UNIVERSITÀ POLITECNICA DELLE MARCHE

FACOLTÀ DI INGEGNERIA

Master degree in Biomedical Engineering

Assessment of human standing balance through wearable inertial sensors

Supervisor:

PALMA LORENZO

Master thesis of:

PRAGLIOLA SARAH

Co-supervisor:

RAGGIUNTO SARA

ACADEMIC YEAR 2021/2022

Abstract

Balance is a fundamental ability for humans and its impairment dramatically reduces the ability to perform activities essential to daily living. The degeneration of balance control system increases the risk of falling, ultimately leading to increased morbidity, mortality, and health care costs. Indeed, balance disorders are one of the major causes of falls in patients with neurological disease, as well as one of the leading causes of injury related to death in older adults. Therefore, the investigation concerning the mechanisms of balance and body postural control represents a growing public concern. Recently, this widespread necessity to assess balance has generated the need for a reliable, low-cost, and easy-to-use clinical measure and inertial sensor technology is turning out to be a possible alternative solution to expensive and immobile force platforms, generally considered as a gold standard in balance assessments. This study has the aim of investigating the accuracy and the validity of inertial sensor against force platform-based evaluations for characterizing the dynamics of standing balance. For this purpose, in collaboration with Santo Stefano Institute in Porto Potenza Picena, a specific measurement protocol was drawn up aimed at the acquisition of synchronized signals between the force plate and the inertial sensor on a total of 17 healthy young adults. The anterior-posterior and medial-lateral trajectories of the center of pressure and center of mass obtained by the two compared measurement systems were strongly matched, with similar paths and oscillations in many of the trials executed. The results confirm that this inertial sensor could be a very promising tool for postural sway assessment.

Contents

Chapter 1

Introduction

Balance can be defined as a generic term describing the dynamics of body posture to prevent falling. It is an imperative skill for quality of life, a fundamental ability to be able to carry out simple daily actions, such as maintaining a correct erect posture and avoid obstacles, and to be able to perform more complex movements such as those, for example, required during the execution of a sporting gesture. However, the human body for its structure is inherently unstable [1] and, thus, the maintenance of balance is a critical challenge to the postural control system, which has to be continuously active to avert falls. In addition, the deterioration in balance function, whether a natural process related to aging or as a result of pathologies, can contribute to falls and fall-related injuries [2, 3].

The integrity of human balance can be quantitatively evaluated employing tests of static and dynamic posturography. In both cases, the posturographic examination consists of the systematic measurement and interpretation of quantities that characterize the performance of the balance control system in upright stance but, static posturography is done on a subject in a condition of quiet standing in a static environment, while the dynamic posturography is performed during a perturbed standing by measuring the response to an applied or volitional perturbation [4].

In the last years, the improvement of quality of life has led to an increase in the aging population and to an increase in life expectancy of the elderly as well, forcing researchers to fully understand human balance. This increasing interest in the study of postural control mechanisms has led to a continuous evolution of the methods used in posturography. Traditionally, it exploits the use of a dynamometric force platform, an instrument that enables to measure the forces exchanged by the subject with the support base and to assess the body's postural sway by recording the displacement of the center of pressure, which is the point of application of the resultant ground reaction force. Nevertheless, even if force platform-based evaluations have been demonstrated as gold standard to perform valid and reliable balance measurements, both in health and diseased subjects, they usually require clinical expertise and an equipped lab space, they are relatively expensive, heavy, difficult to transport, and hence, not practical for out-of-lab (i.e., home) balance assessment necessary in some clinical cases, since a patient may not be able to reach the lab [5]. Therefore, the use of wearable sensors based on miniaturized Inertial Measurement Units (IMUs), in recent years, is increasingly considered a valid solution to overcome these barriers in posturography. Indeed, these sensors are low-cost, easy-to-use, and can be easily worn, using elastic belts or velcro bands, by the tested subjects en-

abling the feasibility of using them in spaces other than the dedicated lab area, since they have reduced size, are lightweight, and are easily portable [6]. This opens to posturographic exams the possibility to perform objective home-based assessments, thus achieving more patients and, for example, simplifying the follow-up of a motor rehabilitation process.

Despite the expanding evidence supporting the use of IMU-based evaluations to carry out posturography, it is important to remember that this area of research is still developing and they have not yet become a standard in tracking patient's postural performance since their precision and reliability for clinical research and practice with respect to the gold standard force platform has not been validated. The objective of this study is to investigate the accuracy and the validity of these novel low-cost portable sensors against force platform-based evaluations for characterizing the dynamics of standing balance.

The following chapter will provide a global view of the state of the art regarding human balance, focusing in particular on the mechanisms and strategies used to control posture. Then, it will pay attention to the procedure to carry on a posturographic analysis providing a brief overview of the use of the force platform and the IMU-based wearable sensor for quantitatively evaluating balance. Moreover, by selecting high-quality papers that adopt wearable inertial sensors to this end, the most important clinical applications in the framework of IMUs, the most common sensor placement and test protocols will be highlighted.

1.1 Control of balance and posture

Posture may be defined as the orientation of any body segment with respect to the gravitational vector [7]. It is associated with the postural sway, an angular measure relative to the vertical direction based on the motion of the individual's center of mass, of body during the maintenance of the upright posture. *Balance*, on the other hand, coincides with the optimal condition of postural changes done to maintain the equilibrium in order to prevent falling [7]. Thus, human *postural control* may be defined as the act of maintaining, achieving, or restoring the state of balance during any body posture or activity [8]. When assessing the implications of balance and postural control it is essential to consider the importance of both the neurological and the mechanical aspects of the control of balance.

1.1.1 Neurological control of balance and posture

Postural control of balance requires the engagement of a complex sensorimotor system, which integrates the information of three main apparatuses [1, 9, 10]:

1. **Visual system**, which has the important task of collecting information regarding the changes that occur in the surrounding environment. It is involved in the organization of locomotion and plays a fundamental role in avoiding possible obstacles along the way;

2. **Vestibular system**, which is located inside of the ear, has the task of detecting changes regarding the head position and speed, making it possible to position the eyes correctly and detect bodily inclinations. It is also able to sense the linear and angular acceleration of the head;

3. **Somatosensory system**, which includes several receptors distributed in the skin, muscles, joints and internal organs, is able to record the different sensations of pressure and contraction. Consequently, it can recognize the mutual position and velocity of the various body segments, determine the position of the different parts of the body with respect to the support surface, sense their contact with external objects and determine the orientation of gravity.

Postural dyscontrol may reflect pathologies affecting one or more components of the sensorimotor system, as well as age-related changes due to the physiological reduced efficiency of the vestibular, visual and proprioceptive functions. This explains why all the neuromusculoskeletal disorders lead to a degeneration of the postural control system [7]. Moreover, the degeneration of the balance control may reflect the inability of the central nervous system to effectively re-weight the sensorimotor system [10, 11]. Indeed, in general, neurological control of posture tends to rely heavily on the somatosensory system in case of conditions of normal stance, but when there are changes in the environmental conditions or balance tasks, it will re-weight its relative dependence on each of the three systems depending on the reliability of the information received [11].

After the integration of all the information coming from the three previously described apparatuses, the central nervous system (CNS) sends signals to the skeletal muscles and the following movements, resulting in small oscillations of the body, serve to maintain balance [4]. This process through which the balance is maintained has been considered from several viewpoints, defining three possible stabilization mechanisms:

- **physical mechanism**, linked to muscle stiffness (i.e., the elastic stiffness of the muscular tissues that influences the effective response given by a muscle to a mechanical disturbance of its state of rest), is an implicit feedback control, which acts instantly, without delay [1];

- **reactive mechanism**, linked to visual, vestibular, proprioceptive and tactile afferents, tries to maintain balance with a control in closed or feedback chain due to which there is an activation of muscles with significant delays of propagation [12];

- **anticipatory mechanism**, linked to the central nervous system, is an open-chain control mechanism or feedforward based on an integration of sensory information and dynamics prediction, able to cancel delays of transduction and propagation of sensory information [13].

The first two mechanisms, being feedback, act in response to external perturbations of the equilibrium, while the third, being a feedforward mechanism, results in muscular actions that are generated in advance of events, in anticipation of the presumed effects to counteract future events that cause loss of balance. This latter is a control based on learning and memory mechanisms and is adaptable to different environmental conditions. In fact, postural control is a skill learned in childhood that improves with experience.

1.1.2 Mechanical control of balance and posture

A man, stationary in the upright position, maintains balance thanks to small but continuous oscillations that have the purpose of counterbalancing the weight force, which would tend, due to the effect of gravity, to make him fall. Indeed, during quiet standing, there are two resultant forces: the weight force and the ground reaction force (GRF), applied respectively to the center of mass (COM) and the center of pressure (COP) [4]. The **center of mass** is the point at which the total body mass can be considered to be concentrated to and it is equivalent to the weighted average of the COM of each segment of the body in the three-dimensional space [1, 4, 7]. The COM's vertical projection on the ground is called the **center of gravity** (COG) [1, 4, 7]. The **center of pressure**, instead, is the location below the body of the resultant reaction vector (i.e., ground reaction force) and it consists of the weighted average of all the pressures over the surface on which the subject stands [1, 4, 7]. In particular, if a subject has only one foot in contact with the ground, the COP lies within that foot, but if the subject has both feet over the ground, it lies between the two feet, depending on the relative weight exerted on each foot [1]. The definitions of the COP, the COM and, the COG are better shown in Figure 1.1.

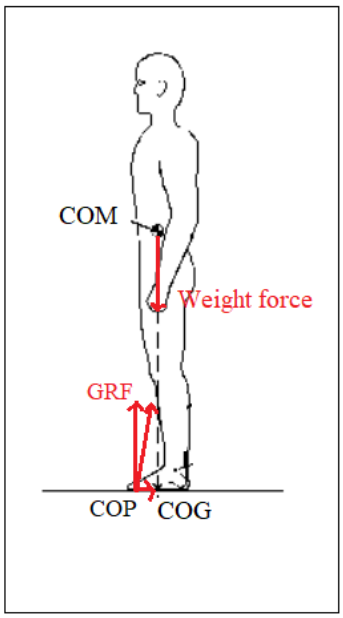

Figure 1.1: The figure shows the position of the Center of Gravity (COG), Centre of Mass (COM) and Centre of Pressure (COP). In addition, the positions of the two resultant forces, one due to gravity (Weight force) and the one caused by the Ground Reaction Force (GRF), are depicted in red.

To have the equilibrium, mechanically, these two resultant forces, the one due to gravity and the one caused by the GRF, have to be equal and opposite because any difference between these two provokes a moment applied to the body that results in destabilization of the postural balance [1, 14].

The relationship between the resultant COP and the COM during quiet stance can be analyzed using a biomechanical model of balance, commonly called **Inverted pendulum model** [1, 7, 15]. This model assumes the body as a single rigid element hinged to the foot via the ankle joint. Modeling the standing body like a pendulum

pivoting around the ankle, the postural control is considered as a feedback control system with the COM as the output and passive variable and the COP as the control variable [1, 7]. Indeed, the center of pressure to avoid postural instability regulates the center of mass by adjusting the position of the vertical projection of the COM (i.e., COG) to keep it inside the support polygon (base of support) of the body [5] (Figure 1.2).

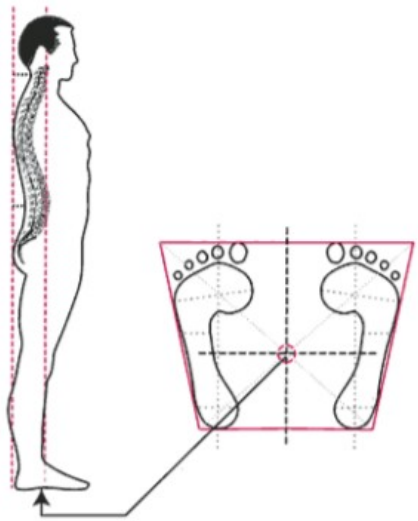

Figure 1.2: The figure represents the support base of a standing subject, with the arms relaxed at the sides. This consists of the trapezoid polygon, depicted in red, with the external sides corresponding to the lateral profile of the feet and with the bases of the polygon corresponding to the lines that join the front and back of the feet [16].

To better understand this regulation we can consider a subject oscillating back and forth to maintain balance while standing erect, as represented in Figure 1.3, which shows a changing situation of different postural conditions in different time instants:

- **Time 1** is characterized by the center of gravity positioned ahead of the COP and by a clockwise angular velocity w. In this situation, the effect of the moment due to the body weight is higher than that due to the vertical reaction force. As a consequence, the body will experience an angular acceleration α in the clockwise direction, which would result in a forward sway. To correct this, the subject will increase his or her COP by increasing the activity of the plantar flexor muscles.

- **Time 2**, instead, has the COP anterior to the position of the body's COG and so the prevailing moment is that due to the reaction force. Thus, since in this case, the angular acceleration α will reverse, it will start to decrease the angular velocity w.

- **Time 3** is characterized by both the angular acceleration α and velocity w that are in the counterclockwise direction and thus the body results in a backward

sway. To correct this posterior shift of the body's COG and thus to decrease the COP, the central nervous system decreases the activity of the plantar flexor muscles and increases the dorsiflexor activation until the COP will lie posterior to the position of the COG.

- **Time 4** has α clockwise again and after some time w will again decrease and reverse.
- **Time 5** is characterized by the body that returns to the original conditions with the COG ahead of the COP position.

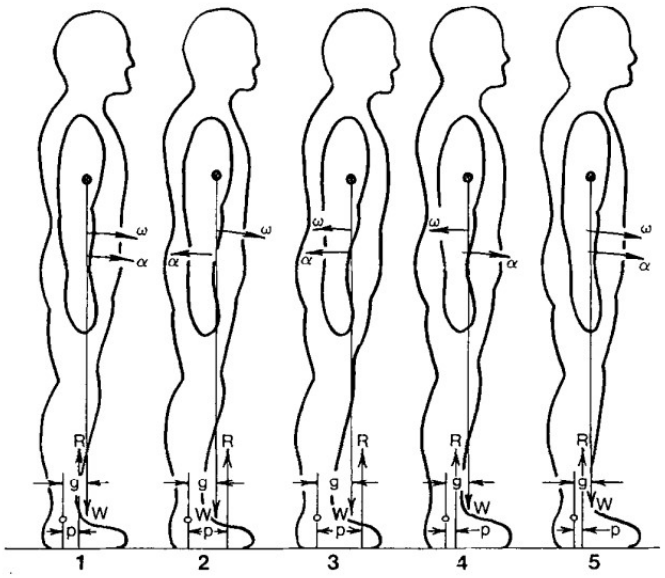

Figure 1.3: A subject swaying back and forth while maintaining balance in the upright position is represented in the figure at five different points in time, showing the center of gravity and the center of pressure locations (g and p respectively), the associated angular acceleration α and velocity w and the position of the two resultant forces (R and W) [7].

Thus, modeling the body as an inverted pendulum, pivoting around the ankle, two moments will act, a counterclockwise moment equal to $R \cdot p$ and a clockwise moment equal to $W \cdot g$, resulting in the following equation:

$$R \cdot p - W \cdot g = I \cdot \alpha \ , \tag{1.1}$$

where W is the body weight, R represents the vertical reaction force, g and p are the moment arms of W and R from the ankle joint, I is the moment of inertia of the total body around the ankle joint, and α is the angular acceleration of the inverted pendulum.
From the equation, we can see that when $Wg > Rp$ (condition described at the time instant 1), the subject will experience a forward sway of the body, instead when $Wg < Rp$ (condition described at time 3) the subject will experience a backward sway of the body. Both these displacements of the COG position need to be correct in order to avert postural instability, therefore, the dynamic range of the COP

must be greater than that of the center of mass because the center of pressure must continuously move forward and backward with respect to the COM position to ensure the maintenance of equilibrium, since the COP represents the control variable.

Moreover, the inverted pendulum model considers the difference (COM-COP) as the error signal of the balance control system provoking the COM's horizontal acceleration, since it states that this difference is proportional to the horizontal linear acceleration of the COM [1, 7]. This can be demonstrated starting from Figure 1.4 and considering small oscillations, thus a small angle θ, we can assume that $\sin\theta = \theta$ and $\cos\theta = 1$; so it can be approximated as follows:

$$g = -d \cdot \theta \ , \tag{1.2}$$

where d is the distance from the ankle joint to the total body COM, θ represents the sway angle and g is the anterior displacement of the COM with respect to the ankle joint.

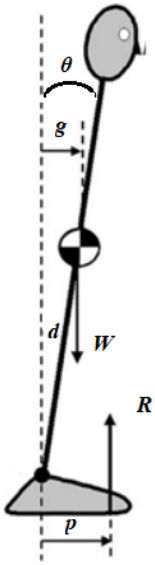

Figure 1.4: Inverted pendulum model in the Anterior-Posterior (A/P) direction, characterized by the pendulum that pivots around the ankle joint [17].

Performing a double differentiation it is possible to obtain the angular acceleration of the inverted pendulum α,

$$\ddot{g} = -d \cdot \ddot{\theta} \rightarrow \quad \ddot{g} = -d \cdot \alpha \rightarrow \quad \alpha = \frac{-\ddot{g}}{d}. \tag{1.3}$$

Then, replacing the angular acceleration in the moment equation:

$$R \cdot p - W \cdot g = I \cdot (\frac{-\ddot{g}}{d}) \ , \tag{1.4}$$

and, considering that in the equilibrium condition the two resultant forces are equal, we can obtain dividing by the weight force:

$$R = W \rightarrow (g - p) = I(\frac{\ddot{g}}{d \cdot W}) \ . \tag{1.5}$$

Assuming K as a biomechanical constant, we have:

$$(g - p) = K\ddot{g} \ , \tag{1.6}$$

which is equivalent to define that the difference between the COM and COP is proportional to the acceleration of the COM:

$$COM - COP = KC\ddot{O}M \ . \tag{1.7}$$

The horizontal acceleration described is in the Anterior-Posterior (A/P) direction but the same applies to the Medial-Lateral (M/L) acceleration. This simplified view of the body as an inverted pendulum in A/P direction is useful for describing the importance of the ankle joint for controlling motion in case of quiet stance [1, 18]. Indeed, as said before, the location of the COP under each foot is achieved by the regulation of the activation of the plantar flexor and dorsiflexor muscles done by the CNS to control the net ankle moment. In fact, an increasing plantar flexor activity moves the center of pressure anteriorly, while an increasing dorsiflexor activity moves the COP in the posterior direction. This is what is defined as the *ankle strategy*. However, viewing the system in this simplified way may not be appropriate for assessing more global postural control mechanisms and a **double or triple segment inverted pendulum model** may be required, with control at the ankles but also at the hips [1, 10, 18], as shown in Figure 1.5. This is because

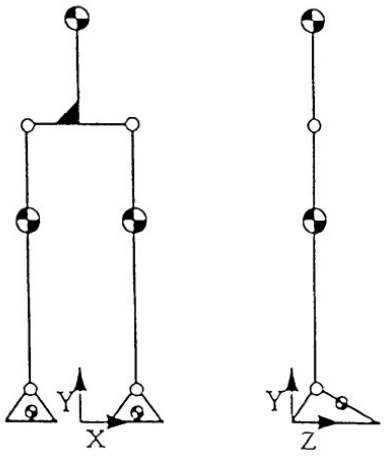

Figure 1.5: The figure represents the biomechanical models for standing. The first depicted model is the one for the frontal plane, which consists of a parallelogram pivoting around both ankle and hip joints, while the second one is in the sagittal plane with the pendulum pivoting around the ankle during quiet standing or around both hip and ankle in case of perturbed stance [7].

the ankle strategy allows maintaining the equilibrium in case of quiet stance and when only small perturbations of the body are involved, while the hip strategy is introduced to counterbalance large bodily displacement. Thus, to prevent the COM-COP difference to fuel the natural tendency to fall, there are two main possible control mechanisms [19] (Figure 1.6):

1. **Ankle strategy**, which consists in acting on the COP by modulating the activation of the ankle muscles. This mechanism is employed for unperturbed

stance and to compensate for slow and low amplitude perturbations of the balance. It requires less muscle strain;

2. **Hip strategy**, which consists in acting on the COM using relative movements of parts of the body. This mechanism is used for faster large amplitude perturbations, in cases in which there is a sudden disturbance of posture to quickly recover a normal postural attitude. It involves a very high energy expenditure since, in these conditions, the perception of the imbalance must be very rapid.

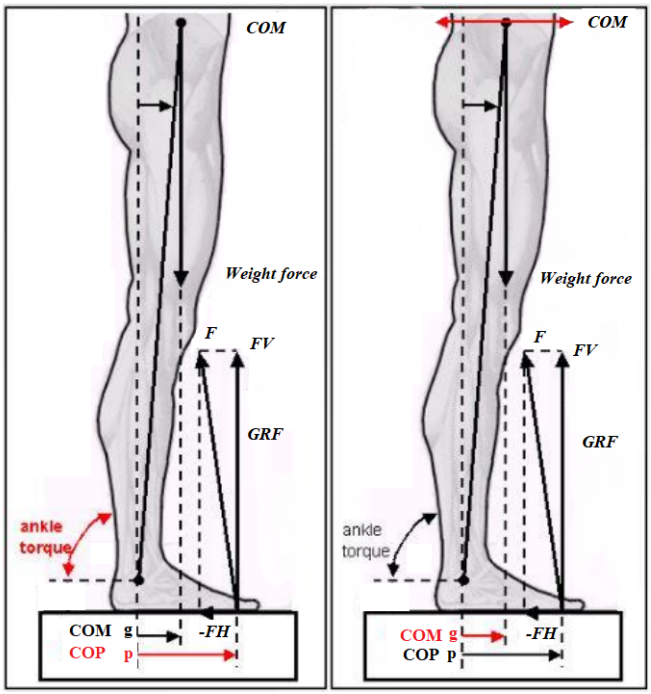

Figure 1.6: Ankle strategy (left) and hip strategy (right) acting on the Centre of Pressure (COP) and the Centre of Mass (COM) respectively [20].

Therefore, in the A/P direction, in case of small oscillations of the body, the ankle strategy will recruit the plantar flexor/dorsiflexor muscles to move the COP anteriorly/posteriorly, while in case of large perturbations the hip strategy will act, alone or in combination with the ankle strategy, to flex/extend the hip to move the center of mass posteriorly/anteriorly. In the M/L direction, instead, the ankle strategy will respond to small oscillations using the invertor or the evertor muscles to obtain the movement of the COP laterally away or toward the midline of the body respectively, while large oscillations of the body will require the action at the hip joints of the abductor/adductor muscles responsible for the loading and unloading of the body weight on one leg with respect to the other. In situations in which the perturbation is so large that ankle and hip strategies are not able to compensate for it, the final line of defense to avoid falls is the **step strategy**. This mechanism consists in taking a step to make the base of support larger, since the center of gravity is pushed very far. All the balancing strategies previously described are summarized in the following figure (Figure 1.7).

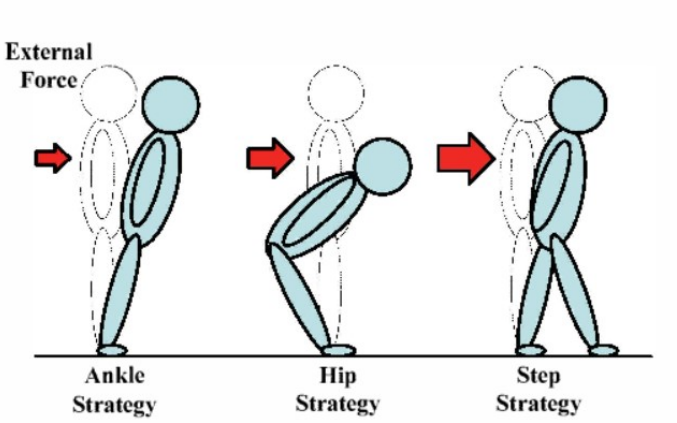

Figure 1.7: The figure depicts three basic balancing strategies: Ankle strategy, Hip strategy, and Step strategy. The red arrows, corresponding to external forces, highlight that these mechanisms are used in conditions of different entities of equilibrium perturbations [21].

1.2 Posturographic analysis

Postural stability varies over the course of life and depends on the degree of maturity and functional integrity of the systems (i.e., visual, vestibular and proprioceptive) responsible for maintaining human balance: from birth to adolescence there is a phase of development and improvement of the ability to maintain in balance the body, while in adulthood this capacity undergoes a physiological decline due to the reduction in efficiency of these systems [2, 3, 22]. This progressive loss of functioning with increased age and several pathologies can contribute to balance deficits and given the association of the latter with falls and fall-related injuries, balance disorders represent a growing public health concern. Indeed, they are one of the leading causes of death afflicting geriatric subjects [22]. Moreover, in economic terms, the direct and indirect costs associated with falls are very high and are growing as the percentage of older people is increasing [22, 23]. As a consequence, trying to understand age-related changes of postural control system is of utmost importance to help in preventing falls and reducing the burden on individuals and society due to injuries following balance disorders.

Posturographic analysis is an excellent investigation tool for this phenomenon. It can be used in clinical settings to appraise balance-related disabilities, such as those characterizing Parkinson's disease, concussion or stroke, to assess fall risk in geriatric subjects, in rehabilitation protocols, or also can be used in sport science to evaluate the balance performances of athletes [6, 24]. Indeed, performing a balance test, it is possible to:

- tease out the contribution of the three systems constituting the postural control system and identify their individual role;
- understand how the redundancy of these systems involved in the control of balance can assist when one of the systems fails or is impaired;
- pertube the balance system in order to quantify the human response;

- confuse the systems by providing conflicting or false sensory inputs.

The techniques, evaluating the integrity of balance control system, within posturography, can be divided in two main groups of *static* or *dynamic* posturography [24].

Static posturography

Static posturography or postural steadiness, describes the dynamics of the postural control system associated with maintaining balance during quiet standing in a static environment [25]. The classical paradigm used to perform this kind of postural analysis consists in analyzing how the examined subject remains in static position with the arms along the sides during quiet stance, either on one leg or two, on a fixed support surface and without external perturbations. The aim of such test is to assess the spontaneous body's sway and small changes in postural sway represents a good postural control.

Dynamic posturography

Dynamic posturography characterizes the performance of the postural control system in pertubed standing by measuring its response to an applied or volitional perturbation [25]. These perturbations can be either voluntarily initiated internal perturbations, such as raising an arm or bending the trunk, or external unexpected disturbances, like a moving platform that translates or tilts. The former aim to study the anticipatory response of the CNS to protect against imbalance, that is proactive control. The last ones are used to test the reactive response of the three sensory systems.

In these tests, to examine the postural stability a time-series analysis based on the center of pressure data is mostly used [25]. There are mainly two different representations of the centre of pressure [24]:

- **Statokinesigram**, which is the graphic representation of the coordinates of the center of pressure during the trial, projected separately in the two planes, sagittal and frontal (i.e., 2-D trajectory of the COP over the test);
- **Stabilogram**, which consists in the time evolution of the anterior-posterior or medial-lateral components of COP.

An example of typical statokinesigram and stabilograms for a healthy young adult during quiet standing are shown in Figures 1.9 and 1.8, respectively.

From COP, then it is common to extract quantitative information characterizing the stability of the subject through the calculation of some parameters in the time or frequency domain [25]. Moreover, postural evaluations often include both eyes-open and eyes-closed trials. Indeed, when a subject is tested with the eyes-closed, he/she is temporarily deprived of the visual system, which is one of the sensory system involved in the control of balance. Thus, performing both tests it is possible to estimate the role of the vision in maintaining standing stability. The ratio of the eyes-closed measure to the eyes-open measure is referred to as the Romberg ratio [25]. From a theoretical perspective, parameters measured from a subject in

condition of closed eyes should be greater than that measured with open eyes, since the closed eyes trial should constitute a more critical situation for the maintenance of the posture due to the deprivation of the visual input. Therefore, the Romberg ratio for each parameter should be greater than one since greater oscillations in the closed eyes trial results into greater parameter values than those in the open eyes trial. However, this is not always true, as a matter of fact some individuals, such as people suffering from a certain pathology, when they are in more critical situations for the control of the posture, they tend to freeze some degrees of freedom, resulting in a reduced amplitude of oscillations and so a Romberg Ratio which could be lower than one.

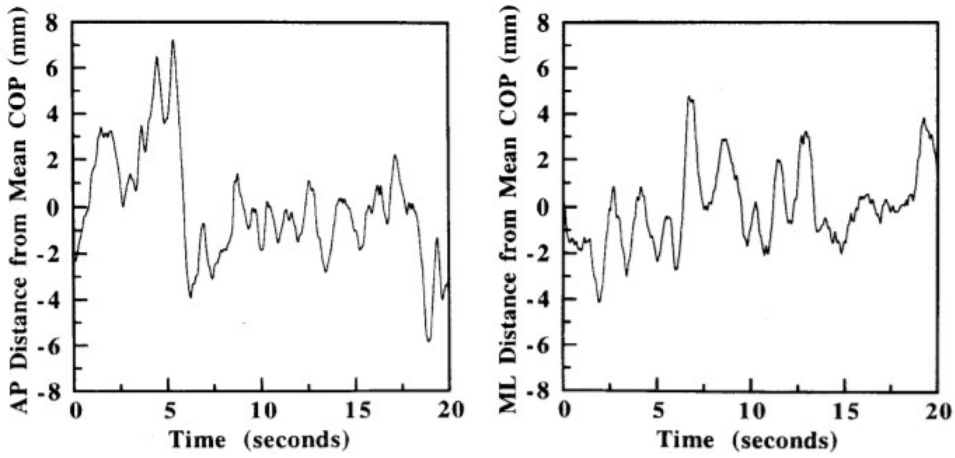

Figure 1.8: Example of stabilogram plots for a healthy young adult during standing balance for 20 seconds with eyes-open: on the left Anterior-Posterior (AP) time series of the displacement from the mean COP and on the right Medial-Lateral (ML) time series of the displacement from the mean COP [25].

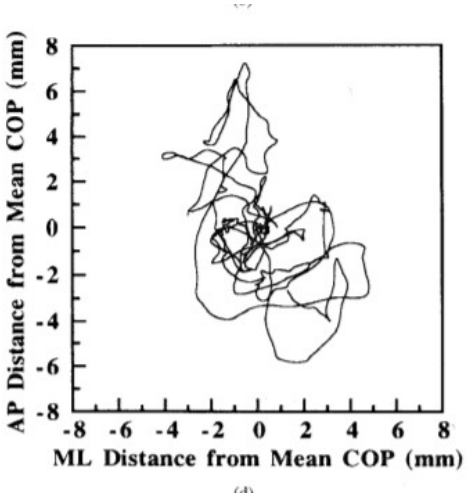

Figure 1.9: Example of statokinesigram representation for a healthy young adult during quiet stance for 20 seconds with eyes-open. The AP and ML time series of the displacement from the mean COP are plotted on the X and Y axis respectively [25].

COP is computed directly from force-platforms, while COM can be indirectly assessed by means of three different methods:

1. **Stereophotogrammetry applied to a multisegmental body model**, which implies the computation of the position of the COM of the total body as the weighted average of a set of points constituting the centre of masses of the various body segments. This procedure requires the use of markers applied to these points and anthropometric tables providing an estimate of the position of centre of masses and of the masses of the various body segments;

2. **COP low-pass filtering**, which is a technique that provides the COM displacement starting from the COP displacement and using a low pass filter with a cut-off frequency of 0.3/0.4 Hz. This method relies on the fact that COM can be seen as a low pass version of COP, with COP frequency band of 0-3 Hz and COM frequency band of 0-0.3 Hz. However, it is important to consider that this method is highly dependent on the chosen cut-off frequency and also on other design parameters of the implemented filter, such as the transition band.

3. **Double integration method**, which implies the use of the following formula:

$$X_{COM} = X_{COM_0} + \dot{X}_{COM_0} \cdot t + \int_0^t \left[\int_0^\tau \frac{F_{0x}}{M} \, d\xi \right] d\tau \right] \, , \tag{1.8}$$

   where X_{COM_0} and $\dot{X}_{COM_0}$ represent the position and the velocity of the COM, respectively, at time $t = 0$; F_{0x} represents the horizontal component of the reaction force vector and M the body mass.

1.2.1 Dynamometric force platform

Currently, a posturographic analysis is most often characterized with measures exploiting the use of a dynamometric force platform [6]. The working principle of a force plate is based on the use of sensors, sensitive to a mechanical action, which translate into an electrical signal the mechanical action to which the platform itself is subjected due to the effect of an applied load [27]. Thus, if a subject is standing on a force platform, it allows us to measure the resulting force exchanged between the feet and the support base.

The dynamometric platforms can be divided into two different types: piezoelectric and strain gauge. The piezoelectric force plate measures foot-to-ground reaction forces using load cells containing piezoelectric crystals. In this case, the applied force causes a deformation of the materials of which it is composed and consequently a physical size variation, since the crystal is compressed when a force from the outside is applied. This provokes a variation of the piezoelectric properties of the material that can be converted into an electrical signal proportional to the force applied on the platform. Strain gauge platforms, on the other hand, consist of metal plates connected to a circuit of electrical resistances (i.e.,Wheatstone bridge). In this force plates, the resistance varies as a function of the deformation to which they are subjected, according to the following law:

$$R = \rho \cdot \frac{L}{A} \, , \tag{1.9}$$

where R is the resistance, ρ is the resistivity of the material, L is the length of the strain gauge and A is the section of the strain gauge. Therefore, if fed with a current of intensity I they are capable of producing a voltage,

$$V = R \cdot I \,, \tag{1.10}$$

which is an electrical signal directly proportional to the applied force.

The simplest force plates measure the vertical component of the ground reaction force and the two coordinates of the center of pressure expressed usually within a coordinate system relative to the force plate. Advanced models measure the three-dimensional components of the equivalent force applied to the surface (i.e., ground reaction force) and the coordinates of its point of application (i.e., COP) as well as the vertical moment applied to the foot.

1.2.2 Inertial measurement unit

Wearable technology refers to any kind of electronic device that can be worn by a subject. Inertial sensing units are wearable sensors using the principle of inertia to measure linear accelerations (i.e., accelerometers) or angular velocities (i.e., gyroscopes) or both amplitude and direction of the local magnetic field (i.e., magnetometers). These inertial sensors can be further integrated into what is defined an inertial measurement unit, which contains a triaxial accelerometer and a triaxial gyroscope, as well as, a triaxial magnetometer in case of what is called a Magneto Inertial Measurement Unit (MIMU). The fusion of data from these sensors used together provides an excellent opportunity to collect a variety of precious and objective outcomes to allow segment orientations, joint angles and sway assessments for evaluating balance. Following the main components and the operating principle of IMU-based sensors will be analyzed.

Accelerometers

Accelerometers are sensors capable of measuring linear accelerations [6, 28, 29]. They are based on different construction techniques and physical principles for the acceleration measurement but conceptually these devices exploit the same principle of operation: they are based on the detection of the inertia of a mass subjected to an acceleration. Indeed, inside of the accelerometer, a mass is connected to an elastic element, generally a spring, in turn linked to a fixed structure and its position over time is acquired by a sensor. If there is no acceleration, the mass is stationary, instead in presence of an acceleration, the mass moves from its rest position (point x_0) in a proportional way to the acceleration acting on it. This displacement of the mass is evaluated by means of the sensor, which on the basis of the traveled space, determines the acceleration and transforms this displacement into an electrical signal. The operating principle of an accelerometer can be better understood from Figure 1.10.

According to Newton's second law of motion, a mass m to which an acceleration a is impressed is subjected to a force:

$$F = m \cdot a \,. \tag{1.11}$$

As a consequence, the elastic element tends to stretch by a Δx value, while the test mass, constrained to it, generates a force opposite to that due to the acceleration,

trying to resist the movement. The elastic element follows Hooke's law, according to which the spring is subjected to an elastic return force proportional to the deformation Δx impressed:

$$FH = k \cdot \Delta x \,, \tag{1.12}$$

where k is the elastic constant dependent on the characteristics of the spring. Balancing these forces we have that:

$$FH = k \cdot \Delta x = F = m \cdot a \,. \tag{1.13}$$

Thus, knowing m and k and by measuring the displacement Δx of the elastic element, it is possible to obtain the acceleration:

$$a = \frac{k \cdot \Delta x}{m} \,. \tag{1.14}$$

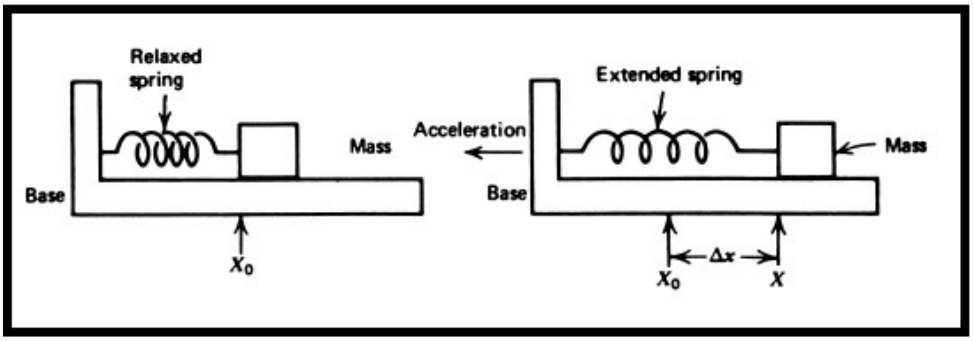

Figure 1.10: Operating principle of an uniaxial accelerometer constituting by a mass attached to a spring [26].

Another schematization of an accelerometer is given by the mass-spring-damper system [28] (Figure 1.11). In this case, the proof mass moves relative to its supporting frame according to the undergone acceleration, the elastic constant of the spring k and the viscoelastic constant of the damper b, forming a second-order system. Applying Newton's second law we have:

$$m \cdot a = m \cdot \frac{d^2x}{dt^2} + b \cdot \frac{dx}{dt} + k \cdot x \,, \tag{1.15}$$

where x is the displacement of the mass m with respect to its frame and a is the external input acceleration.
Based on this, the accelerometers, in the kinematic analysis of human movement, allow to measure the acceleration of the various body segments on which they are placed.

Generally, accelerometers are uniaxial and in this case they are able to measure only the acceleration component parallel to their sensitive direction. Since it is often necessary to monitor the acceleration along the three spatial axes, it is possible to build a triaxial accelerometer by assembling three uniaxial accelerometers so that each identifies one of the three spatial axes. This is achieved just connecting the test mass with three orthogonal elastic elements.

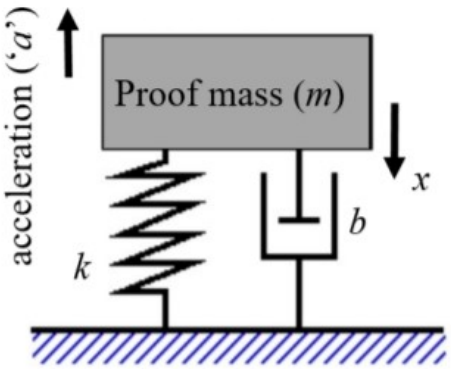

Figure 1.11: The figure shows the mass-spring-damper configuration of an accelerometer [28].

Gyroscopes

The gyroscope is a rotating device which, due to the law of conservation of angular momentum, tends to keep its axis of rotation oriented in a fixed direction [29, 30]. It allows us to measure the angular velocity around a certain axis, so as to be able to calculate through it the variation of angle undergone around the same axis.

Current technology makes it possible to build gyroscopes that exploit different operating principles; the most common are the mechanical, optical and microelectronic (MEMS) gyroscopes with vibrating mass. The mechanical gyroscope (Figure 1.12) consists of a rotor having a certain angular velocity around its own axis of rotation (also named spin axis), kept inside a gimbal suspension. The rotor, possessing a high angular momentum L, which is given by the product between its moment of inertia I and the angular speed of rotation w, will tend to maintain its initial orientation, leading to a phase shift of the angle of one of the hinges of the suspension [31].

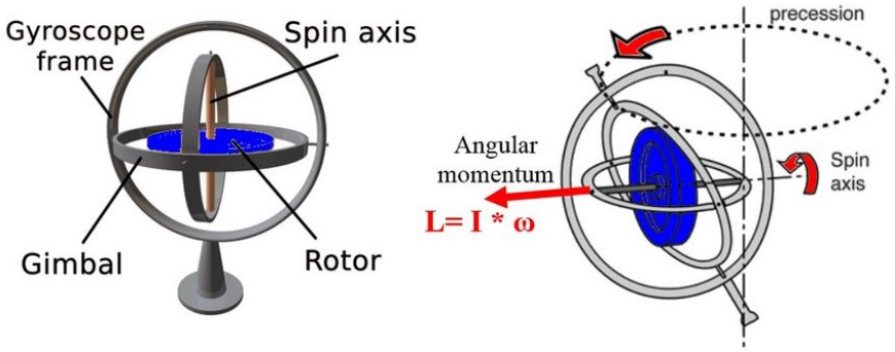

Figure 1.12: The figure shows the operating principle of the mechanical gyroscope [31].

The optical gyroscope (Figure 1.13) measures the angular velocity exploiting the *Sagnac effect*: two rays of light are sent inside an optical fiber, in opposite directions, so that when the sensor is placed in rotation, a round is completed out of phase, since the ray traveling in the opposite direction to the rotation will take less time [33]. From this phase shift it is possible to obtain the measurement of the angular

velocity.

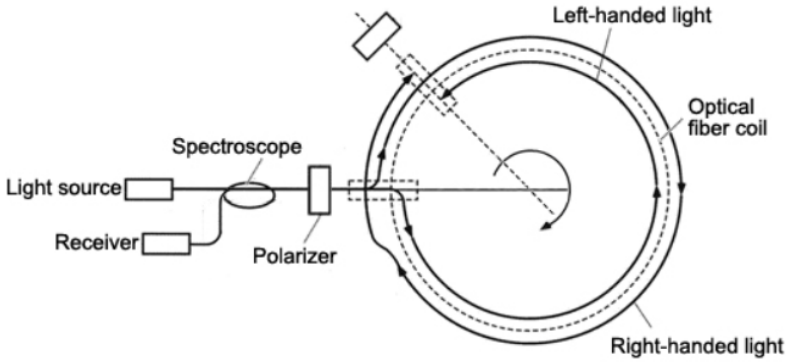

Figure 1.13: The figure shows the configuration and the operating principle of an optical gyroscope [32].

The mechanical and optical gyroscopes are widely used in the field of navigation, but they are not suitable to perform the analysis of human movement as they are both expensive and bulky. Vibrating mass gyroscope, on the other hand, are small, light, and they have low power consumption and cost [34]. Therefore, they are ideal for analyzing human movement. This latter sensors exploit the effect of the Coriolis Force FC, i.e., an apparent force to which a body is subjected when its motion from a reference system in circular motion is observed with respect to an inertial reference system (Figure 1.14). These gyroscopes are made by a vibrating mass connected to springs, as depicted in Figure 1.15, and in the absence of rotation, this element oscillates continuously along a given trajectory with a certain velocity V. The rotation of this structure with an angular velocity w, around an axis perpendicular to the plane of vibration of the mass, induces the formation of the Coriolis force. This causes a new oscillation of the mass in an orthogonal direction to the plane in which is contained and the amplitude of this out-of-plane vibration is proportional to the angular velocity applied. The intensity of FC is proportional to the vibrating mass m and to its own velocity V and the angular velocity of the rotating reference system w, depending on the relation [29, 34]:

$$FC = -2m(w \times V)\,. \tag{1.16}$$

This force FC is opposite to the elastic one produced by the spring and obtainable from Hooke's law, $FH = k \cdot x$. In equilibrium condition we have that:

$$FC = -2 \cdot m(w \times V) = FH = k \cdot x\,, \tag{1.17}$$

from which measuring x and knowing the elastic constant of the spring k and the rotation speed of oscillation V it is possible to find the angular velocity:

$$w = \frac{k \cdot x}{2 \cdot m \cdot V}\,. \tag{1.18}$$

Based on this, gyroscopes are sensors able to measure the angular velocity of the body segments on which they are positioned. Thus, in the kinematic analysis of human movement, they are generally used to derive the different gait parameters,

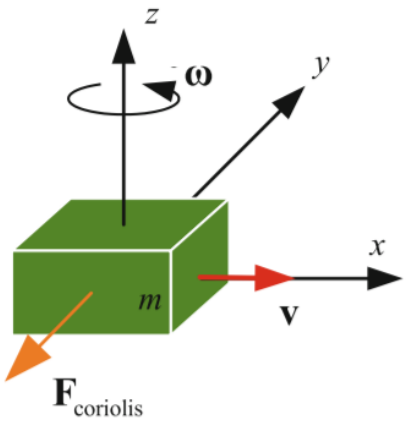

Figure 1.14: The figure shows the Coriolis force acting on a vibrating mass m with a velocity of oscillation V and with w as angular velocity of the rotating reference system [29].

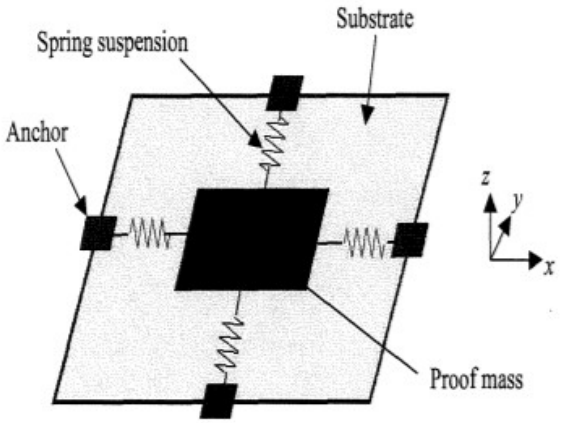

Figure 1.15: The figure shows a schematic representation of a MEMS vibrating gyroscope [30].

since from the angular velocity variables such as the speed, walking cycle and stride length and time of stance and swing can be easily obtained, or, in association with an accelerometer, they can be also used to determine specific motor patterns.

A triaxial gyroscope can be obtained as a combination of three monoaxial gyroscopes. The output of this is the angular velocity expressed in the sensor reference system, i.e. the angular velocity measured with respect to the three orthogonal axes X, Y, and Z. Then, simply by performing a discrete integration of it over time, the angular rotations are obtained:

$$\Delta\alpha = w \cdot \Delta t\,, \tag{1.19}$$

where α represents a generic angle of rotation around one of the three axes X, Y, Z of the gyroscope, w is the angular velocity referred to each axis and Δt is the sampling time of the sensor.

The main problem with gyroscopes is that the measure of the detected angular velocity is affected by an intrinsic offset called bias. This offset, during the inte-

gration process, necessary to evaluate the orientation changes, leads to a diverging linear error called drift which, over time, leads to the complete inconsistency of the measurements.

Magnetometers

The magnetometer is an instrument measuring the magnetic field surrounding it [6]. In particular, according to the type of information measured, magnetometers are divided into scalars or vectors, respectively if they measure the magnitude of the magnetic field or the component of the magnetic field along the magnetometer sensitive axis. These sensors are very important because one of the main problems of 3D inertial sensing is the need of external references [35]. Using accelerometers we can use the gravity force as a reference in the vertical plane, at least in static situations, but we still don't have a reference for the horizontal plane, which instead can be obtained using magnetometers. The earth's magnetic field has a component parallel to the earth's surface always pointing towards magnetic north, consequently its projection on the horizontal plane can be used to determine the orientation of the magnetometer in the space. Thus, it can be used as a device to detect and obtain the orientation of an object or a body.

The operating principle of the magnetometer is shown in Figure 1.16, where depending on the orientation of the magnetic field, a torque is generated and can be calculated in order to obtain the angle of incidence of the sensor axis [35].

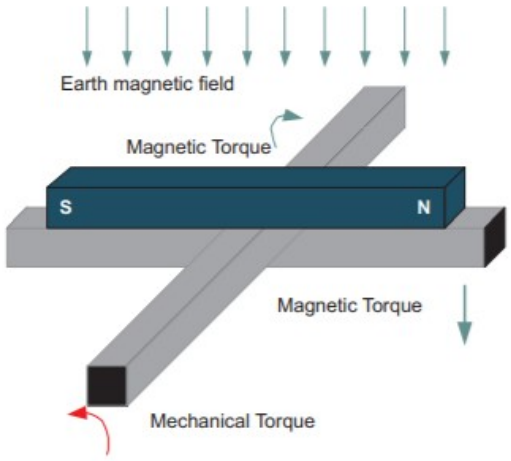

Figure 1.16: The figure shows the operating principle of a magnetometer [35].

The triaxial magnetometer provides the components of the magnetic field present in the environment along the three X, Y, Z axes. In addition, the use of the magnetometer is useful as, through trigonometry and known the roll ϕ and pitch θ angles, it is possible to determine the yaw angle ψ. In particular, if the Z axis is parallel to the gravity force vector, it is possible to obtain the yaw angle using the following equation:

$$\psi = atan(\frac{My}{Mx}) \,, \tag{1.20}$$

where Mx and My represent the components of the magnetic field along the axes of the magnetometer X and Y.

Inertial sensors

In recent years, inertial sensors are increasingly considered an attractive solution for 'in the field' motion analysis, as demonstrated by the high number of papers focusing on this topic reported in literature. However, before such technology can be used routinely, its reliability and validity need to be studied to compare its performance against a gold standard. Research in the past years has focused on investigating this validity and reliability of IMU-based approaches for many different purposes, including, for example, for analyzing gait [36, 37], static and dynamic balance [38, 39, 40, 41], upper arm mobility [42], and for classifying and characterizing daily-life movement activities in both healthy and pathological populations. For example, Noamani et al.[39], investigate the accuracy of IMUs against in-lab equipment (motion-capture cameras and force plate) for characterizing standing balance. In their study, each participant was asked to stand still on a force plate for a two-minute standing test for estimating inter-segmental moments and center of pressure position in a four-segment model. IMU-based approach resulted in high accuracy compared to the reference. Equally positive results were achieved by the studies done by Sun et al.[43] and Mancini et al.[44], that examined the concurrent validity of a wireless skin-mounted inertial sensor and a body-worn accelerometer system respectively, by comparing measurement agreement between these novel sensors and the force plate during quiet stance. In the first study, each participant standing on a force plate completed three balance assessment conditions (eyes open/firm surface, eyes closed/firm surface, and eyes open/foam surface) twice for 30 s each, with the sensor placed on the skin on the posterior trunk at the level of L5. In the second study, instead, all the participants had to maintain the standing position on a force plate and simultaneously wear the wearable sensor with 3-D accelerometers at the level of L5, for a total of three trials of two minutes performed all with eyes open. In both studies, researchers compare sway from force plate and inertial sensor and concluded that sensor based measures of sway were just as sensitive as the one from the gold standard. Instead, Jacob et al.[45], investigate the validity and accuracy of inertial sensors for IMUs-based gait analysis. Therefore, they compared gait parameters measured by the wearable system and the motion capture system as the gold standard. Their results indicate that wearable sensors generate valid gait parameters compared to the motion capture system and can consequently be used for clinically relevant gait recordings in flexible environments. In the context of validity of IMUs for gait analysis, significant is also the study done by Fusca et al.[46], that presented a set of guidelines to design a validation protocol for inertial measurement.

A thorough research in literature demonstrated a broad heterogeneity of methods generally used to assess the integrity of the postural control system with IMU-based measurements. Following a brief overview of the different functional tests and motion parameters that are most commonly with inertial sensor evaluations is reported:

- **Gait analysis**: To this end, accelerometers are most often used to derive spatio-temporal gait parameters such as, cadence or step length [48]. Moreover, inertial measurement units using accelerometers in combination with gyroscopes have become increasingly popular for gait analysis as they allow kinematic characterisation of gait, supplementary to spatio-temporal gait parameters [47]. A previous systematic review of the literature [37] demonstrated high accuracy for most IMUs compared to gold standard systems.

Clinical applications of inertial measurement units include single or multiple linked sensor set-ups to measure a wide variety of different motion parameters including for example the range of motion of the trunk and pelvis, joint angles of the hip, knee and ankle as well as angular velocity of the thigh and shank. Research shows that IMU-based gait analysis is a feasible and sophisticated tool for functional outcome assessment in orthopaedics, since electromyography (EMG) determines the electric activity from muscles and wearable EMG sensors have become available in fusion with IMUs to enrich kinematic gait analysis with muscle activity [49].

- **Sit-to-stand test** (STS): In literature, the STS test has been enhanced thanks to the use of an IMU sensor fixed on the trunk (e.g., lumbar spine or sternum) to measure the trunk inclination as known compensation mechanism adopted to avoid pain or as a result of persistent muscle weakness [47]. In particular, a study demonstrated that to measure the trunk movement, using a single inertial sensor, the optimal placement of the IMU is at a level of the L1 [50]. Other studies in this field reported experimental protocols characterized by the use of multiple linked inertial sensors to allow additional assessment of joint kinematics from the hip and knee.

- **Timed Up-and-Go test** (TUG): Some studies performed this test using inertial measurement units to achieve a precise timing of the test transition phases and to measure motion parameters from each of these latters. To this end, IMUs are most often placed on the trunk, sternum, thigh, tibia and shin in order to determine the trunk acceleration, the lower limb angular velocity and the hip and knee range of motion.

- **Stair climbing test**: Works described evaluations done with IMUs placed on the sternum, sacrum, hip, thigh and tibia, capturing trunk and lower limb acceleration and angular velocity to detect frailty in elderly patients, to assess functional outcome after total joint replacement, and in general to establish safety and independence of elderly patients [47].

- **Balance tests:** Balance is measured across a wide range of clinical populations, especially patients with neurological disorders such as elderly at risk for falls [6]. In particular, two systematic reviews are specifically focused on the objective estimation of fall risk in geriatric populations: the first one addresses the use of inertial sensors for fall risk assessment [51], while the second one considers novel sensing technologies (including IMUs) in fall risk assessment in older adults [52]. Among the various pathologies affecting balance performance, it is widely recognized that Parkinson's Disease (PD) is a condition that may greatly benefit from an innovative clinical management of patients based on wearable monitoring technologies [6]. A systematic review discussed inertial sensors and the principal postural parameters that should be analyzed for assessing PD [53]. Another, analyzed the use of wearable sensors to assess standing and walking balance in people with PD [54]. Another commonly reported balance disorder that may strongly benefit from the use of inertial sensors is Multiple Sclerosis (MS) [55]. A recent systematic review analyzed the validity of the use of sensors to study mobility and balance in MS patients.

In general, studies focused on balance test used IMUs to measure three-dimensional body sway from the centre of mass, hips and ankles.

In literature, several different inertial sensor placements were described in the experimental protocols, depending on the considered postural task. For example, many studies [40, 41] placed the wearable sensors near the position of the COM on the lower back, mainly in correspondence of the lumbar region of the trunk at L5 and the sacral region of the trunk at S2. Other papers [56, 57] instead used protocols with sensors fixed on the lower limb, for example, on the thigh, malleolus, and shank, or on the sternum. Some [58, 59] also put these sensors on the upper back on the thoracic region of the trunk, or on the upper limb [60], in particular on the wrists, or on the forehead. The main sensor placements reported in experimental protocols found in literature are summarized in Figure 1.17.

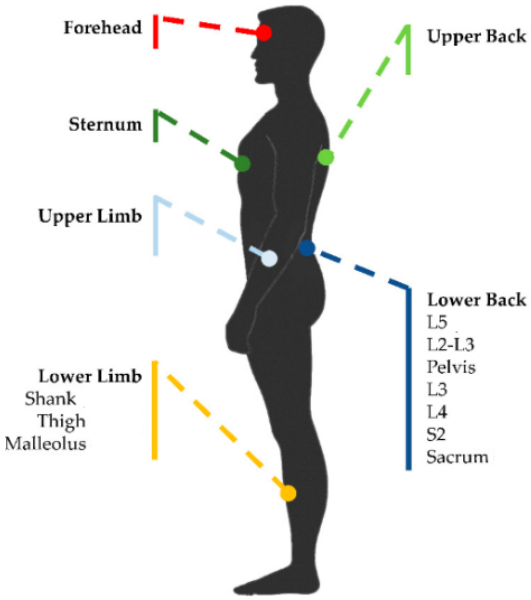

Figure 1.17: The figure summarizes the main sensor placements reported in different experimental protocols found in literature [6].

Chapter 2

Materials and Methods

This chapter outlines the primary objective that this work presents: the validation of the precision and accuracy of wearable inertial sensors against the gold-standard reference (i.e., dynamometric force platform) to compare these two solutions. In particular, in this study we verify:

1. the concurrent validity of an IMU sensor in standing balance assessment compared to a reference force plate;

2. whether IMU-based evaluations can reveal differences between the different tasks, therefore between the different positions and the different challenge conditions for the postural control system, assumed by the examined subjects during the tests, as well as force platforms can do.

In the following paragraphs the development process that led to the implementation of the proposed validation algorithm will be described, starting from description of the protocol used for the acquisitions to the procedure for processing and comparing the experimental data obtained from the two measurement systems.

2.1 Literature review

Search strategy and study selection

In this work it was decided to perform the validation of inertial measurement units focusing only on their use to evaluate standing balance. For this purpose, a preliminary literature research was performed on several web sites (e.g., Scopus, Pubmed, Google Scholar, IEEE and Elsevier) to find recent studies involving inertial sensors in static posturographic assessments. The entered keywords were: “inertial sensor”, “IMU”, “MIMU”, “postural sway”, “postural control”, ”standing balance”, ”posturography”, and “accelerometers”. The search criterion consists in the selection of papers in which the IMUs sensors were used together with a force platform, added as a comparison tool. Furthermore, articles were excluded if they were out-of-topic with respect to the aims of the present work, i.e., the study of standing balance using IMUs sensors. Hence, studies focused on gait analysis, walking balance, fall detection, anticipatory postural adjustments, and other dynamic tasks such as sit-to-stand and time-up and-go tests have been excluded. In addition, if a study included both gait and balance analysis, only the balance part of the study has been considered. Moreover, studies using inertial sensors found in smartphones

or others devices for personal use were excluded. At the end, twenty studies, dated from 2011 to 2022, regarding the validation of IMU-based evaluations against the gold standard were chosen.

The next step was to organize the information related to the type of instrumentation used, the type of experimental protocols and tasks carried out, the number and state of health of the subjects analyzed. A summary of this main characteristics of the articles included is reported in Table 2.1.

Article	Partecipants	Strumentation	Sensor Placement	Test condition
Kutilek et al. [61]	9 VS patients	-Xbus Master IMU (100Hz) -Synapsis posturography system	L2-L3	Double stance (EO/EC) Surface: firm and foam 60 s
Sun et al. [43]	39 MS 15 healthy	-BioStamp MC10 (50 Hz) -BERTEC force plate 4060-05-PT-1000	L5	Double stance (EO/EC) Surface: firm and foam 30 s
Alessandrini et al. [62]	13 UVB	-IMU Captiks Movit (50 Hz) -EDM Euroclinic force plate	L5	Double stance (EO/EC) Surface: firm and foam 60 s
Doherty et al. [63]	15 with concussion 15 healthy	-IMU Shimmer 3 (102.4 Hz) -AMTI force plate	L3-L5	Double stance (EO) Single or tandem stance (EO) 20 s
Kim et al. [64]	elderly and athletes	-IMU (50 Hz) -TekScan Inc	S2	Single stance (EO) 30 s
Melecky et al.	10 DCA 11 healthy	-XSens MTx IMU (100 Hz) -Synapsis posturographic system	L2-L3	Double stance (EO/EC) Surface: firm and foam 60 s
Hejda et al. [66]	10 DCA 11 healthy	-Xsens MTx IMU(100 Hz) -Synapsis posturographic system	L2-L3	Double stance (EO/EC) Surface: firm and foam 60 s
Neville et al. [67]	10 healthy	-Motion Intelligence IMU (250 Hz) -Kistler 9287 force plate -12 camera VICON 512 motion capture system	L5	Double stance (EO/EC) Tandem stance (EO/EC) Surface: firm and foam 30 s
Halicka' et al. [68]	20 healthy	- two 2-D ADXL203 (100 Hz) accelerometers -force platform	L5, Th4	Double stance (EO) Surface: firm and foam 50s
Heebner et al. [69]	23 healthy controls	-3D accelerometer (1000 Hz) -force platform	L5	Double stance (EO/EC) Single stance (EO/EC) Tandem stance (EO/EC) Surface: firm and foam 30s
Hsieh et al. [70]	30 elderly	-XSens Mtx IMU (100 Hz) -Synapsys posturographic system	L2-L3	Double stance (EO/EC) Surface: firm and foam 60 s
Mancini et al. [44]	30 PD 29 healthy	-XSens Mtx IMU (50 Hz) -AMTI OR6-6 force plate	L5	Double stance 2 minutes (EO)
Mancini et al. [71]	13 PD 12 healthy	-XSens Mtx IMU (100 Hz) -AMTI OR6-6 force plate	L5	Double stance (EO/EC) 40 s
Mancini et al. [72]	13 with PD 12 healthy	XSens Mtx IMU (50 Hz) -AMTI OR6-6 force plate	L5	Double stance (EO) 30 s
Rouis et al. [73]	15 healthy	-3D accelerometer (50 Hz) -AMTI force platform	L5	Double stance (EO/EC) 30 s
Whitney et al. [74]	81 healthy	-2D ADXL213AF accelerometer (100 Hz) -EquiTest machine	pelvis	SOS test Surface: firm and foam
Frames et al. [75]	7 healthy	-IMU -force platform	lower back	Double stance (EO) Surface: firm and inclined 90 s
Najafi et al. [5]	17 DPN 21 healthy	-2 BalanSens Biosensics IMU -Emed-x system force plate	lower back, shin	Double stance (EO/EC) Surface: firm and foam 30 s
Noamani et al. [39]	10 healthy	-4 MTws Xsens IMUs (100 Hz) -AMTI force plate	Foot,tibia, sacrum, sternum	Double stance (EO) 2 minutes

Table 2.1: Summary of the main characteristics of the articles included in the current study. VS=Vestibular Schwannoma; MS=Multiple Sclerosis; UVB=Unilateral Vestibular Failure; DCA=Degenerative Cerebellar Ataxia; PD=Parkinson's Disease; DPN=Diabetic Peripheral Neuropathy; SOT=Sensory Organization Test; EO=Eyes open; EC=Eyes Closed.

This first step of the study has been done to define and justify the data collection and data processing methods used in the current research.

2.2 Experimental protocol

The aim of this study was to establish if it is possible to derive the information provided from a traditional posturographic analysis, therefore exploiting most often a force platform, using an inertial sensor as an alternative. For this purpose, a specific measurement protocol was drawn up aimed at the acquisition of synchronized signals between the force plate and the inertial sensor on healthy subjects, of different sex and anthropometric characteristics, during static posturographic tests.

Following, the choice of the subjects involved in the current study, the experimental set-up and finally the acquisition protocol are described in detail.

2.2.1 Examined subjects

For this investigation, a total of 17 healthy subjects, of different sexes and anthropometric characteristics, aged between 23 and 63, were involved. Partecipants were recruited at the Santo Stefano Institute in Porto Potenza Picena. To be subjected to the test, all subjects were required to be free from injury at the time of testing and from neurological or orthopedic pathologies that could impact on postural stability. All subjects gave written informed consent prior to participation in the study.

The anthropometric characteristics and age are shown in Table 2.2.

	Weight	Height	Age	COM-Ankle Distance	Gender
Subject 1	81 Kg	1.76 m	38	94 cm	Male
Subject 2	95 Kg	1.80 m	38	89 cm	Male
Subject 3	46 Kg	1.61 m	32	91 cm	Female
Subject 4	52 Kg	1.60 m	25	88 cm	Female
Subject 5	48 Kg	1.58 m	25	87 cm	Female
Subject 6	65 Kg	1.78 m	34	94 cm	Male
Subject 7	46 Kg	1.61 m	32	91 cm	Female
Subject 8	95 Kg	1.80 m	38	89 cm	Male
Subject 9	82 Kg	1.79 m	33	96 cm	Male
Subject 10	60 Kg	1.68 m	23	90 cm	Female
Subject 11	48 Kg	1.58 m	25	87 cm	Female
Subject 12	74 Kg	1.78 m	34	94 cm	Male
Subject 13	65 Kg	1.78 m	34	94 cm	Male
Subject 14	52 Kg	1.68 m	29	91 cm	Female
Subject 15	44 Kg	1.60 m	54	85 cm	Female
Subject 16	69 Kg	1.60 m	63	84 cm	Female
Subject 17	81 Kg	1.76 m	38	94 cm	Male

Table 2.2: Data of subjects included in the study.

In the table the *COM-ankle distance* represents a fundamental parameter to determine, following, the displacement of the centre of mass, since it represents the length of the inverted pendulum model used to analyze the control of posture. This distance corresponds to the distance between the ankle joint and the subject's COM position, which is considered as the point in the lumbar area where the sensor was placed. Before starting each battery of motor tasks done by a subject, the COM-ankle distance was measured for each individual as shown in the Figure 2.1. It is of

significant importance to be careful in measuring this distance because an incorrect or inaccurate value of such measure can distort the performed test.

Figure 2.1: The figure shows the procedure done for taking the measurement of the *COM-ankle distance* for each subject involved in the study.

2.2.2 Description of the measurement set-up

Laboratory set-up

The acquisition system consists of three different parts: a force platform, an inertial measurement unit and a force sensing resistor sensor for the synchronization of the inertial sensor data with the one acquired by the force plate.

1. Force-Sensing Resistor (FSR) sensor:
FSR sensor is a device that allow measuring static and dynamic forces applied to a contact surface [76]. It is made of a conductive polymer which exhibits the unique property of changing its electric resistance based on the force applied to its surface. In general, when unloaded, the sensor has a high resistance that drops as a force is applied and the more force applied to the surface of the sensor, the lower the resistance. Thus, the resistance change is inversely proportional to the applied force, as shown in Figure 2.2.

The FSR sensors are generally supplied as a polymer sheet or ink that is applied as screen printing. In this sensing film, there are electrically conducting and non-conducting particles, generally of sub-micrometer sizes. When a force is applied to the surface of the sensing film, then the particles touch the conducting electrodes and thus the resistance of the film changes. Typical FSR sensors are shown in the following Figure 2.3.

In this study, the FSR sensor was positioned above the inertial sensor fixed on the velcro belt worn by the tested subject, as shown in Figure 2.4. This was done to allow the simultaneous recording of the acquisitions between the force plate and

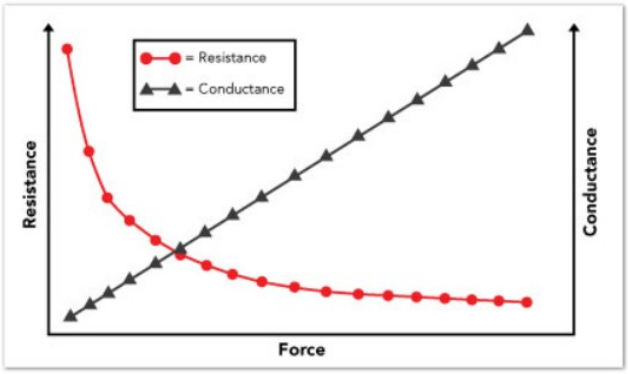

Figure 2.2: The resistance change is inversely proportional to the applied force. The conductance (i.e., inverse of resistance) response as a function of force is linear within the sensor's designated force range [77].

Figure 2.3: Force Sensing Resistor (FSR) sensors.

the IMU sensor. Indeed, the force plate and the inertial measurement unit recorded data independently, thus, a physical event was required to synchronize the two systems. This physical event was achieved by instructing a person to tap the FSR sensor three consecutive times with the finger before starting the execution of each task from the subject. The synchronizing event resulted in large acceleration spikes on the inertial sensor, which were used to achieve the synchronization of the IMU's data with the one acquired by the force platform. The synchronization between the data of the two systens was not carried out in real-time during the acquisitions but in the post-processing phase using as software MATLAB, as described in the next section. The FSR sampling frequency used in the study was 1000 Hz.

Figure 2.4: The figure illustrates the position of the force sensing resistor sensor.

2. A 6-axis AMTI force platform:
To collect the center of pressure data, a six-axis AMTI force plate (AMTI OR6-7-2000; Advanced Mechanical Technology Inc.) (Figure 2.5) was used. The platform measures the three orthogonal force components along the X, Y and Z axes and the moments around the three axes, producing a total of six outputs. To measure forces and moments, the OR6-7 force platform uses strain gauges mounted on four precision strain elements. The technical characteristics of the OR6-7 model biomechanics force platform used are summarized in Table 2.3. The force plate data collection sampling frequency used in the study was 1000 Hz.

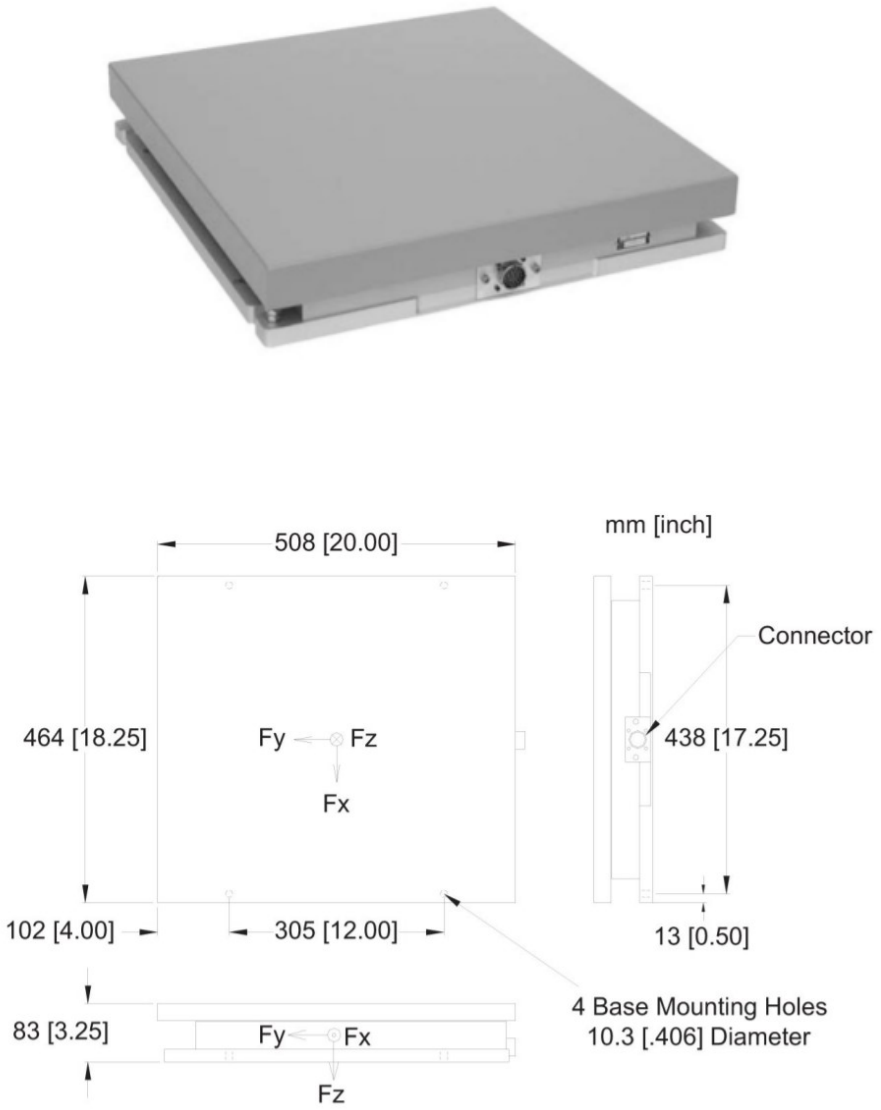

Figure 2.5: The figure shows the layout of the force platform used in the current study (i.e., AMTI OR6-7-2000 model).

OR6-7 -2000 Force platform specifications	
Fx, Fy Capacity (N)	4450
Fz Capacity (N)	8900
Mx, My Capacity (Nm)	2300
Mz Capacity (Nm)	1100
Fx, Fy Natural Frequency (Hz)	370
Fz Natural Frequency (Hz)	530
Fx, Fy Sensitivity ($\mu V/[V * N]$)	0.34
Fz Sensitivity ($\mu V/[V * N]$)	0.08
Mx, My Sensitivity ($\mu V/[V * Nm]$)	0.79
Mz Sensitivity ($\mu V/[V * Nm]$)	1.69
Height (mm)	82.5
Weight (Kg)	32
Top Plate Material	Alluminium

Table 2.3: Technical characteristics of the OR6-7 model biomechanics force platform.

2. Inertial measurement unit: the next generation IMU sensor
The Next Generation IMU (NGIMU) is a compact inertial measurement unit and data acquisition platform that combines on-board sensors and data processing algorithms with a broad range of communication interfaces to create a versatile platform well suited to both real-time and data-logging applications [78]. The structure of this sensor is shown in Figure 2.6.

Figure 2.6: External structure of next generation IMU sensor used in the current study [78].

The on-board sensors included in the NGIMU device are a triple-axis gyroscope, a triaxial accelerometer, and a triple-axis magnetometer, as well as a barometric pressure sensor and a humidity sensor. Their technical specifications are summarized in Table 2.4. The on-board sensor fusion algorithm, on the other hand, is the Attitude and Heading Reference System (AHRS), which is an orientation filter, implemented directly in the microprocessor of the device, used to provide a single estimate of the orientation of a body through the fusion of the measurements taken by the gyroscope, accelerometer and magnetometer. Indeed, combining inertial and magnetic measurements, the AHRS sensor algorithm is able to provide a drift-free measurement of orientation relative to the Earth [78]. This is because, the drift due to the gyroscope is compensated by two vectors of reference, the gravity

SENSORS		
Gyroscope	Range: Sample rate: Resolution:	2000°/s 400 Hz 16 bit
Accelerometer	Range: Sample rate: Resolution:	16 g 400 Hz 16 bit
Magnetometer	Range: Sample rate: Resolution:	1300 uT 20 Hz 0.3 uT
Pressure	Range: Sample rate: Resolution:	300-1100 hPa 25 Hz 24 bit
Humidity	Range: Sample rate: Resolution:	0-100 % 25 Hz 0.008 %

Table 2.4: Technical specifications of on-board sensors included in the NGIMU device [78].

AHRS algorithm	
Outputs	Quaternion Rotation matrix
Update rate	400 Hz
Static accuracy (Pitch/ Roll)	<1° RMS
Static accuracy (heading)	<2° RMS

Table 2.5: Technical specifications of AHRS sensor fusion algorithm included in the NGIMU device [78].

(provided by the accelerometer) and the earth's magnetic field (acquired through the magnetometer). The technical specifications of AHRS algorithm are reported in Table 2.5. The internal hardware structure of the device is depicted in Figure 2.7. The device takes advantage of a real-time communication via USB, serial, Wi-Fi but it also has a micro-SD card that allows to save the data acquired during the tests. In the current study, the communication used was the wireless one, connecting the device to a personal computer used then for the processing of the data. As shown in Table 2.4, the sample frequency of the sensors (i.e., gyroscope, accelerometer, magnetometer) included in the device were 400 Hz, for the present work before the acquisition session it was set to 200 Hz for each sensor.

The kinematic data of the sensor were captured through a set of three retro-reflective passive markers, positioned on the sensor as shown in Figure 2.8, and an infrared 6-chamber optoelectronic system (Vicon, Oxford Metrics Ltd, Oxford, UK) sampled at 100 Hz.

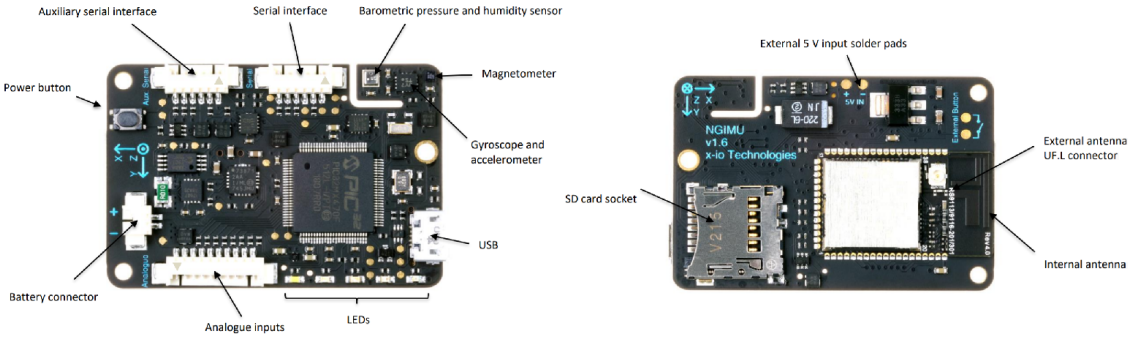

Figure 2.7: Internal structure of NGIMU sensor: top view of board on the left, bottom view of board on the right [78].

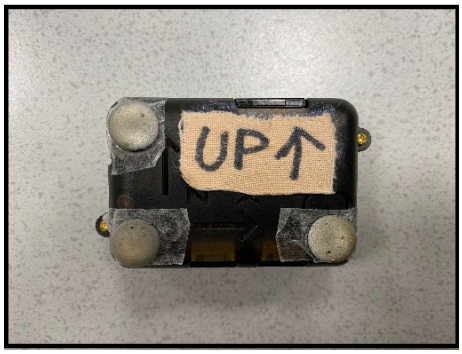

Figure 2.8: Three retro-reflective passive markers positioned on the sensor for the acquisition of the sensor displacement.

Subject set-up

The sensor was positioned posteriorly on the subject's trunk, in the lumbar region L4-L5, taking the subject's iliac crests as anatomical reference, in order that the sensor was placed near the center of mass of the subject. This is the most common sensor location used in the vast majority of IMU-based evaluations for static posturography [6]. A snug elastic velcro band was used to wear the sensor from each subject, as shown in Figure 2.9. Before starting the motor task session, the subject wearing the sensor positioned himself/herself with the feet at the width of the shoulders inside the platform, standing upright (Figure 2.10). A visual target (image) was placed at a distance of about 4 meters and fixed at a height of about 1.70 m to minimize the influence from the environment during the open eye tests and avoid any artifacts due to the alteration of the head position.

2.2.3 Acquisition protocol procedure

For carrying out the standing balance tests and data acquisition, the Movement and Posture Analysis Laboratory (L.A.M.Po) of the Santo Stefano Institute was used. After the initial calibration of the instrumentation, the acquisition session was started. At the beginning of each acquisition, the inertial sensor was positioned on the subject's back and the COM-ankle distance was measured as shown previously in Figure 2.1. Then, the subject was invited to get on the platform wearing his/her own socks, to assume the position indicated by the considered motor task and to remain

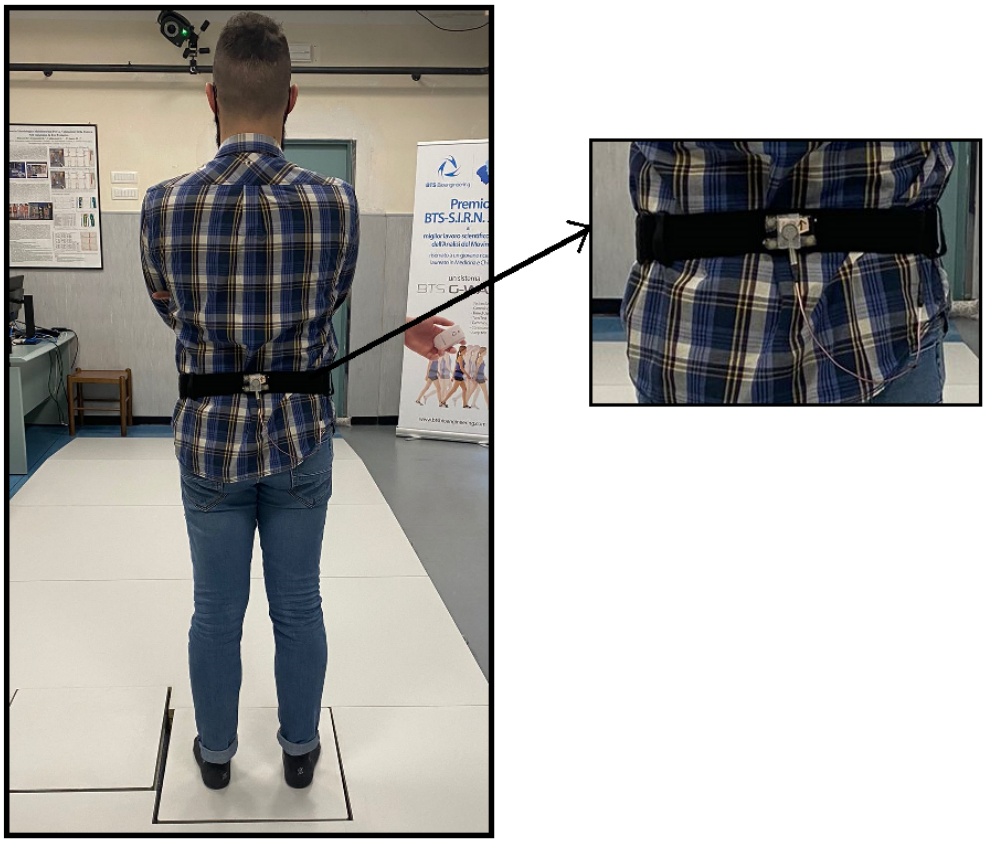

Figure 2.9: Sensor position on the subject's trunk in the lumbar region L4-L5.

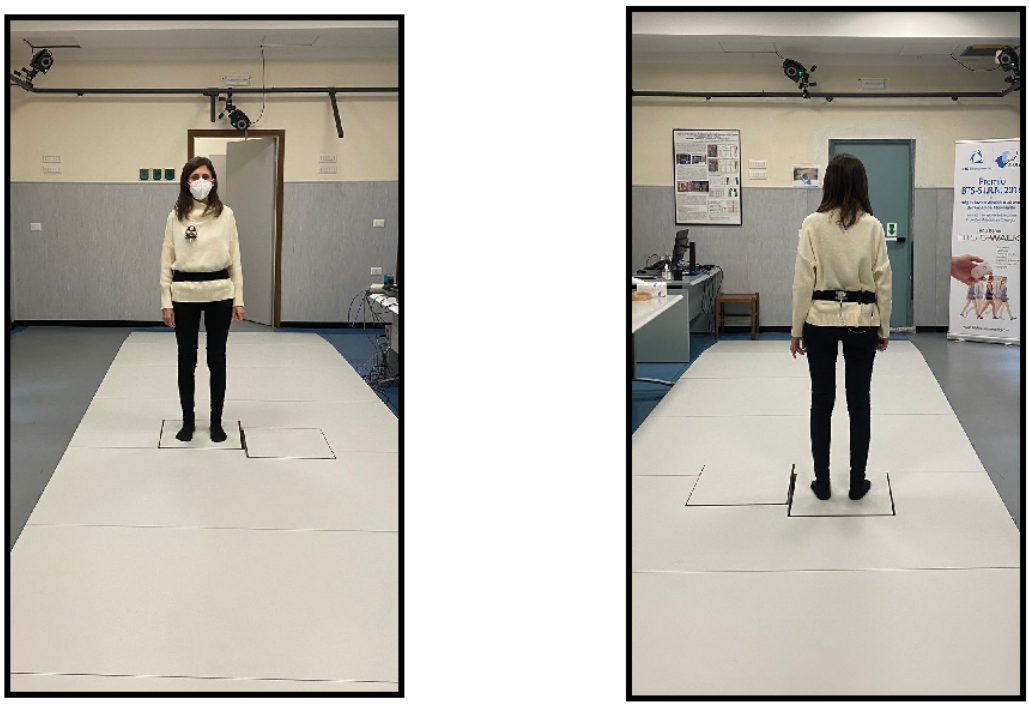

Figure 2.10: The figure shows the subject set-up.

silent. The data acquisitions of the platform and inertial sensor was started and the operator tapped three consecutive times the FSR sensor to create the physical event necessary for the synchronization of the two systems. After the synchronization, the subject executed the motor task. Before ending the acquisition, the operator hit again three times the FSR sensor to mark the end of the recording in the data of both the acquisition systems. Before proceeding with a new acquisition, a few seconds was waited before starting the test to limit fatigue phenomena.The instructions were provided by the same operator for all tests, furthermore, movements and noises in the laboratory room were limited so as to not interfere with the instrumentation and distract the subject. The procedure defined for the acquisition protocol can be summarized in four main phases, described in detail following:

1. Laboratory calibration

At the beginning of the measurement session, a calibration of the optoelectronic system was carried out to define the global laboratory reference system and set to zero the force platform. The calibration procedure was performed in two phases: a static phase in which a rigid calibration wand was placed flat on the floor to identify the origin coordinates and axes of the global reference system, and a dynamic phase, in which the wand was moved throughout the empty measurement volume in which the cameras were concentrated, ensuring that the markers on the wand were visible to the cameras and allowing each camera to record the wand in several orientations. Following, also the inertial sensor calibration was done using the NGIMU GUI, which has a section (Figure 2.11) allowing to see in real-time the movements of the sensor to check if the perceived orientation from the interface is the actual one of the sensor. Thus, before using the sensor for the acquisition, the latter connected to the GUI was calibrated as follows:

1. the inertial sensor was kept still on the table;
2. the AHRS initialise command in the interface was used to reinitialise the AHRS algorithm;
3. the correctness of the calibration was verified by rotating the sensor in each direction while checking that its representation in the interface is moving in the same direction.

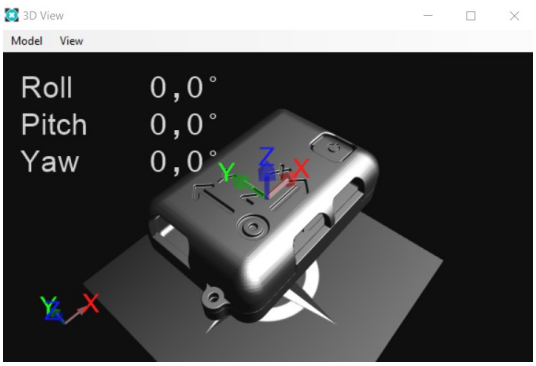

Figure 2.11: NGIMU GUI interface used to verify initial inertal sensor calibration.

2. Alignment of the sensor's and laboratory's global reference systems

In this second phase of the procedure, the inertial sensor was placed at the extremity of the force platform in order to align the IMU's reference system with the global laboratory reference system, as shown in the following representative schematization (Figure 2.12). After that an acquisition of 60 seconds was performed in order to identify the initial offset.

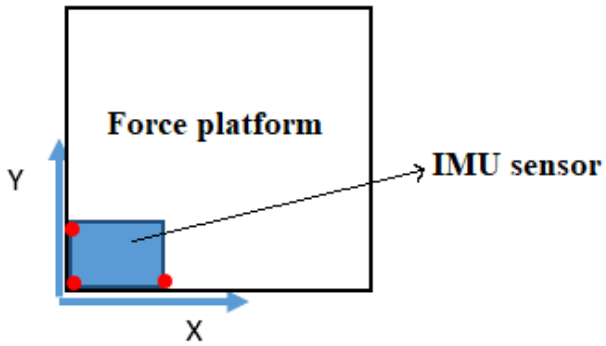

Figure 2.12: The figure shows how the sensor was positioned to align its reference system to the global one of the laboratory. The blue rectangle represents the inertial sensor placed on the force plate, while the red circles fixed on it represent the three markers used to capture the kinematic data of the device.

3. Synchronization of the inertial sensor with the force platform

As described before, at the beginning of each task performed by the subjects 3 taps were given on the force-sensing resistor sensor, positioned on the inertial sensor, so that both devices were able to read three perturbations to be synchronized and allow the simultaneous recording of the acquisitions between the IMU and the force platform.

4. Execution of the tasks by each subject included in the study.

Eight different motor tasks were performed for each subject in different equilibrium conditions so as to establish if the inertial sensor was able to distinguish between the different conditions as it is already possible to do with the force platform. The tests included two modes of vision (i.e., closed and open eyes), since in this way it is also possible to estimate the role of the visual system in maintaining balance. Also, data collection was divided into single- and double-legged stance categories. Indeed, also standing on one leg is a posture used in daily life, such as employed walking normally, when navigating stairs, and stepping over obstacles. In addition, people are most likely to fall due to a shift in the center of gravity while standing on one leg. During the double stance data collection phase, two different position of the feet on the support surface were considered, since it is widely recognized that it heavily influences the postural sway because it modifies the base of support. Each task had a duration of 30 s. The tasks were performed in the absence of environmental

noise and external perturbations. The battery of tasks performed by each subject included the trials listed below:

- TASK 1: **Double stance eyes open with an enlarged base**, in which the subject places his/her feet parallel in a comfortable position with arms crossed, staring at the image positioned in front of him/her.
- TASK 2: **Double stance eyes closed with widened base**, in which the subject places the feet parallel in a comfortable position with arms crossed and with closed-eyes.
- TASK 3: **Double stance open eyes with a narrow base**, in which the subject stands with his/her feet joint together, the arms crossed, staring at the image positioned in front of him/her.
- TASK 4: **Double stance eyes closed with a narrow base**, in which the subject stands with the eyes closed, with feet joint together and the arms crossed.
- TASK 5: **Single stance eyes open dominant limb**, in which the subject remains standing on the single dominant limb. The arms are kept at his/her sides and the eyes look straight ahead staring at the image.
- TASK 6: **Single stance eyes closed dominant limb**, in which the subject remains standing on the single dominant limb with his/her eyes closed and the arms at the sides.
- TASK 7: **Single stance eyes open non-dominant limb**, in which the subject remains standing on the single non-dominant limb. The arms are kept at his/her sides and the eyes look straight ahead staring at the image.
- TASK 8: **Single stance eyes closed non-dominant limb**, in which the subject remains standing on the single non-dominant limb with his/her eyes closed and the arms at the sides.

2.3 Description of standing balance data analysis algorithm

In this section the analysis algorithm implemented to process and validate the NGIMU-based data against the reference force plate will be explained in detail. The code will be illustrated following the subsequent organization:

1. Acquisition step;
2. IMU-data processing phase;
3. Force plate-data processing phase;
4. Synchronization of the inertial sensor with the force plate data;
5. Comparison of inertial sensor against force plate data.

All the following steps and procedures described were coded in a MATLAB programming environment.

2.3.1 Acquisition step

The dataset includes the signals acquired on a total of 17 subjects submitted to the standing balance tests. Thus, it was organised in 17 folders containing the raw data obtained after the acquisition session. Each folder, identified by 'Subjectx' (where x=01,02...17 indicates the subject's identification number), includes two sub-folders, one with the data acquired through the inertial sensor (i.e., Subjectx-Inertial.csv and Subjectx-quaternion.csv files) and one with the data acquired from the force plate and FSR sensor (i.e., Subjectx.txt file). Tha data collected by the inertial sensor were the following:

- Acceleration measured by the accelerometer;
- Angular velocity measured by the gyroscope;
- Magnetic field measured by the magnetometer;
- The quaternions identifying the orientation of the sensor system with respect to its global reference system, i.e. the earth reference system, for all the entire duration of the test done by the subject. These are provided directly as outputs by the NGIMU, thanks to the AHRS fusion algorithm, which combines the information obtained by accelerometer, gyroscope and magnetometer.

The first phase of the algorithm deals with loading for each subject these files as input.

2.3.2 IMU-data processing phase

To make the data estimated from the NGIMU comparable with those of the force platform it was necessary that both were expressed with respect to a single global reference system. Thus, starting from the raw data of the on-board sensors of NGIMU (i.e., the three components of the angular velocity, acceleration and magnitude of the magnetic field on the x, y, z axes of the gyroscope, accelerometer and magnetometer respectively) and the quaternions obtained during the execution of the subject's task, and also from the raw data obtained from the inertial sensor placed on the surface of the force plate during the alignment phase (i.e., alignment phase of the sensor's and laboratory's global reference system described in the previous section), an orientation filter was implemented. In this way, it was possible to provide the orientation of the sensor with respect to its initial position, in terms of Euler angles, i.e. Yaw, Pitch and Roll angles. Such representation represents the actual orientation of the subjects with respect to the initial fixed global frame as the simple composition of three elementary rotations. Following, also the values of the accelerations measured by the triple-axis accelerometer were reported in the initial reference system of the sensor and the static acceleration due to gravity, removing the mean value, was eliminated obtaining only dynamic acceleration.

After these initial steps of alignment, it was possible to compute the displacement and the position of the center of mass, both A/P and M/L. Supposing the subject modeled as inverted pendulum to describe the oscillations performed by the body to maintain balance in the upright position (see subsection 1.1.2 for further information), the estimate of the displacement of the center of mass, in the

anterior-posterior direction, was derived from the following equation:

$$COM_{AP} = d \cdot sin\theta\,, \tag{2.1}$$

where θ is the A/P oscillation angle of the body and d is the distance between the COM and the ankle of each subject. Assuming that the inertial sensor was placed on the individual's COM, it was possible to approximate the oscillation angle, θ, to the Roll angle, θ_{Roll}, measured by the device and, hence, estimate the anterior-posterior displacement of the COM as:

$$COM_{AP} = d \cdot sin\theta_{Roll}\,. \tag{2.2}$$

To obtain the displacement for the entire duration of execution of a task, at each sampling instant, the angular increase of the Roll angle was obtained and subsequently, through the above formula, the increase in the position of the COM in A/P direction was evaluated. Then, the total displacement of the A/P component of the center of mass was obtained from the sum of all the position increments. The medial-lateral displacement of the center of mass, COM_{ML} was calculated using the Pitch angle ϕ_{pitch} :

$$COM_{ML} = d \cdot sin\phi_{pitch}\,. \tag{2.3}$$

Also in this case, to obtain the displacement for the entire task's duration, the angular increase of the Pitch angle, at each sampling instant, was derived and, using the previous formula and summing all the position increments of the COM in the M/L direction, its total medial-lateral displacement was obtained. The raw anterior-posterior and medial-lateral displacements were filtered with a zero lag fourth order Butterworth filter with a cut-off frequency of 1 Hz.

The A/P and M/L displacements of the center of pressure were instead computed from the acceleration of the COM taking advantage of the relation linking the difference between the position of the COM and COP and the acceleration of the center of mass a_{COM}:

$$COP = COM - \frac{d}{g} \cdot a_{COM}\,, \tag{2.4}$$

where g is the gravity acceleration and d the COM-ankle distance. Next, the obtained anterior-posterior and medial-lateral COP displacements were filtered with a zero lag fourth order Butterworth filter with a cut-off frequency of 2 Hz.

2.3.3 Force plate-data processing phase

After the acquisition step of the force plate data, the two coordinates of the center of pressure were obtained. The X coordinate represents, in the different sampling instants, the medial-lateral trend of the COP, while the Y coordinate shows the anterior-posterior displacement. To remove the noise affecting the recordings a bidirectional Butterworth filter of order 2 was used in order to filter out the components of the center of pressure. The cut-off frequency of the filter was set to 5 Hz. The COM estimated by the platform is calculated by performing the COP low pass filtering method. For this purpose, a bidirectional Butterworth filter of fourth order with a cut-off frequency of 0.4 Hz applied to the COP coordinates was implemented. Also in this case the X coordinate represents, in the different sampling

instants, the medial-lateral movement of the COM, while the Y coordinate shows the anterior-posterior trend. Finally, the mean was removed from both COM and COP components to eliminate the continuous component of the signals. Moreover, a resampling step was performed. This was done because the sampling frequency of the gyroscope, the magnetometer and the accelerometer in the NGIMU sensor was set to 200 Hz, but the acquisition frequency of the force platform was 1000 Hz. Therefore, to facilitate the subsequent comparison of the results, the data recorded from the force plate, both COP and COM, were resampled at a frequency of 200 Hz, as the inertial sensor.

2.3.4 Synchronization of the inertial sensor with the force plate data

The force plate and the inertial sensor record data independently. Hence, to compare the data obtained from the two measurement system it was necessary to create a specific event to synchronize the recordings. As explained before, this was achieve using a force sensing resistor sensor placed on the IMU worn by the subject and instructing a person to perform three taps at the beginning and the end of each motor task. This resulted in large spikes in the acceleration signal and also visible in the FSR signal. An example of these three perturbations present in the two signals is shown in Figure 2.13, representing the FSR singal and the acceleration signal of a subject involved in the current study. In this section of the algorithm, a

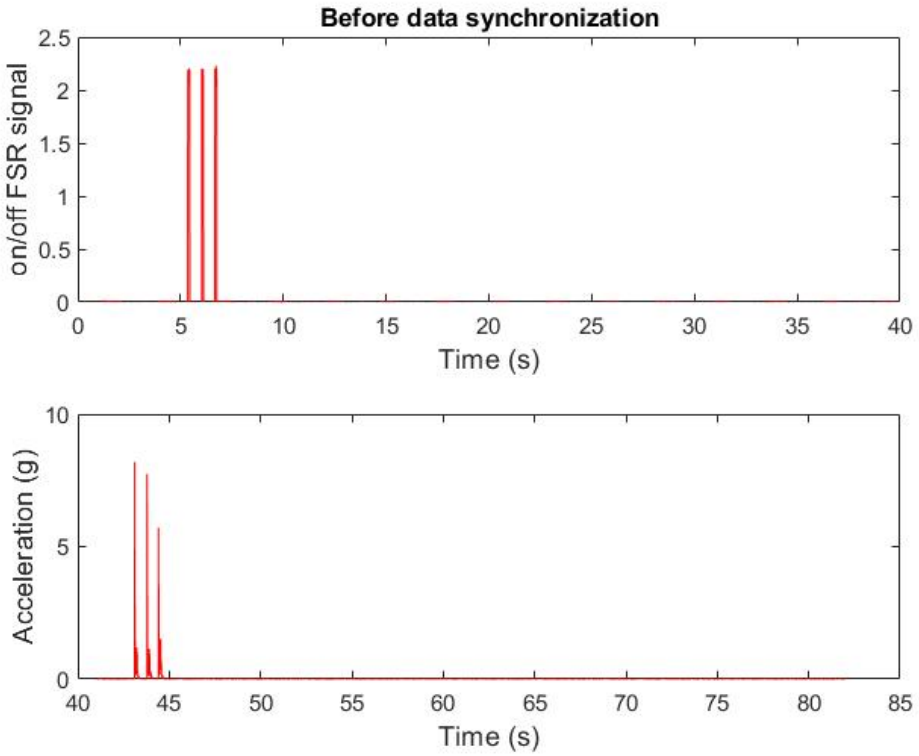

Figure 2.13: The plot is an example of the three perturbations visible in both the FSR signal and the acceleration signal. These signals refers to the Task 1 of Subject 7 involved in the current study.

function capable of automatically synchronizing the third peak present in the two signals was created. This was done by setting, for the acceleration and the FSR data, empirical threshold levels, obtained carrying out an initial visual inspection of the data, on the basis of their static values. In this way, the part of the signals comprised between the two physical events consisting in the start and the end of each motor task was synchronized. An example of synchronization achieved is illustrated in Figure 2.14. Furthermore, since the beginning of the inertial sensor signal could be affected by the adjustment movements of the inertial sensor following the three taps given on the FSR sensor, positioned on the IMU, this has been excluded from the analyses. Thus, all the synchronized data of the force plate and the inertial sensor were further cut in order to select the same 20 central seconds.

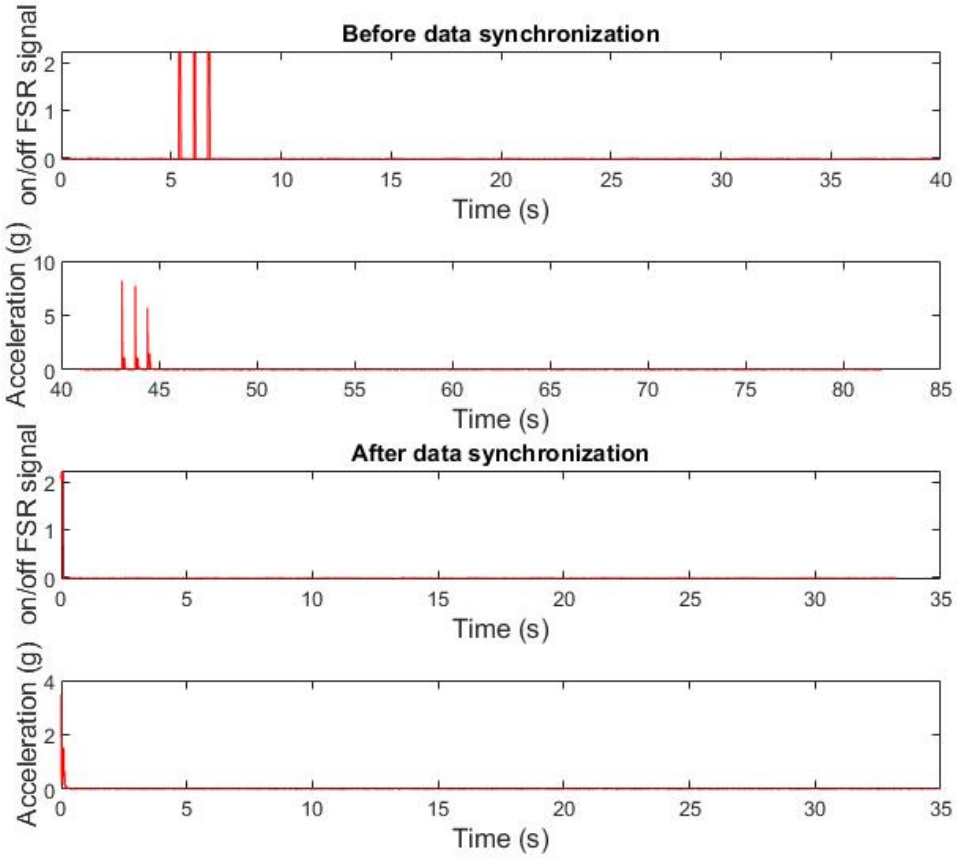

Figure 2.14: The plot is an example of the synchronization obtained between the FSR signal and the acceleration signal. These signals refers to the Task 1 of Subject 7 involved in the current study.

2.3.5 Comparison of inertial sensor against force plate data

This step of the algorithm consists of the final phase of visualization and analysis of the results obtained. The trajectories of the center of pressure obtained from the inertial sensor and the force platform were superimposed to compare their trend. The same was also done for the displacement of the center of mass. In addition,

to quantitatively measure the differences between the displacement of the COM estimated through the inertial sensor and the one obtained from the force plate, assumed as the reference one, the root-mean-square errors (RMSE) or root-mean-square deviations (RMSD) were computed. This was obtained using the following formula:

$$RMSE = \sqrt{\sum_{i=1}^{n} \frac{(\hat{y}_i - y_i)^2}{n}}, \tag{2.5}$$

where $\hat{y}_i$ (with $i = 1...n$) represent the values of the center of mass at each time instant estimated from the inertial sensor, y_i represent the values of the center of mass at a certain time instant obtained from the force plate, and n is the number of samples considered. The same was also computed for the center of pressure, calculating the RMSE between the displacement of the COP obtained from the two measurement systems. Furthermore, to objectively track the similarity of the COP trajectory obtained using the inertial sensor and the one obtained using the force plate, the cross-correlation between them was also computed. Then, also the cross-correlation coefficients of the COM trajectories relative to the two measurement systems were determined. The cross-correlation between these discrete-time sequences to determine how they match up with each other in the different tasks was obtained using the MATLAB function *xcorr*.

Chapter 3

Results

In this work, a comprehensive validation of the accuracy of assessing the dynamics of standing balance via wearable IMUs against gold-standard force platform was performed. This chapter will describe the results obtained from this validation. First, the results relative to the comparison of the trajectories of the center of pressure derived from the two measurement systems, of the 17 subjects submitted to the study, will be presented. Next, also the results relative to the comparison of the displacements of the center of mass will be shown. For both center of pressure and center of mass the root mean square errors and the cross-correlation coefficients, computed between the trajectories obtained from the inertial sensor and the force platform assumed as reference, will be reported. Furthermore, an analysis of the inertial sensor data obtained for the different performed motor tasks was carried out to understand whether IMU-based evaluations can reveal differences between the different positions and the different challenge conditions for the postural control system, assumed by the examined subjects during the tests, as well as force platforms can do. To this end, the results obtained from the statokinesigram plots (i.e., the displacement of the center of pressure in the anterior-posterior direction versus the medial-lateral displacement of the center of pressure) will be described.

Comparison COP trajectories

The recording session was divided into single and double stance trials. The first fourth motor tasks executed from each subject were the one related to the double stance phase, in which the subject was in a less critical situation for the maintenance of balance having both feet as support resting on the ground. The superimposition of the anterior-posterior and medial-lateral displacement of the center of pressure obtained by the force plate and the inertial measurement unit, in these first tasks, has shown that the trajectory of the center of pressure obtained from the processing of the acceleration signals of the inertial sensor generally follows the trend of the oscillation of the force plate-COP. These results can be appreciated in Figures 3.1, 3.2, 3.3, 3.4, and 3.5 reporting the comparison of the A/P and M/L trajectories of the COP in the double stance motor tasks for Subject 4, Subject 7, Subject 8, Subject 10 and, Subject 17, respectively. Similar results, in these four trials, were obtained also for the other subjects involved in the analysis.

Subject 4

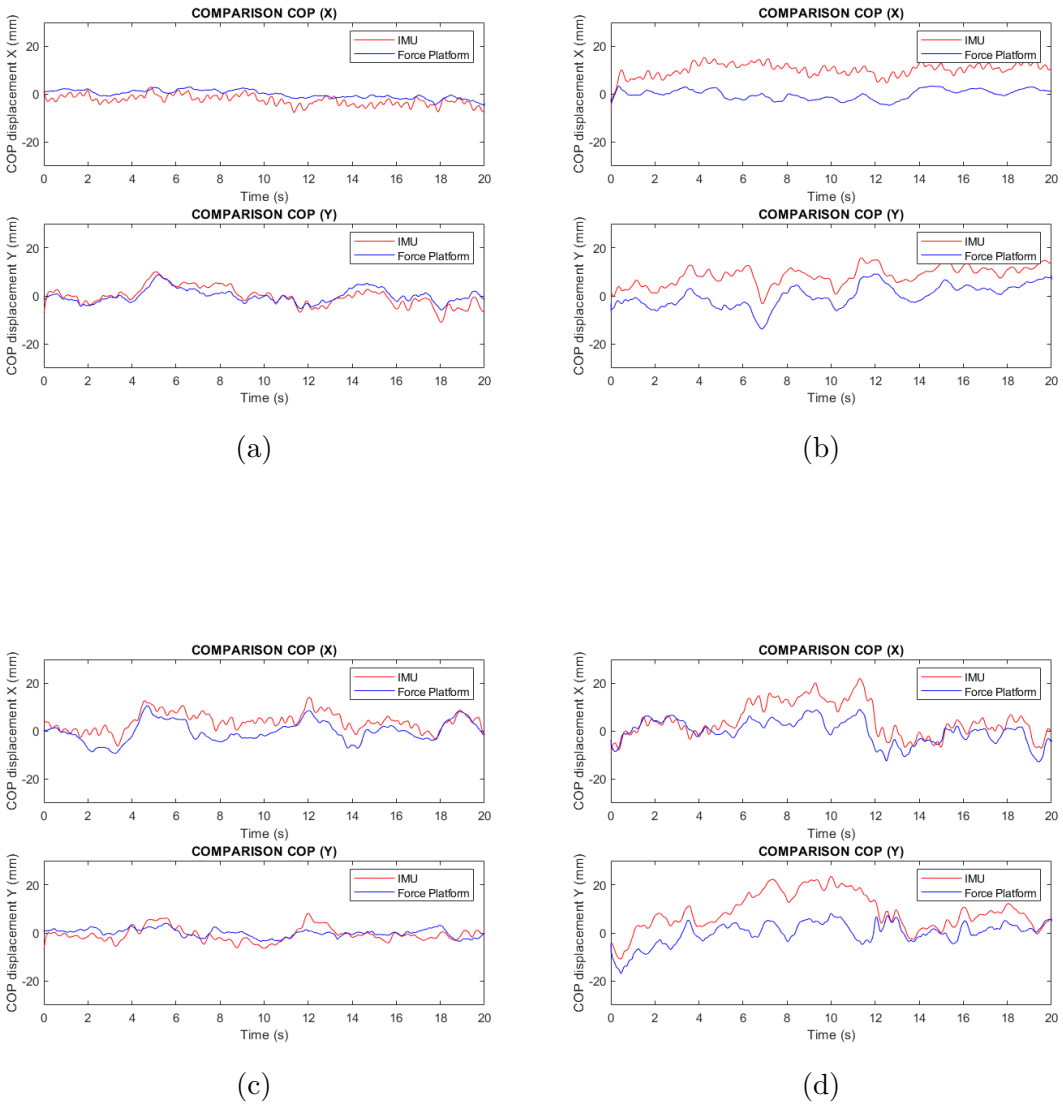

Figure 3.1: Stabilograms representing A/P and M/L time series of the center of pressure displacement for Subject 4: (a) Task 1, (b) Task 2, (c) Task 3, (d) Task 4 of double stance phase. The center of pressure trajectory from the inertial sensor is depicted in red, the force plate-COP is depicted in blue.

Subject 7

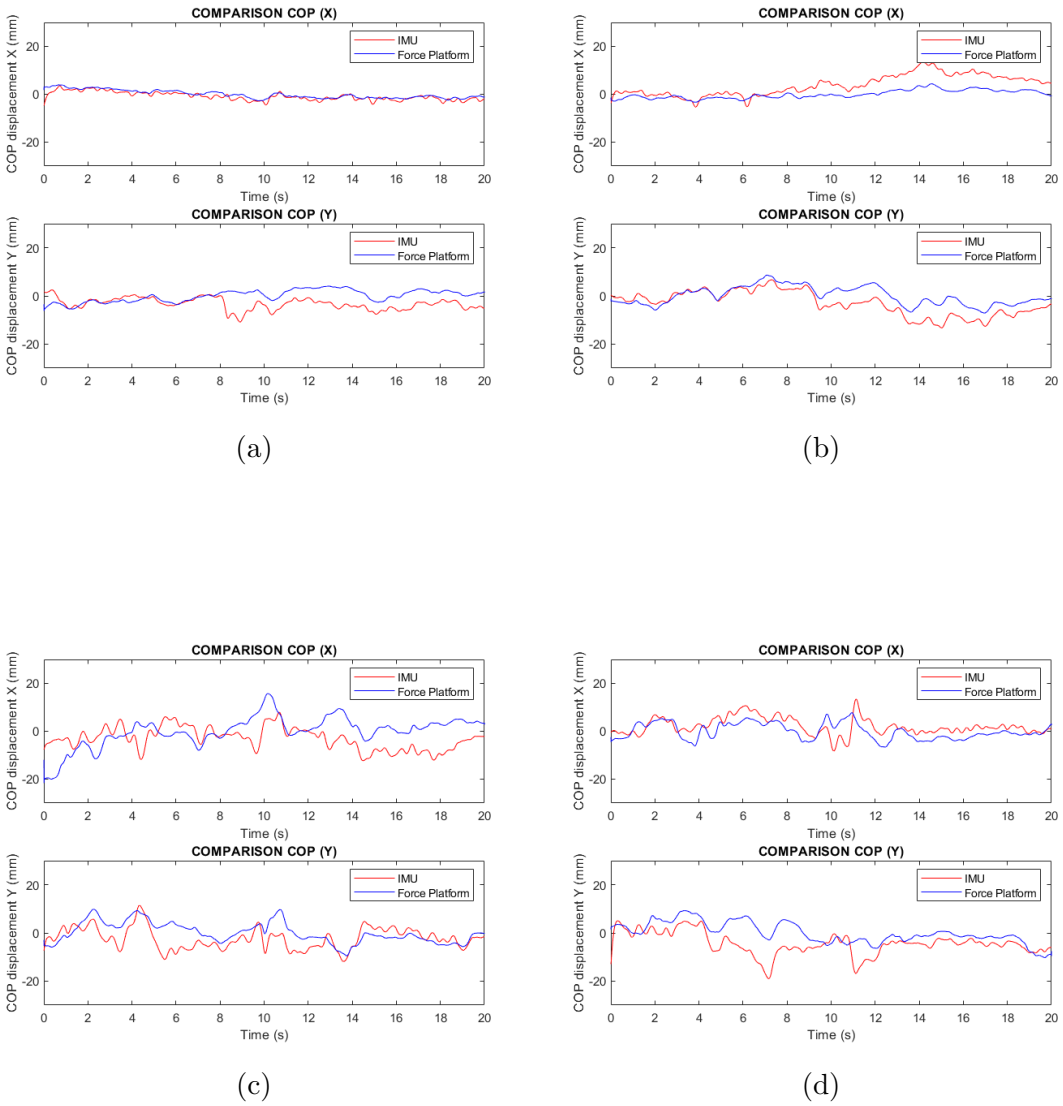

Figure 3.2: Stabilograms representing A/P and M/L time series of the center of pressure displacement for Subject 7: (a) Task 1, (b) Task 2, (c) Task 3, (d) Task 4 of double stance phase. The center of pressure trajectory from the inertial sensor is depicted in red, the force plate-COP is depicted in blue.

Subject 8

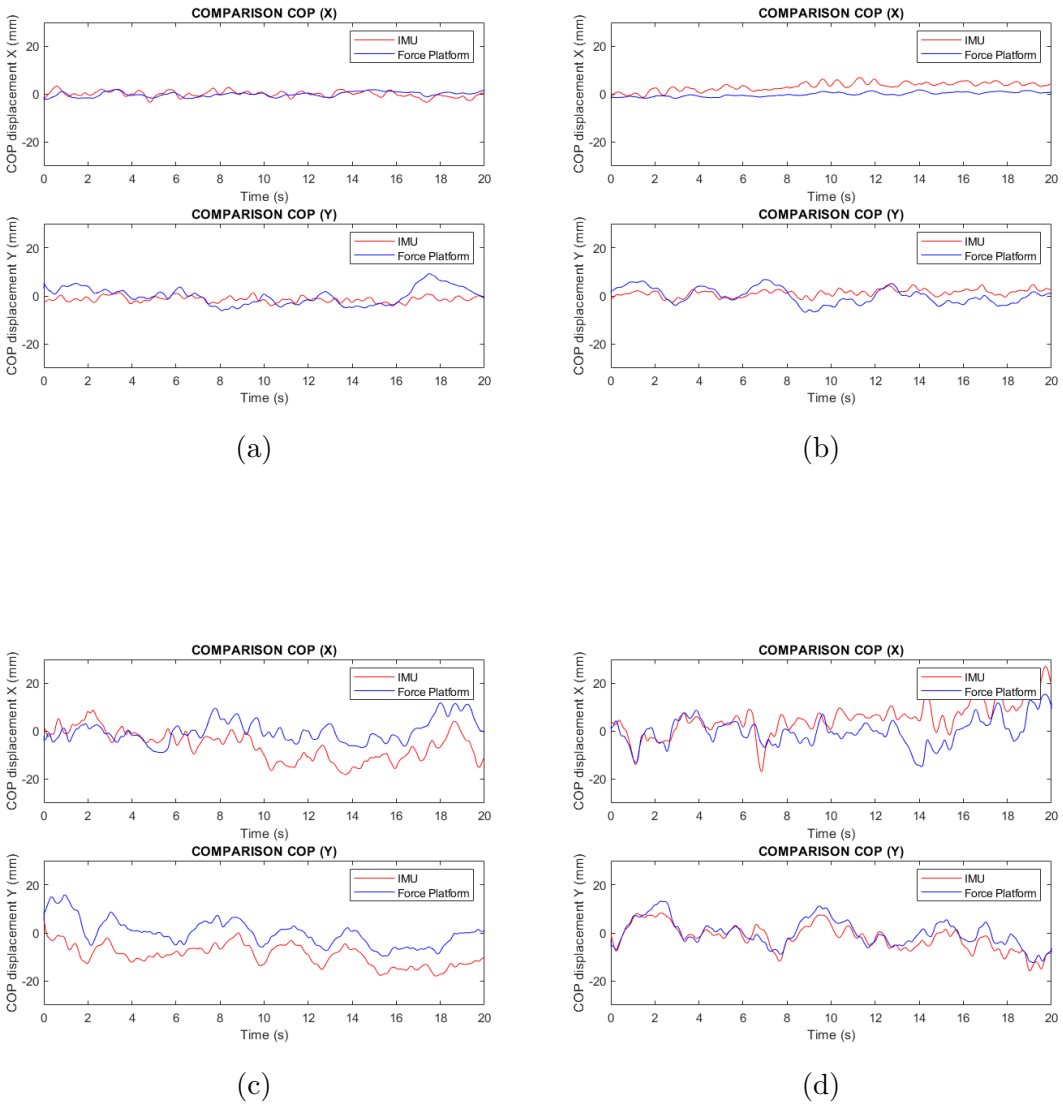

Figure 3.3: Stabilograms representing A/P and M/L time series of the center of pressure displacement for Subject 8: (a) Task 1, (b) Task 2, (c) Task 3, (d) Task 4 of double stance phase. The center of pressure trajectory from the inertial sensor is depicted in red, the force plate-COP is depicted in blue.

Subject 10

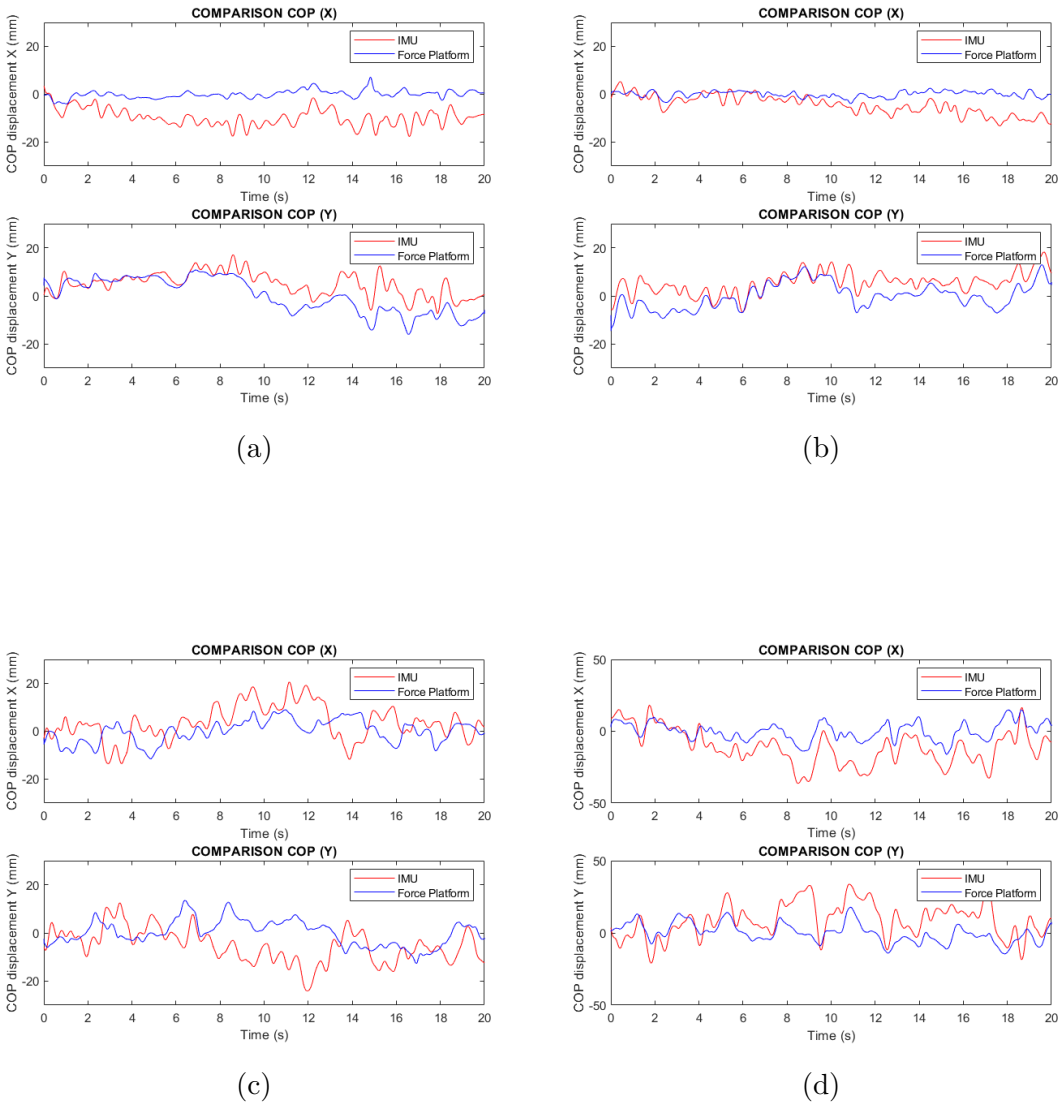

Figure 3.4: Stabilograms representing A/P and M/L time series of the center of pressure displacement for Subject 10: (a) Task 1, (b) Task 2, (c) Task 3, (d) Task 4 of double stance phase. The center of pressure trajectory from the inertial sensor is depicted in red, the force plate-COP is depicted in blue.

Subject 17

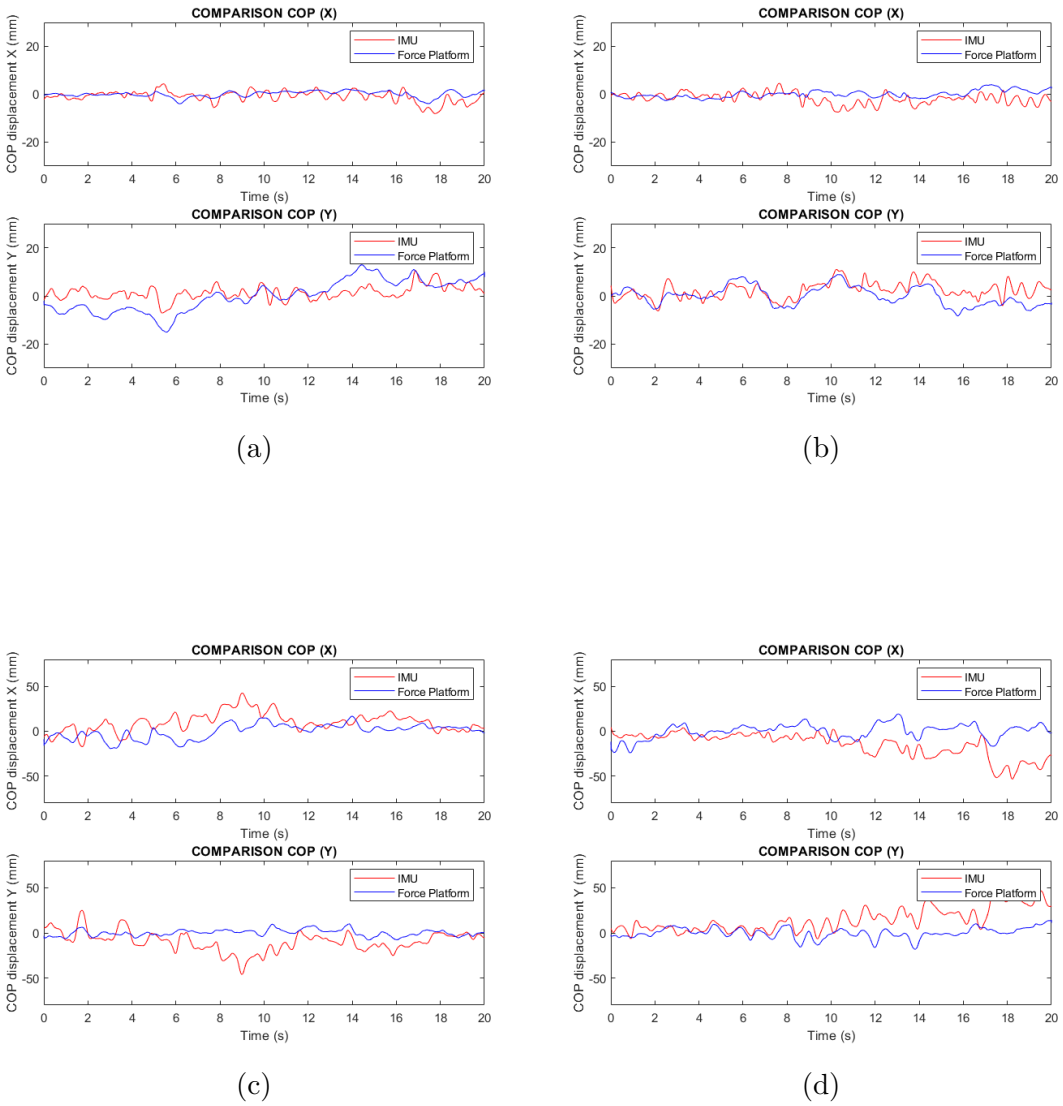

Figure 3.5: Stabilograms representing A/P and M/L time series of the center of pressure displacement for Subject 17: (a) Task 1, (b) Task 2, (c) Task 3, (d) Task 4 of double stance phase. The center of pressure trajectory from the inertial sensor is depicted in red, the force plate-COP is depicted in blue.

However, the comparison of the center of pressure trajectories in the single stance trials did not produce equally good results for all the subjects analyzed. In fact, this second phase of data collection required the subject to support himself/herself only with one foot resting on the ground, but not all the subjects analyzed were able to complete the 30 s of task without repeatedly placing the other foot on the ground. Furthermore, in most cases the subjects losing their balance placed the foot of the swinging leg outside the force platform, making the comparison of the trajectories of the center of pressure obtained from IMU and force plate not possible.

For example, subject 8 was one of those having difficulty performing single stance tests. As can be seen from the trajectories shown in the Figure 3.6, the traces move further away when the subject recovers balance by placing the foot on the ground outside the platform. On the other hand, Subject 14 (Figure 3.7) of the study, for example, was one of those able to carry out these last tasks without placing the second foot outside the force platform to avoid the fall but only trying to recover the balance, when necessary, by placing within the shape of the platform the foot of the raised leg for a few seconds and then raise again it. For this reasons, due to these difficulties in performing the tasks properly, the data of the 17 subjects recorded from these last four motor tasks were discarded from the validation part of the study.

Subject 8

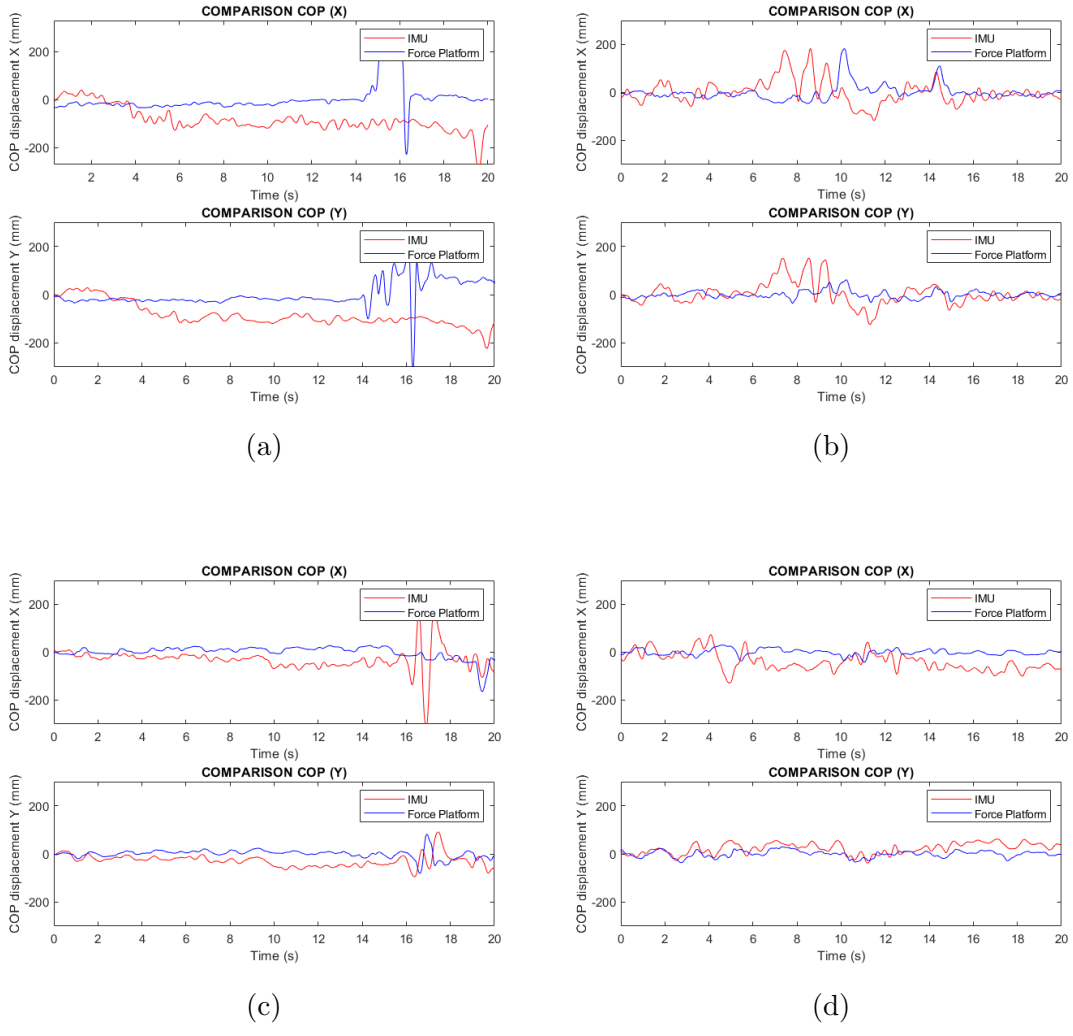

Figure 3.6: Stabilograms representing A/P and M/L time series of the center of pressure displacement for Subject 8: (a) Task 5, (b) Task 6, (c) Task 7, (d) Task 8 of single stance phase. The center of pressure trajectory from the inertial sensor is depicted in red, the force plate-COP is depicted in blue.

Subject 14

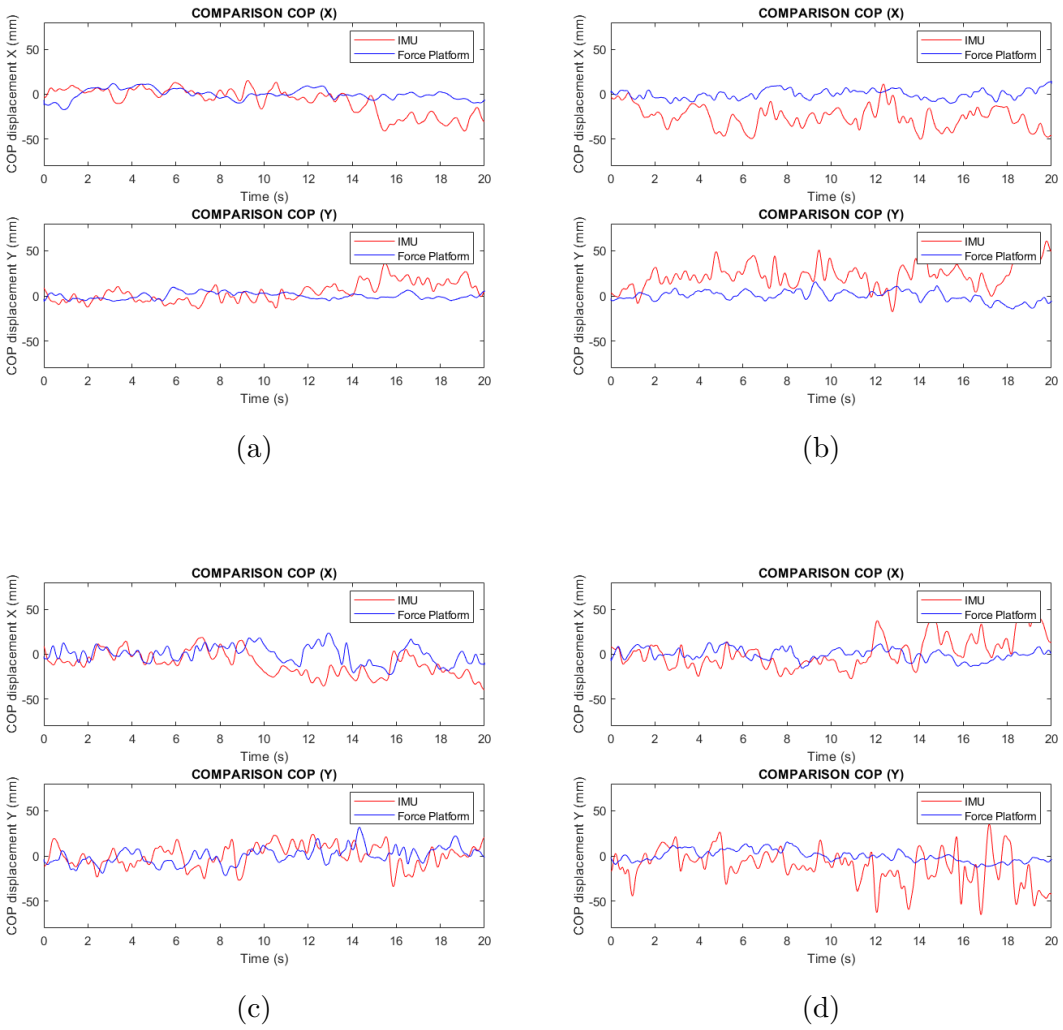

Figure 3.7: Stabilograms representing A/P and M/L time series of the center of pressure displacement for Subject 14: (a) Task 5, (b) Task 6, (c) Task 7, (d) Task 8 of single stance phase. The center of pressure trajectory from the inertial sensor is depicted in red, the force plate-COP is depicted in blue.

Furthermore, to have a quantitative measure of the difference between the displacements of the center of pressure provided by the two analyzed solutions, the root-mean-square errors between them were computed for the tasks involved in the validation of the inertial sensor. The results of this calculation are summarized in Table 3.1. Moreover, to have an objective measure of the similarity of the COP trajectory obtained using the inertial sensor and the one obtained using the force plate, also the cross-correlation between them was computed. For example in Figures 3.8 and 3.9, the cross-correlations obtained for the double stance tasks for Subjects 7 and 17 are reported. The values of the cross-correlation coefficients obtained for the other subjects involved in the study are summarized in Table 3.2.

	Task 1	Task 2	Task 3	Task 4
Subject 1	3.1172	3.2259	15.2430	21.7610
	3.0897	3.6420	14.2421	10.5255
Subject 2	1.7515	2.6561	7.2730	6.5493
	4.8685	4.8342	7.0514	9.3610
Subject 3	1.7712	4.7495	4.1882	5.5501
	2.4980	5.4615	6.5287	5.7608
Subject 4	2.7478	10.6642	4.9026	6.1744
	2.3755	8.8641	2.6791	10.1285
Subject 5	3.5696	3.1984	16.3100	13.7966
	2.6093	2.7347	12.0712	18.4034
Subject 6	3.8417	4.0647	6.2310	8.1151
	3.9244	4.9989	6.1012	7.6067
Subject 7	1.1934	4.6747	8.0958	4.1918
	4.8684	4.4835	5.0927	6.2991
Subject 8	1.3809	3.5078	8.7965	7.8734
	3.6194	3.3385	9.7880	3.1139
Subject 9	4.7611	3.6000	24.7982	25.6427
	2.8059	7.0141	22.4902	22.0147
Subject 10	10.3035	5.9118	8.6949	13.6583
	6.7680	6.3913	10.3945	14.0652
Subject 11	3.4673	2.6520	5.7088	9.5065
	4.3743	3.5773	6.0173	9.7633
Subject 12	4.0572	1.5183	8.3988	24.0095
	4.9506	3.7573	11.5140	22.5689
Subject 13	1.8234	2.0311	6.5738	9.5651
	3.3462	3.6193	7.3212	9.9973
Subject 14	2.8496	4.6363	17.4210	10.9702
	5.2582	4.4033	19.6039	8.0711
Subject 15	2.8918	2.6099	7.1562	15.2799
	6.5987	3.1836	7.9033	14.0901
Subject 16	3.4231	3.1821	5.7033	14.1232
	5.4231	8.1821	6.7033	18.1232
Subject 17	2.1941	3.2119	15.1515	21.9312
	5.7298	4.1073	14.9199	19.8435

Table 3.1: The table summarizes the root mean square errors between the displacement of the center of pressure obtained from the inertial sensor data and the one obtained from the force platform. For each subject the first row refers to the component X of the center of pressure, while the second row refers to the component Y of the center of pressure.

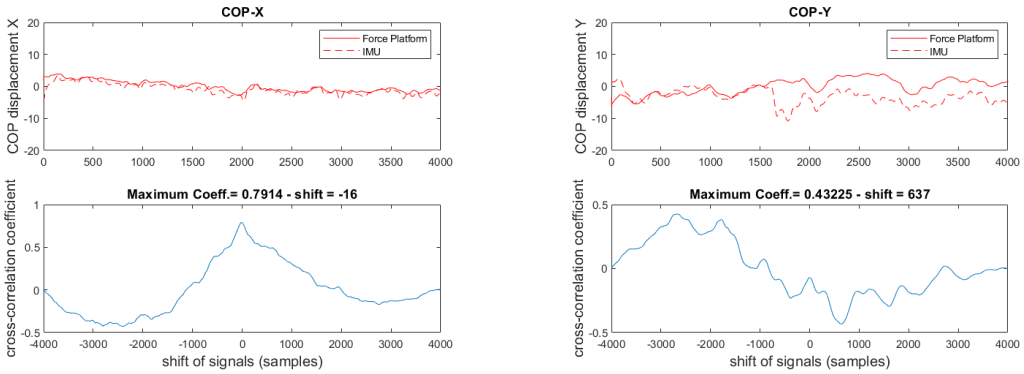

(a)

(b)

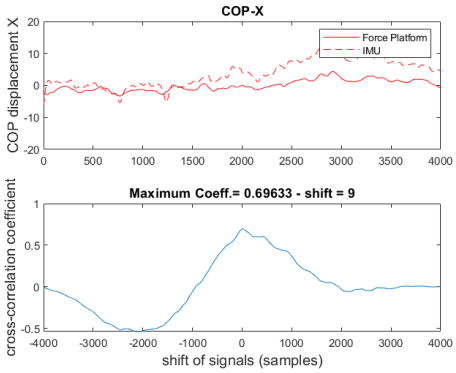

(c)

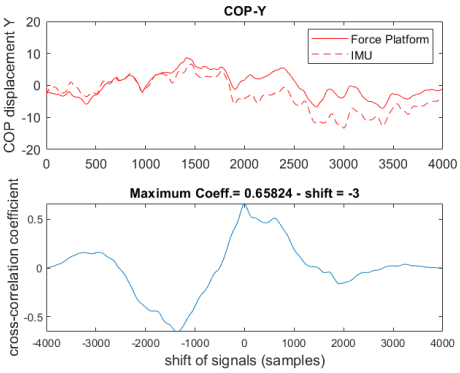

(d)

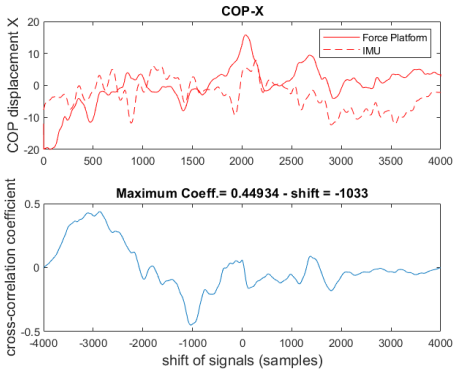

(e)

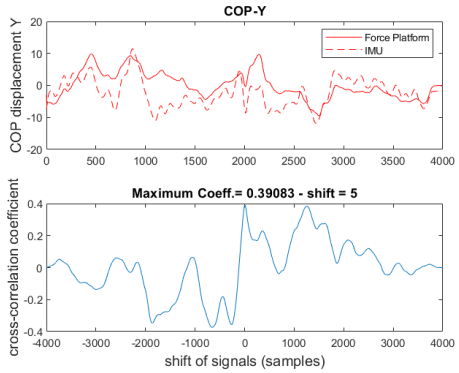

(f)

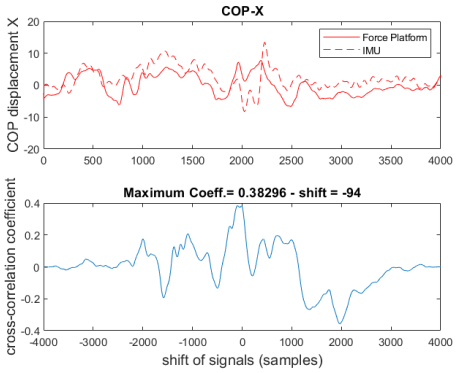

(g)

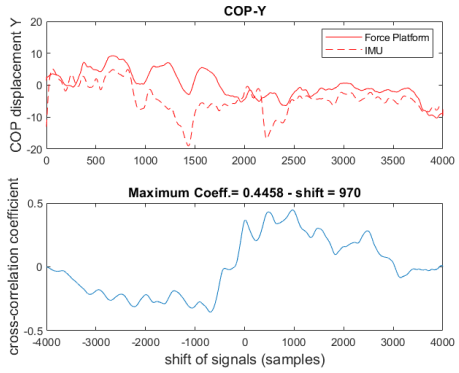

(h)

Figure 3.8: Cross-correlation (blue) of the COP trajectories (red) for Subject 7: (a - b) Task 1, (c - d) Task 2, (e - f) Task 3, (g - h) Task 4.

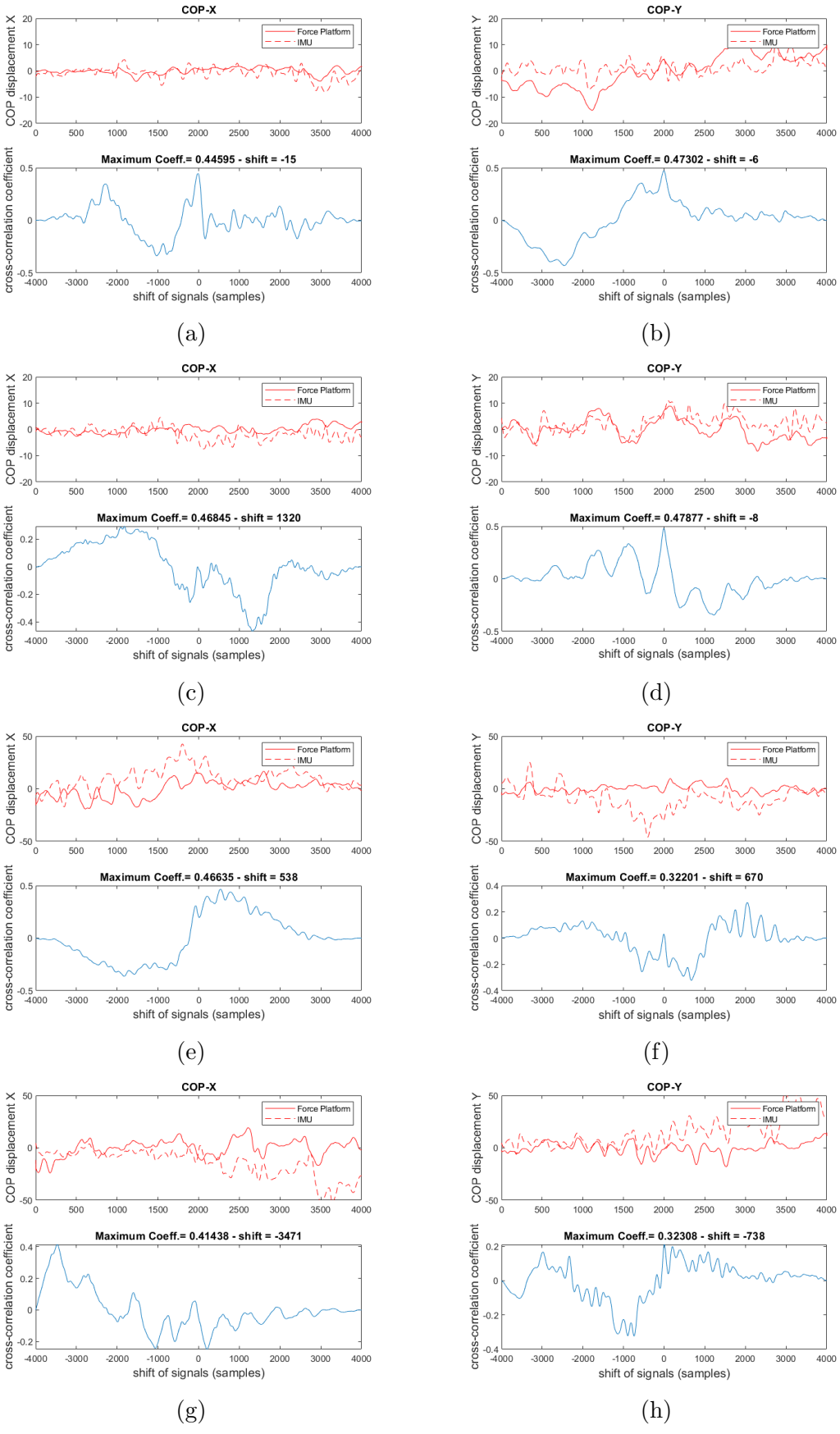

Figure 3.9: Cross-correlation (blue) of the COP trajectories (red) for Subject 17: (a - b) Task 1, (c - d) Task 2, (e - f) Task 3, (g - h) Task 4.

	Task 1	Task 2	Task 3	Task 4
Subject 1	0.25556	0.35409	0.37852	0.32719
	0.89753	0.92896	0.41002	0.39135
Subject 2	0.48516	0.30567	0.34001	0.27296
	0.47976	0.29059	0.24707	0.41733
Subject 3	0.22855	0.32179	0.47422	0.52730
	0.37046	0.18968	0.61311	0.30622
Subject 4	0.54184	0.29320	0.53553	0.66684
	0.79715	0.42454	0.47688	0.42310
Subject 5	0.40493	0.47654	0.38548	0.39501
	0.61501	0.70326	0.26204	0.27322
Subject 6	0.46613	0.29804	0.32303	0.24680
	0.23645	0.39456	0.38170	0.27178
Subject 7	0.79140	0.69633	0.44934	0.38296
	0.43225	0.65824	0.39083	0.44580
Subject 8	0.39961	0.51132	0.28425	0.50143
	0.28233	0.46379	0.36914	0.84632
Subject 9	0.18683	0.25115	0.30898	0.41051
	0.35103	0.43653	0.27736	0.29163
Subject 10	0.30430	0.27970	0.68529	0.59171
	0.56908	0.48995	0.51534	0.38063
Subject 11	0.36785	0.44728	0.66864	0.58702
	0.38650	0.45466	0.47298	0.38202
Subject 12	0.45859	0.68329	0.64837	0.36073
	0.45155	0.33969	0.51942	0.34047
Subject 13	0.32916	0.26894	0.33655	0.30511
	0.33923	0.48014	0.43204	0.30927
Subject 14	0.79140	0.30004	0.34906	0.49369
	0.28223	0.35121	0.40109	0.42194
Subject 15	0.34783	0.33078	0.30011	0.26167
	0.42128	0.51032	0.40549	0.31101
Subject 16	0.43567	0.33210	0.31245	0.41200
	0.33923	0.45512	0.37654	0.32160
Subject 17	0.44595	0.46845	0.46635	0.41438
	0.47302	0.47877	0.32201	0.32308

Table 3.2: The table summarizes the cross-correlation coefficients between the displacement of the center of pressure obtained from the inertial sensor data and the one obtained from the force platform. For each subject the first row refers to the component X of the center of pressure, while the second row refers to the component Y of the center of pressure.

Comparison COM trajectories

An equal comparison to that carried out for the center of pressure was made for the trends of the center of mass. The displacements of the COM obtained by the inertial sensor, assuming this positioned directly on the center of mass of the subject, were compared with the trajectories of the COM obtained by filtering the force platform COP-data. Also in this case the results generally provided "closer" traces with a similar trend of the center of mass obtained from the two measurement systems for the first four motor tasks performed by the subjects. This can be noticed in the stabilograms of the A/P and M/L trajectories of the COM in the double stance motor tasks for Subject 4, Subject 7, Subject 8, Subject 10, Subject 17 reported following in Figures 3.10, 3.11, 3.12, 3.13, 3.14, respectively. Similar results were obtained also for the other subjects involved in the analysis.

Subject 4

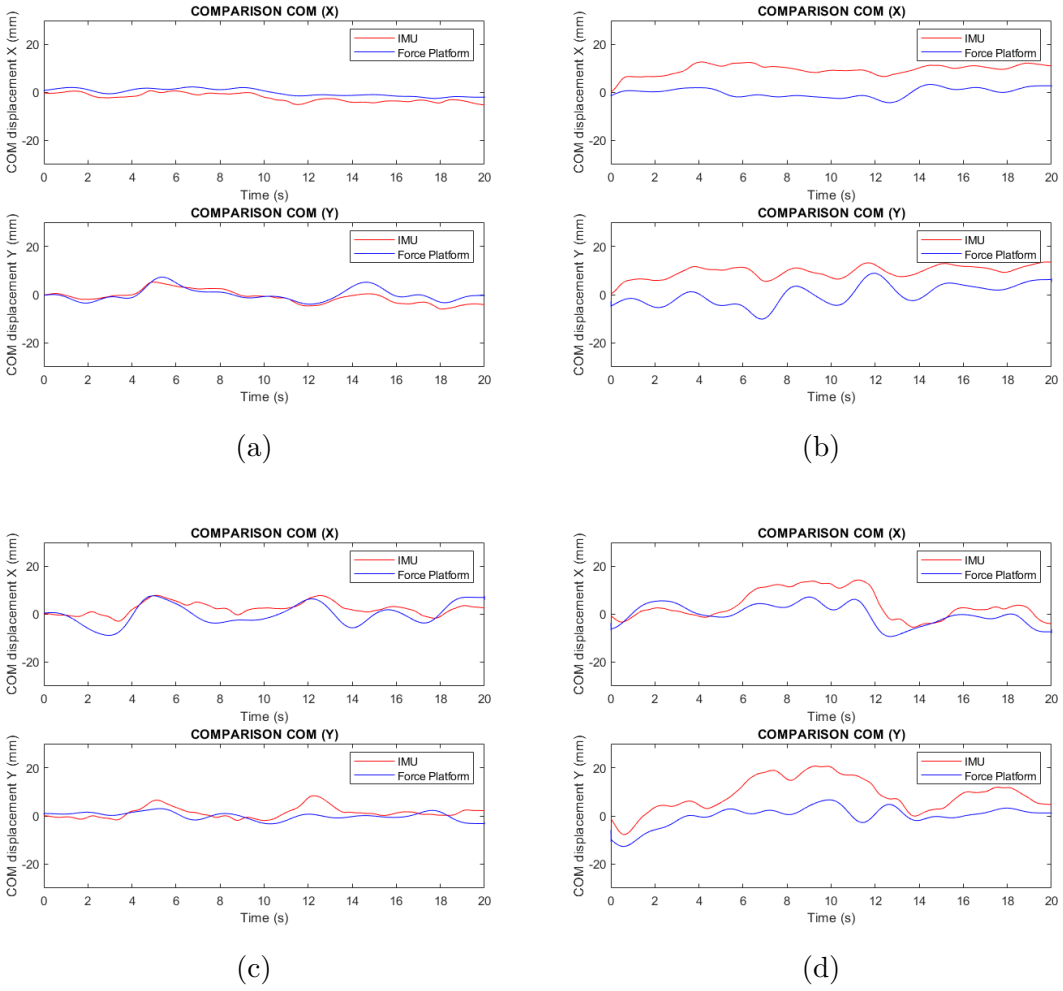

Figure 3.10: Stabilograms representing A/P and M/L time series of the center of mass displacement for Subject 4: (a) Task 1, (b) Task 2, (c) Task 3, (d) Task 4 of double stance phase. The center of mass trajectory from the inertial sensor is depicted in red, the force plate-COM is depicted in blue.

Subject 7

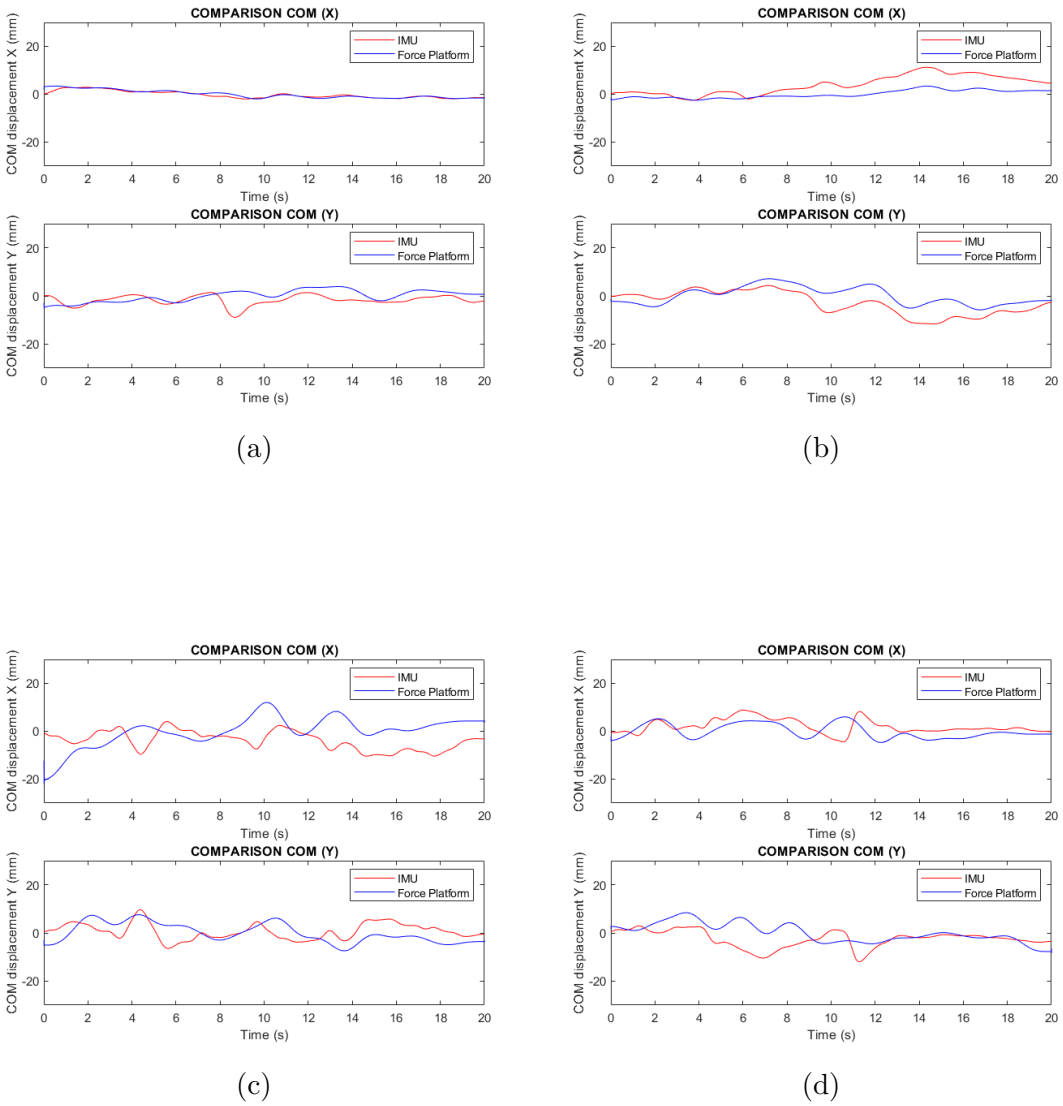

Figure 3.11: Stabilograms representing A/P and M/L time series of the center of mass displacement for Subject 7: (a) Task 1, (b) Task 2, (c) Task 3, (d) Task 4 of double stance phase. The center of mass trajectory from the inertial sensor is depicted in red, the force plate-COM is depicted in blue.

Subject 8

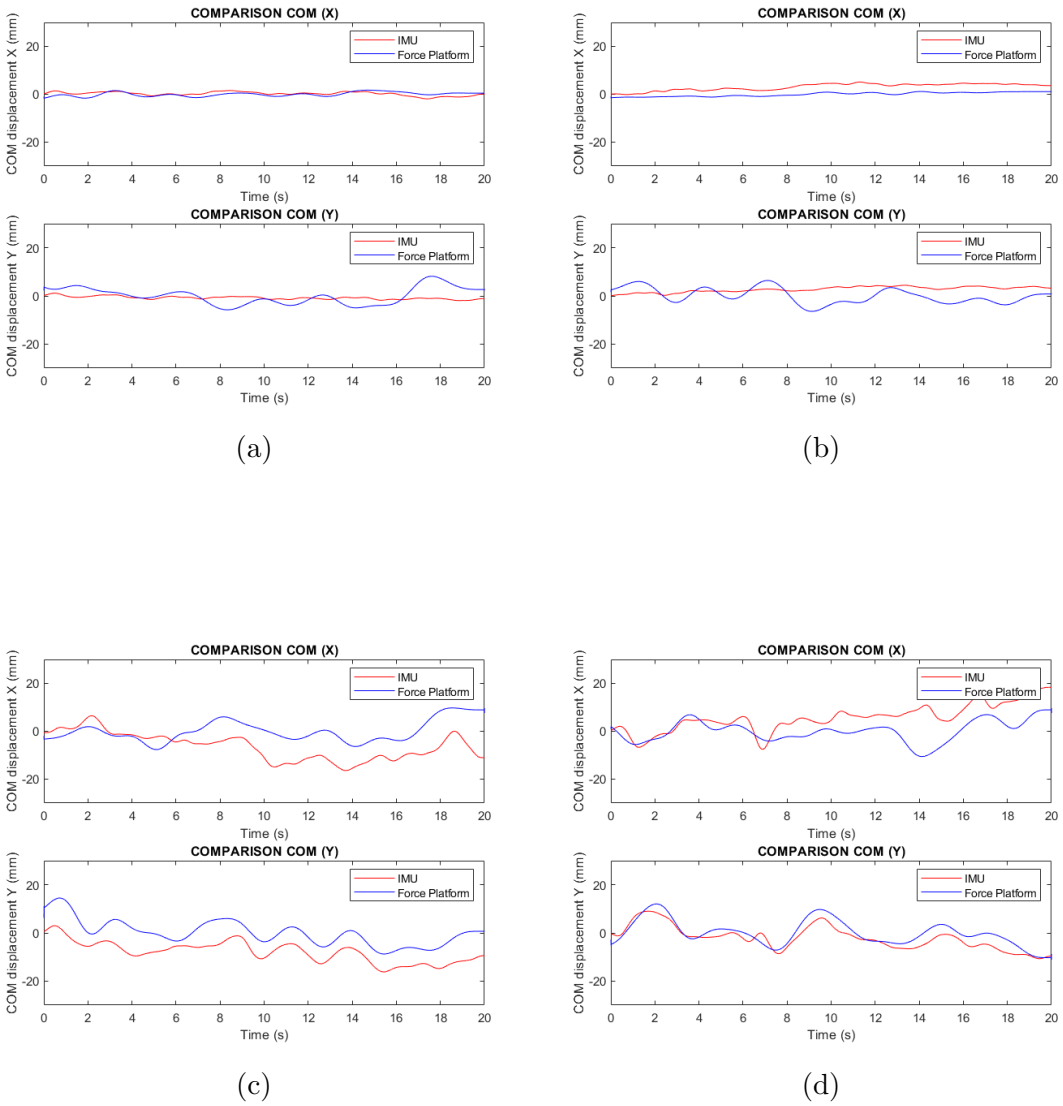

Figure 3.12: Stabilograms representing A/P and M/L time series of the center of mass displacement for Subject 8: (a) Task 1, (b) Task 2, (c) Task 3, (d) Task 4 of double stance phase. The center of mass trajectory from the inertial sensor is depicted in red, the force plate-COM is depicted in blue.

Subject 10

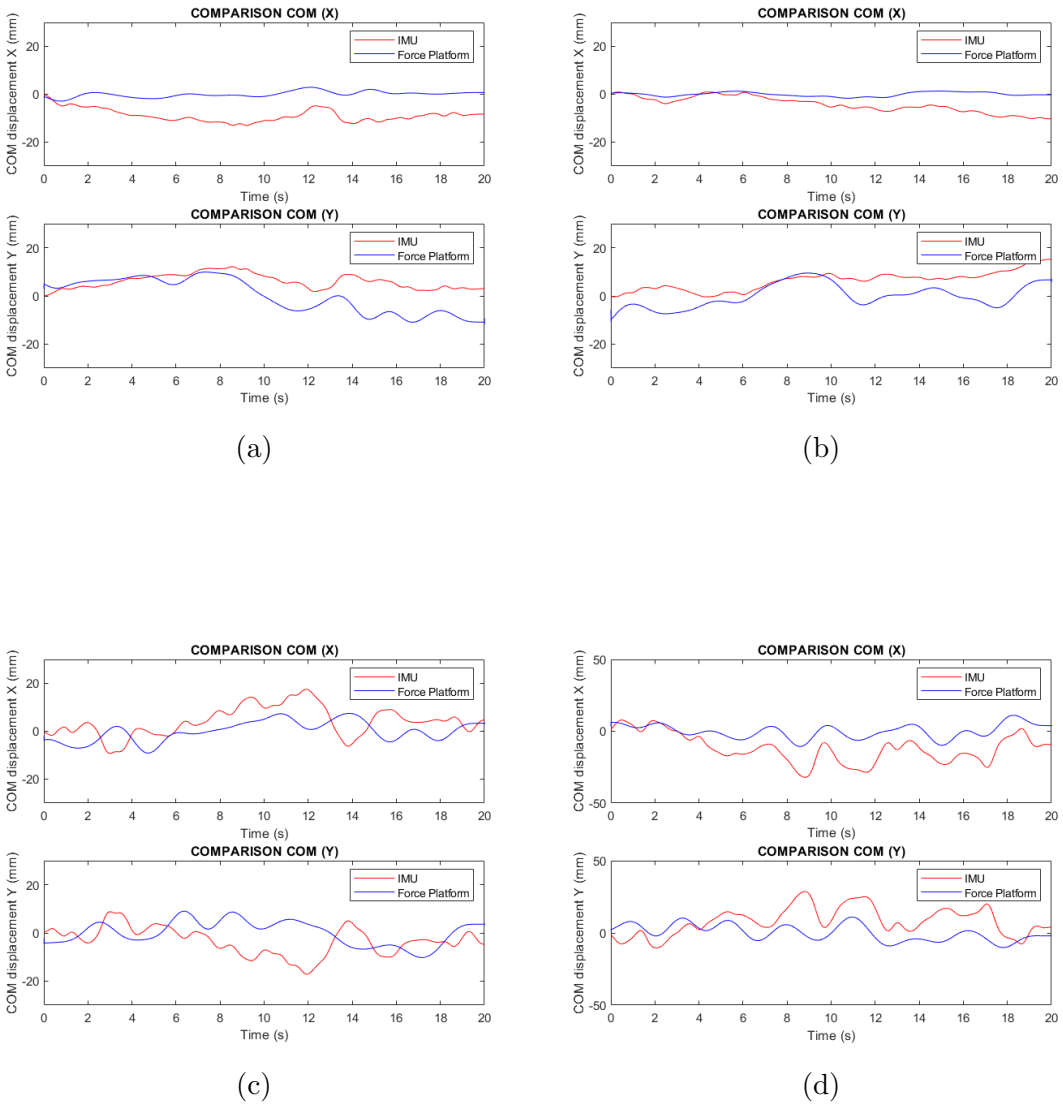

Figure 3.13: Stabilograms representing A/P and M/L time series of the center of mass displacement for Subject 10: (a) Task 1, (b) Task 2, (c) Task 3, (d) Task 4 of double stance phase. The center of mass trajectory from the inertial sensor is depicted in red, the force plate-COM is depicted in blue.

Subject 17

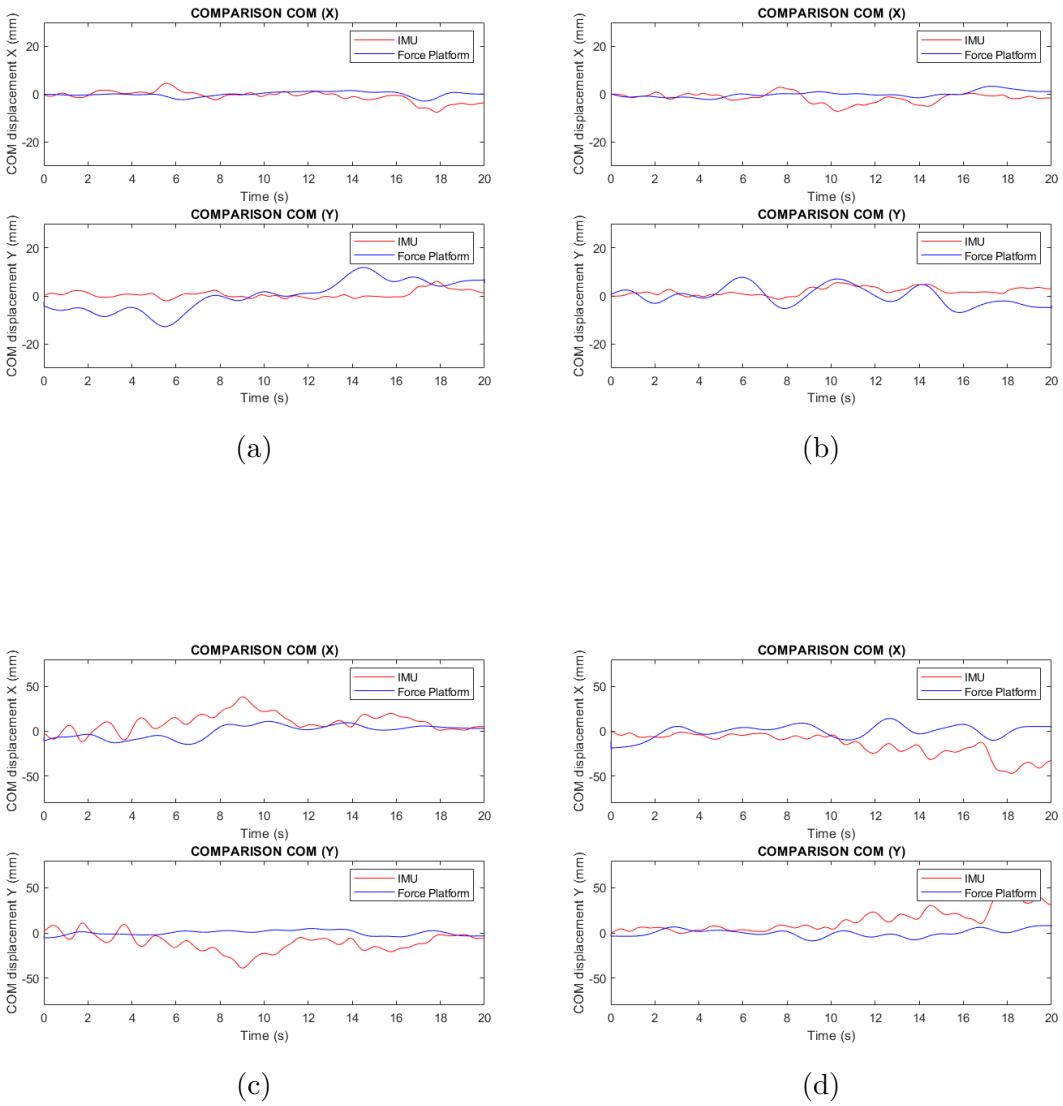

Figure 3.14: Stabilograms representing A/P and M/L time series of the center of mass displacement for Subject 17: (a) Task 1, (b) Task 2, (c) Task 3, (d) Task 4 of double stance phase. The center of mass trajectory from the inertial sensor is depicted in red, the force plate-COM is depicted in blue.

The superimposition of the trajectories of the COM from the data related to the single stance phase, as for the case of the center of pressure, did not provide as satisfactory results as those obtained from the double stance phase. Reasonable, considering that the COM relating to force platform measurements is obtained simply by applying a butterworth filter to the components of the COP. For this reason, with the same considerations made for the center of pressure, the results obtained from tasks 5, 6, 7 and 8 characterized by the single stance support were discarded from the validation study. The values obtained from the computation of the root-mean-square errors between the center of mass displacement obtained from IMU

and the one derived from the force plate for the double stance tasks are summarized in the following Table 3.3.

	Task 1	Task 2	Task 3	Task 4
Subject 1	2.7981	2.9392	8.4510	21.5988
	2.2558	3.7055	8.4210	10.0447
Subject 2	1.6391	2.1997	7.0724	5.5952
	6.2120	4.5381	7.2375	8.7042
Subject 3	1.1540	4.4659	2.7866	3.6722
	2.3347	5.0966	5.9443	4.7851
Subject 4	2.1925	9.9069	3.9707	5.6102
	2.0725	10.0002	2.8544	10.0097
Subject 5	3.2476	2.4193	15.7884	13.3474
	2.2598	2.5996	11.9699	17.3486
Subject 6	3.3532	3.3796	6.2243	7.3517
	4.6030	4.9375	6.3120	6.7260
Subject 7	3.3235	4.7686	8.6959	4.0000
	0.6355	4.54660	4.7306	5.2480
Subject 8	1.0915	3.1884	8.9385	7.6451
	3.5906	4.5580	8.2294	3.0564
Subject 9	3.6472	3.8317	24.3677	23.9034
	2.4214	5.9066	24.2561	22.0350
Subject 10	9.3616	5.3012	7.6642	13.7188
	8.4621	7.4357	9.0197	12.957
Subject 11	3.2471	1.7019	5.4270	7.9926
	3.9224	2.9380	5.1474	8.1034
Subject 12	3.3715	1.0930	8.0703	23.3728
	5.0910	3.4435	10.7378	22.8319
Subject 13	1.342	1.8106	6.3263	8.5237
	1.642	2.8410	5.1248	9.4031
Subject 14	2.9972	2.9369	17.2031	9.7282
	4.4036	4.9921	18.8994	8.0310
Subject 15	1.5171	1.9798	6.0483	14.8200
	6.8109	3.1640	7.1159	13.7658
Subject 16	3.1211	3.4520	6.1102	14.0120
	6.1102	8.2257	6.8220	18.4790
Subject 17	2.4720	2.8406	13.9722	21.4596
	6.1673	4.0981	15.4581	18.4755

Table 3.3: The table summarizes the root mean square errors between the displacement of the center of mass obtained from the inertial sensor data and the one obtained from the force platform. For each subject the first row refers the component X of the center of mass, while the second row refers to the component Y of the center of mass.

Also in this case, as for the COP trajectories, the cross-correlation of the COM displacement obtained using the inertial sensor and the one obtained using the force plate, was computed. In Figures 3.15 and 3.16, the cross-correlations obtained for the double stance tasks for Subjects 7 and 17 are reported. Table 3.4, instead, summarizes the values obtained fo the other subjects involved in the current validation study.

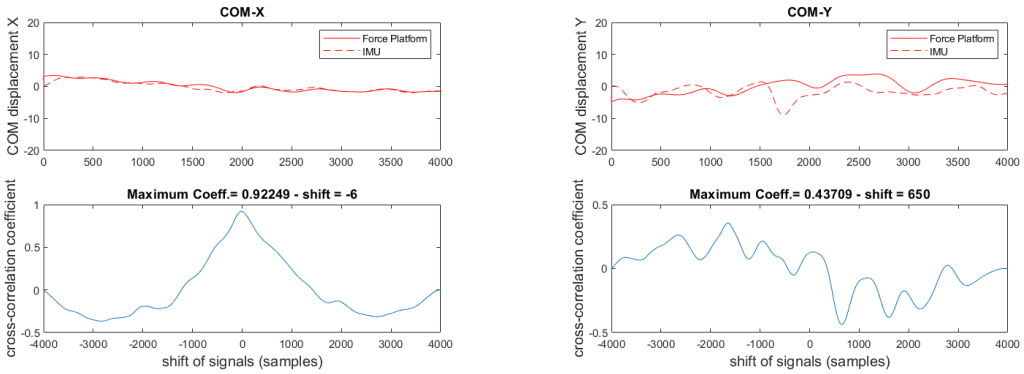

(a)

(b)

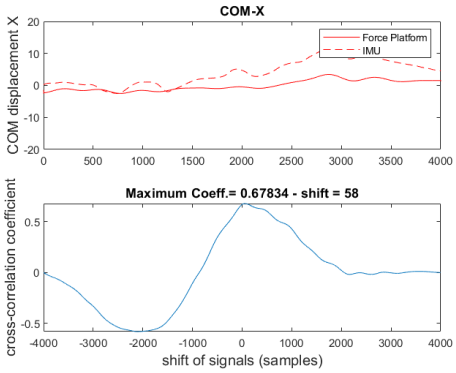

(c)

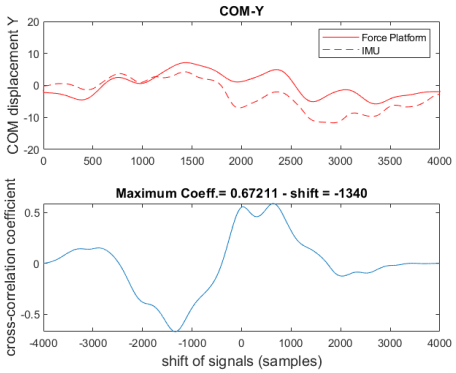

(d)

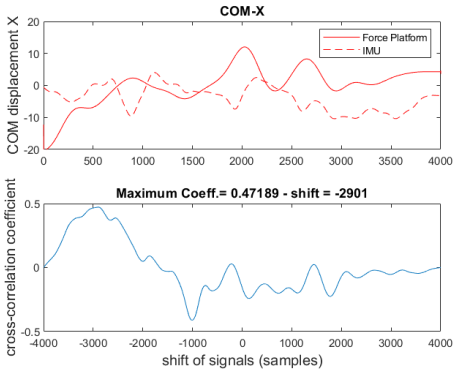

(e)

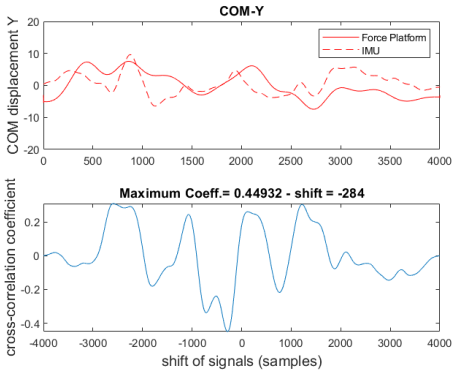

(f)

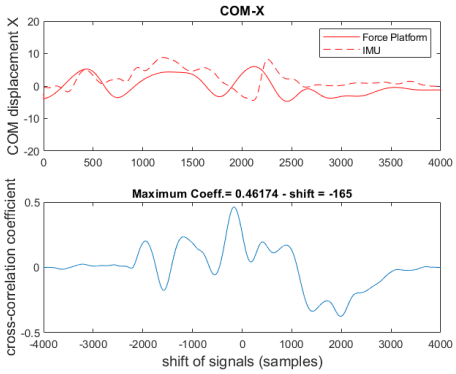

(g)

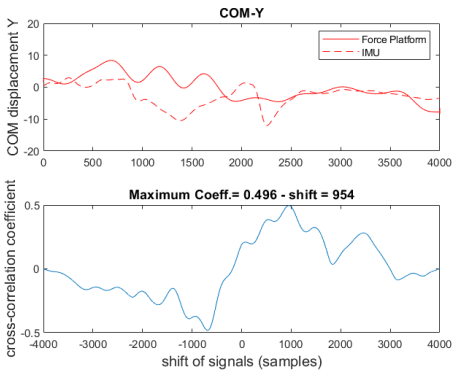

(h)

Figure 3.15: Cross-correlation (blue) COM trajectories (red) for Subject 7: (a - b) Task 1, (c - d) Task 2, (e - f) Task 3, (g - h) Task 4.

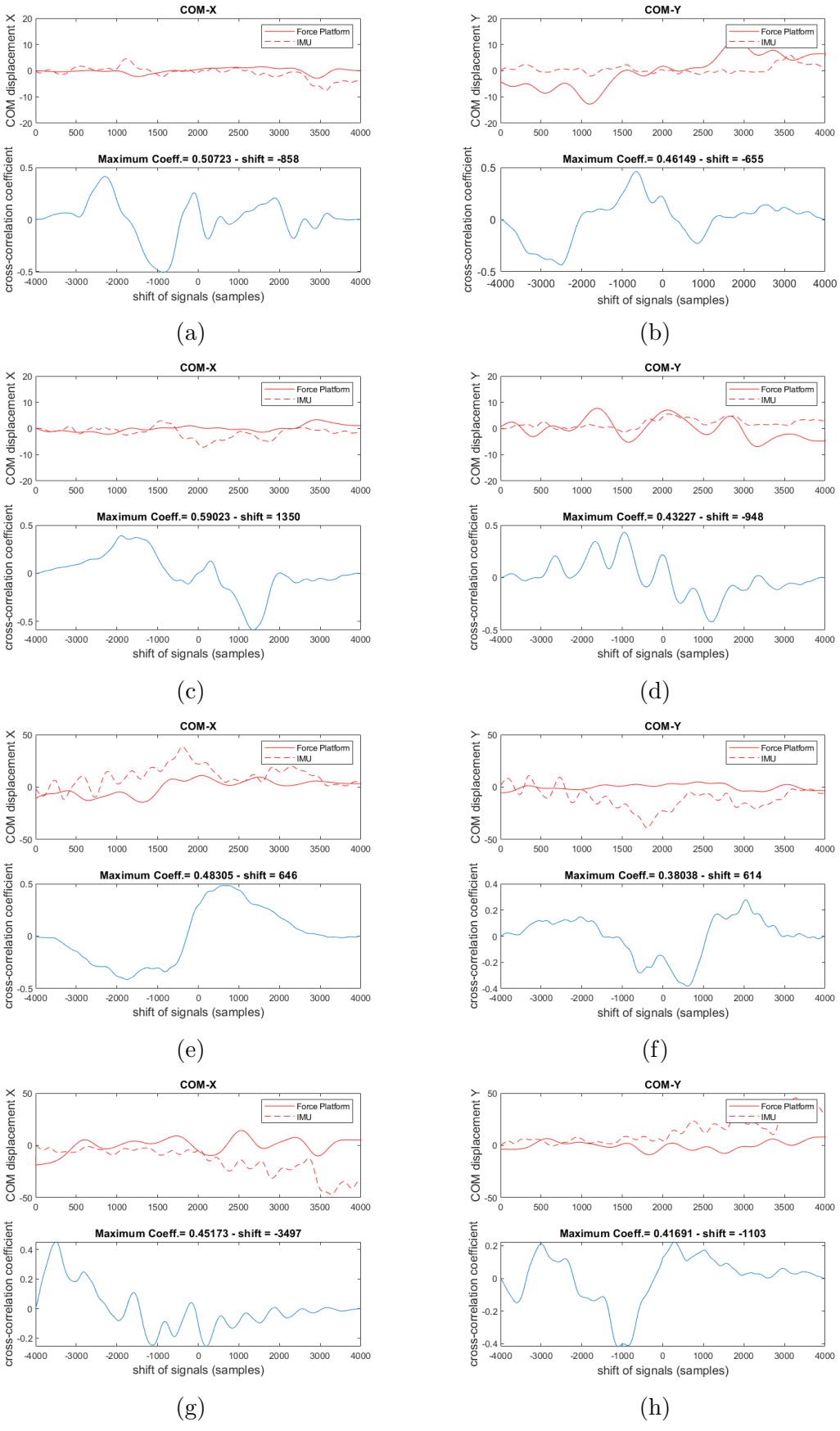

Figure 3.16: Cross-correlation (blue) COM trajectories (red) for Subject 17: (a - b) Task 1, (c - d) Task 2, (e - f) Task 3, (g - h) Task 4.

	Task 1	Task 2	Task 3	Task 4
Subject 1	0.33165	0.43328	0.45976	0.42082
	0.86336	0.88480	0.43991	0.35913
Subject 2	0.62405	0.42460	0.40131	0.27941
	0.52214	0.44230	0.27385	0.35572
Subject 3	0.38544	0.42696	0.64718	0.63610
	0.32778	0.21640	0.59236	0.32948
Subject 4	0.62873	0.34267	0.53149	0.64781
	0.72261	0.41936	0.31238	0.46133
Subject 5	0.47795	0.56136	0.32273	0.37272
	0.51267	0.54718	0.30896	0.36455
Subject 6	0.47836	0.26272	0.36716	0.30099
	0.26739	0.48120	0.51827	0.34714
Subject 7	0.92249	0.67834	0.47189	0.46174
	0.43709	0.67211	0.44932	0.49600
Subject 8	0.61796	0.56809	0.29258	0.40051
	0.35391	0.41187	0.44173	0.83039
Subject 9	0.29144	0.13589	0.27270	0.35610
	0.56030	0.47065	0.38836	0.36446
Subject 10	0.39130	0.39525	0.68197	0.50752
	0.58084	0.38655	0.69655	0.46408
Subject 11	0.46930	0.42568	0.59318	0.50038
	0.49960	0.22256	0.46767	0.26650
Subject 12	0.48557	0.55962	0.63653	0.19367
	0.53741	0.47841	0.55131	0.24983
Subject 13	0.41443	0.40061	0.39122	0.46202
	0.37499	0.62525	0.45010	0.38597
Subject 14	0.92249	0.44871	0.31960	0.54169
	0.35391	0.48179	0.51312	0.53306
Subject 15	0.58474	0.45817	0.37456	0.34023
	0.48469	0.56861	0.47895	0.38332
Subject 16	0.35210	0.42171	0.31341	0.42356
	0.45742	0.42191	0.31240	0.33120
Subject 17	0.50723	0.59023	0.48305	0.45173
	0.46149	0.43227	0.38038	0.41691

Table 3.4: The table summarizes the cross-correlation coefficients between the displacement of the center of mass obtained from the inertial sensor data and the one obtained from the force platform. For each subject the first row refers to the component X of the center of mass, while the second row refers to the component Y of the center of mass.

Statokinesigram analysis

The postural oscillations of the subjects derived from the inertial sensor were represented on the horizontal plane using the values of the displacement of the center of pressure in the anterior-posterior and medial-lateral directions. This typical maps of the 2D trajectory of the center of pressure over the task time are called statokinesigrams. The representations obtained using inertial sensor-COP presented a very similar aspect to the traditional sway path of statokinesigrams obtained in a classical posturographic analysis using the center of pressure data from the force plate. Indeed, as expected, by comparing the 2D COP trajectories among the various tasks it is possible to notice that passing from a trial with open eyes to the same motor task performed with closed eyes, the size of the track on the plane in terms of occupied area grows. This is reasonable, since the closed-eyes condition is a more critical situation for the maintenance of balance. Moreover, from the comparison also emerged as a different support base of the subject heavily influenced the body's postural sway. Indeed, comparing for example the trials characterizing by the feet apart at the shoulder width with those with feet together it possible to observe that the width of the statokinesigram in the medial-lateral direction increased due to the fact that with a wide base of support in this direction, the subject tends to become more unbalanced in the anterior-posterior direction. These considerations can be better appreciated by looking in the following Figures 3.17 and 3.18, the postural sways obtained for Subject 8 in the double and single stance tasks, respectively.

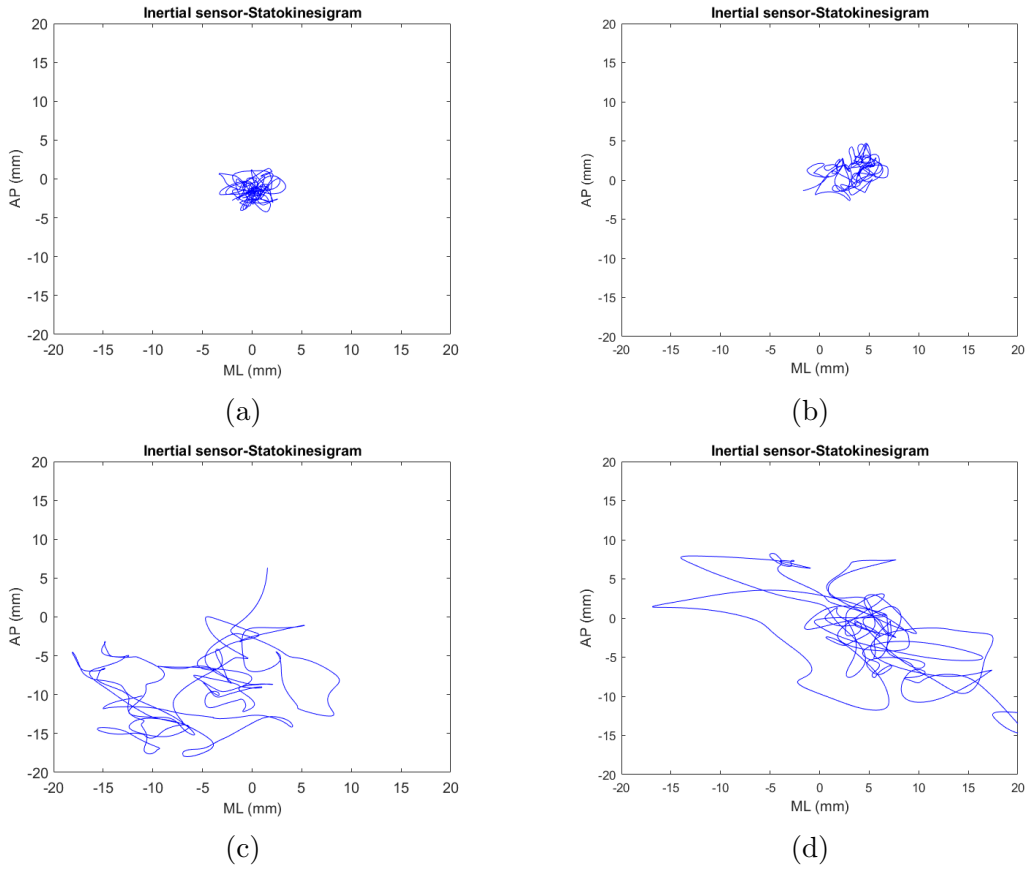

Figure 3.17: Statokinesigrams of center of pressure displacement during double stance trials of Subject 8: (a) Task 1, (b) Task2, (c) Task 3, (d) Task 4.

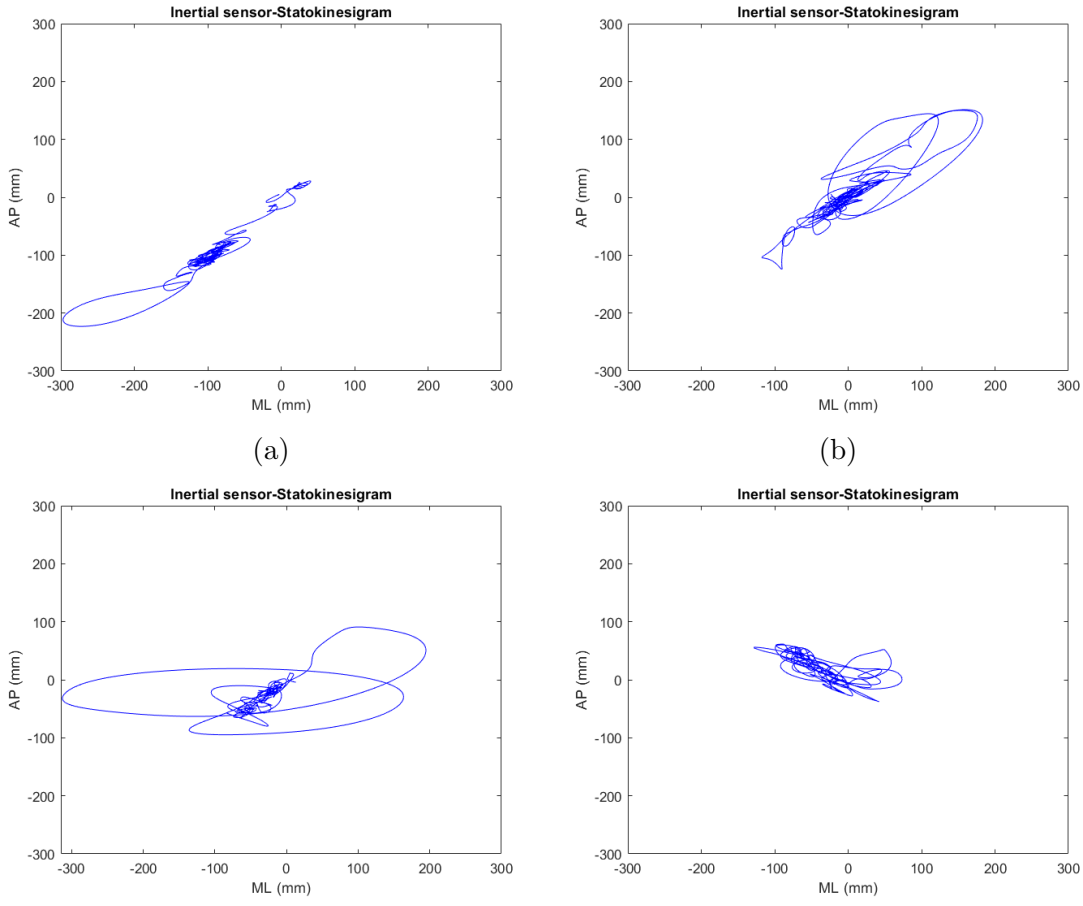

Figure 3.18: Statokinesigrams of center of pressure displacement during double stance trials of Subject 8: (a) Task 5, (b) Task6, (c) Task 7, (d) Task 8.

Chapter 4

Discussion

The maintenance of balance and body orientation in the standing position is essential for guaranteeing the performance of daily life activities and the practice of physical and sport movements. Balance is a responsibility of the postural control system, based on the functions of the nervous, sensory, and motor systems [5]: the sensory system provides information regarding the position of body segments in relation to other segments and to the environment; the motor system is responsible for the correct and adequate activation of the muscles to perform movements; the central nervous system integrates the information provided by the sensory system, and then sends nervous impulses to the muscles, which generate neuromuscular responses. Mechanically, instead, balance depends on the forces and torques applied on it. Indeed, a body is in mechanical equilibrium when the sum of all the forces (F) and torques (M) that act on it is equal to zero: $\sum F = 0$ and $\sum M = 0$. The forces acting on the body can be classified as external and internal forces: the external forces are mainly the gravitational force and the ground reaction force; the internal forces can be physiological disturbances (e.g., heartbeat and breathing) or perturbations created by the muscles activation for the maintenance of posture and the performance of the body's own movements [1]. All these forces, when transmitted to the environment, provoke the continuous acceleration of the human body in all the directions around its center of gravity. Therefore, from the mechanical point of view, the human body is never in a condition of perfect equilibrium, because the forces acting on it are only temporarily null [5]. Thus, it is possible to state that the human body is constantly unbalanced, in an incessant search for balance. Moreover, the postural stability varies over the course of life and depends on the integrity of the systems responsible for maintaining human balance. This degeneration of balance with increased age, as well as several pathologies, contributes to balance deficits that increase the risk of falling, ultimately leading to increased morbidity, mortality and health care costs [22, 23]. Therefore, the investigation concerning the mechanisms of balance and body orientation control represents a growing public concern and has awakened the interest of professionals in several fields, including medicine, physical therapy, physical education, engineering, physics, among others. These professionals have used different techniques of measurement and assessment that often generate different results. In research settings, balance is commonly measured using force platform-based postural sway evaluations that have been demonstrated as valid and reliable measures of balance, in health and disease, and are considered a gold standard [6]. However, force platforms are relatively expensive, immobile

and hence not practical for clinical and home-based assessments. For this reason, recently, this widespread necessity to assess balance has generated the need for a reliable, inexpensive, and quantifiable clinical measure and body-wearable sensor technology is turning out to be a possible new avenue for accurately detecting and monitoring body motion and physical activity of an individual. In this context, the assessments made using wearable sensors based on inertial measurement units are placed. Indeed, these latters, consisting in the combinations of multiple gyroscopes, accelerometers and magnetometers, provide an opportunity for measuring the three-dimensional kinematics of the body. The key adavantages of these sensors are that they are inexpensive, do not require a specific measurement environment or the installation of any particular infrastructure and allow the monitoring of balance under free conditions. IMU-based evaluations are a very promising modality for tracking patient's postural performance but, since they are a very recent technique, further studies are necessary to understand their precision and reliability with respect to the gold standard force platform. For this reason, the aim of this work was to investigate the accuracy and the validity of these novel sensors against force platforms for assessing standing balance. To this end, after a preliminary literature research focused on the selection of papers regarding the use of IMUs sensors against the force plate in static posturography, a specific validation protocol was drawn up to perform simultaneous acquisitions of data from the two measurement systems on 17 healthy subjects executing eight motor tasks of double or single stance with open or closed eyes. The first objective of the validation of the inertial sensors consisted in comparing the trajectories of the center of mass and the center of pressure, obtained by processing the acquired data, of the IMU and of the force platform. The results obtained showed that, in the trials in which subjects have both legs as support, both the IMU-based COM and COP generally followed the path of the traces of the force platform. Unfortunately the comparisons made between the force plate and the inertial sensor in the single stance tests had to be discarded, since not all the subjects analyzed were able to complete these tasks with only one foot resting on the ground. In most cases the subjects losing their balance placed the foot of the raised swinging leg outside the force platform, making the comparison of the trajectories derived from the two systems not possible.

An explanation to some errors and differences in the comparison, especially in the trajectories of the most unstable subjects, may be in the model assumed to describe the oscillations of the subjects. Indeed, in the processing of the inertial sensor data, the estimation of the displacement of the center of mass in the anterior-posterior direction and in the medial-lateral direction was made assuming the body mass as a single inverted pendulum rotating around the ankle joint (supposing a negligible motion of the hip joint) to maintain balance in the upright position. However, subjects do not sway strictly as inverted pendulums, in fact, even quiet stance in young healthy subjects includes some hip strategy and the amount of hip strategy used to control stance posture have been shown to increase with age. Thus, although this approach may produce accurate results during quiet stance, it may be inappropriate for assessing the COM displacements when the subject sways significantly. To overcome this, future works could use a two-segmental model of the body probably more appropriate to describe the maintainance of balance. For example Najafi et al.[5], suggest to use, instead of a single inertial sensor positioned on the lower back near the COM and to use the inverted pendulum model, two inertial sensors, one applied

on the back and one on the shin, capable of providing respectively the angle of ankle and hip joints, then using a two-link model of the human body. Additionally, the force plate and inertial sensor recordings were not hardware synced. Therefore, it was necessary to create an event to allow the synchronization of the captured data. In this study, it was chosen to use a force sensing resistor sensor, positioned directly on the inertial sensor worn by the subject, and as physical synchronization event, three taps given by a person on the FSR sensor were used. This physical event resulted in three perturbations visible in both the inertial sensor and the FSR sensor and used to achieve, in the post-processing phase, synchronization of the IMU's recordings with those of the force platform. However, due to unforeseen technological problems, not always all three hits were detected by both sensors. Therefore, in this situations, a perfect agreement of the acquisitions cannot be defined with extreme certainty, and consequently this results in errors affecting also the calculated RMSEs and correlation coefficients of COP and COM. Nevertheless, generally the superimposed trajectories of the center of pressure and of the center of mass of the two systems were comparable and the RMS errors were less than 25 mm.

To investigate the validity of the use of inertial sensors to assess standing balance, the second goal of the current study consisted in analysing the sensitivity of the device, trying to understand whether IMU-based evaluations could reveal differences among the different tasks, thus among the different feet positions and the different visual conditions assumed by the examined subjects during the tests, as well as force platforms are able to do. In general, IMU-based measures of sway resulted to be just as sensitive as force plate COP measures in differentiating between the different tasks conditions, since, as expected, by comparing the 2D center of pressure trajectories (i.e., A/P COP displacement versus M/L displacement) among the different motor tasks it was possible to notice the effect of situations that required more effort to restore balance on the size and the shape of the statokinesigrams. Indeed, the obtained results confirmed that closing the eyes significantly deteriorates postural control strategy resulting in greater body's oscillations than those characterizing open eyes tasks and, hence, greater size, in terms of occupied area, of the track on the plane. Also, from the comparison emerged as the motor tasks performed with the feet joint together (i.e., Task 3-4) were characterized by larger displacements with respect to those with the feet apart (i.e., Task 1-2). As predictable, the most unstable motor tasks were found to be those in which the subjects had to stand on one leg, especially those in which the subjects were also deprived of visual system information. Therefore, this postural sway increasing when standing under altered sensory conditions obtained in the results was in good agreement with the traditional considerations obtained in classical posturographic tests using force platforms. Moreover, it is worth noting that in the current investigation, the two compared measurement systems actually measure different physical quantities. The force platform gave as output the components of the center of pressure from which those of the center of mass were then obtained by filtering, while the inertial sensor by combining the information of the gyroscope, accelerometer and magnetometer allowed to estimate, using the sensor quaternions subsequently converted to Euler angles, the position of the center of mass, from which the COP was then estimated.

Overall, this method demonstrated, under controlled conditions, a good level of similarity of the trajectories of the center of pressure and mass compared to force plate.

Conclusion

This study suggests evaluations based on inertial wearable sensors to assess standing balance, since IMU-based measurements could offer a patient-friendly, inexpensive and efficient alternative recording technique useful to qualify postural control. For this purpose, an investigation of the validity of analysing the dynamics of standing balance via wearable IMUs against gold-standard in-lab equipment was performed. 17 subjects underwent static posturography tests characterized by the simultaneous use of a force platform and an inertial sensor to compare the trajectories of the center of pressure and mass obtained by the two measuring devices. The experimental set-up developed was in agreement with previously published studies. The anterior-posterior and medial-lateral displacement of the center of pressure and center of mass obtained by the inertial measurement unit strongly matched, with similar path and oscillations, those of the validated force platform in many of the trials executed. Differences and errors emerged more in tests where the subject fluctuated more. Results of this study have some limitations:

- Only a small number of subjects were included in the study. The results will need to be confirmed with a larger sample.
- Only healthy subjects underwent validation of the inertial sensor. Other studies should be addressed to explore also the impact of unhealthy and unstable subjects with balance disorders on the results.
- Only one inertial sensor positioned on the lower back on the L4-L5 was taken into consideration. Future studies could improve the results considering the possibility of using two sensors and a two-link model of the human body to include also the movements done to restore the equilibrium thanks to the hip strategy.

Despite these limitations, it is possible to conclude by stating that the results confirm that this system has the potential for extended clinical as well as research applications. It is clear that this system could be a very promising tool for postural sway assessment.

Bibliography

Bibliography

[1] Winter D.A., *Human Balance and posture control during standing and walking*, Gait & Posture, 1995, Vol. 3: 193-214.

[2] Abrahamová D., Hlavacka F., *Age-related changes of human balance during quiet stance*, Physiol Res., 2008, Vol. 57: 957-964 NO. 6

[3] Konrad H.R., Girardi M., Helfert R., *Balance and aging*, Laryngoscope, 1999, Vol. 109: 1454-60 NO. 9

[4] Duarte M., Freitas S.M., *Revision of posturography based on force plate for balance evaluation*, Rev Bras Fisioter, 2010, Vol. 14: 183-92, NO. 3

[5] Najafi B., Horn D., Marclay S., Crews R.T., Wu S., Wrobel J.S., *Assessing postural control and postural control strategy in diabetes patients using innovative and wearable technology*, J. Diabetes Sci Technol., 2010, Vol. 4:780-91 NO. 4

[6] Ghislieri M., Gastaldi L., Pastorelli S., Tadano S., Agostini V., *Wearable Inertial Sensors to Assess Standing Balance: A Systematic Review*, Sensors (Basel), 2019, Vol. 19 NO. 19

[7] Winter D.A., Patla A.E., Frank J.S., *Assessment of balance control in humans*, Med Prog Technol., 1990, Vol. 16:31-51

[8] Pollock A.S., Durward B.R., Rowe P.J., Paul J.P., *What is balance?*, Clin Rehabil., 2000, Vol. 14:402-6 NO.4

[9] Wade M.G., Jones G., *The role of vision and spatial orientation in the maintenance of posture*, Phys Ther., 1997, Vol. 77:619-28 NO. 6

[10] Horak F.B., *Postural orientation and equilibrium: what do we need to know about neural control of balance to prevent falls?*, Age Ageing, 2006 Vol. 35

[11] Peterka R.J., *Sensorimotor integration in human postural control*, J Neurophysiol., 2002, Vol. 88:1097-118 NO. 3

[12] Masani K., Vette A.H., Popovic M.R., *Controlling balance during quiet standing: Proportional and derivative controller generates preceding motor command to body sway position observed in experiments*, Gait & Posture, 2006, Vol. 23: 164-172

[13] Jacono M., Casadio M., Morasso P.G., Sanguineti V., *The Sway-Density Curve and the underlying postural stabilization process*, Human Kinetics Journal, 2004, Vol. 8: 292-311 NO. 3

[14] Hong C.Y., Guo L.Y., Song R. et al.,*Assessing postural stability via the correlation patterns of vertical ground reaction force components*, BioMed Eng OnLine, 2016, Vol. 15 NO. 90

[15] Sung J.L, Hong C.Y., Liu C.H., Posen L., Guo L.Y., Lin N.H., Yen C.W, Liaw L.J., *Characterizing the Validity of the Inverted Pendulum Model for Quiet Standing*, Journal of Healthcare Engineering, 2021

[16] Chiari L., Morasso P.G., Rocchi L., *Analisi posturografica*, Bioingegneria della postura eretta e del movimento, Cappello A., Cappozzo A., 2007, Patron Editore, 375-412.

[17] Bottaro A., Casadio M., Morasso P.G., Sanguineti V., *Body sway during quiet standing: Is it the residual chattering of an intermittent stabilization process?*, 2005, Human Movement Science, Vol. 24:588-615, NO. 4

[18] Colobert B., Crétual A., Allard P., Delamarche P., *Force-plate based Computation of the Ankle and Hip Strategies from a Double Inverted Pendulum Model*, 2006, Clinical Biomechanics., Vol. 21

[19] Blenkinsop G.M., Pain M.T.G., Hiley M.J., *Balance control strategies during perturbed and unperturbed balance in standing and handstand*, 2017, R. Soc. Open Sci., Vol. 4 NO. 7 Biomechanics., Vol. 21

[20] Morasso P.G., Bottaro A., Casadio M., Sanguineti V.,*Preflexes and internal models in biomimetic robot systems*, 2005, Cognitive Processing

[21] Ono H., Sato T., Ohnishi K., *Balance recovery of ankle strategy: Using knee joint for biped robot*, 2011, 1st International Symposium on Access Spaces (ISAS), 236:241

[22] Sturnieks D.L., George St R., Lord S. R., *Balance disorders in the elderly*, 2008, Neurophysiologie Clinique/Clinical Neurophysiology, Vol. 38:467-478, NO. 6

[23] Burns E.R., Stevens J.A., Lee R., *The direct costs of fatal and non-fatal falls among older adults — United States*, 2016, J Safety Res.

[24] Visser J.E., Carpenter M.G., Kooij H., Bloem B.R.,*The clinical utility of posturography*, 2008, Clinical Neurophysiology, Vol. 119:2424-2436, NO. 11

[25] Prieto T.E., Myklebust J.B., Hoffmann R.G., Lovett E.G., Myklebust B.M., *Measures of postural steadiness: differences between healthy young and elderly adults*, IEEE Trans Biomed Eng., 1996, Vol. 43:956-66 NO.9

[26] Johnson C.D., *Process Control Instrumentation Technology*, 2014, Pearson Education Limited, Eighth Edition

[27] Beckham G., Suchomel T. and Mizuguchi S., *Force Plate Use in Performance Monitoring and Sport Science Testing*, 2014, New Studies in Athletics, NO. 3.2014

[28] Mohammed Z., Elfadel I-A.M., Rasras M., *Monolithic Multi Degree of Freedom (MDoF) Capacitive MEMS Accelerometers*, 2018, Micromachines, Vol. 9 NO. 11

[29] Quan Q., *Sensor Calibration and Measurement Model*, 2017, Springer Nature Singapore

[30] Rashed R., Momeni H., *System modeling of MEMS Gyroscopes*, 2007, Mediterranean Conference on Control & Automation

[31] Hamza-Lup F.G., *Kinesthetic Learning – Haptic User Interfaces for Gyroscopic Precession Simulation*, 2018, International Journal of Human-Computer Interaction, Vol. 11, NO. 3

[32] https://www.neubrex.com/htm/applications/gyro-principle.htm

[33] Haykm T., *PHOTONIC-CRYSTAL FIBERS GYROSCOPE*, Scientific Journal «ScienceRise» , 2015

[34] Sung W.T., Kang T., Lee J.G., *Controller Design of a MEMS Gyro-Accelerometer with a Single Proof Mass*, 2008, International Journal of Control Automation and Systems, Vol. 6: 873-883, NO. 6

[35] Brunetti F., Moreno J.C., Ruiz A.F., Rocon E., Pons J.L.,*A new platform based on IEEE802.15.4 wireless inertial sensors for motion caption and assessment*, 2006, Annual International Conference of the IEEE Engineering in Medicine and Biology Society

[36] Moon K.S., Lee S.Q., Ozturk Y., Gaidhani A., Cox J.A., *Identification of Gait Motion Patterns Using Wearable Inertial Sensor Network*, 2019, Sensors.

[37] Vienne A., Barrois R.P., Buffat S., Ricard D., Vidal P.P., *Inertial Sensors to Assess Gait Quality in Patients with Neurological Disorders: A Systematic Review of Technical and Analytical Challenges*, 2017, Psychology

[38] Lee C.H., Sun T.L., *Evaluation of postural stability based on a force plate and inertial sensor during static balance measurements*, 2018, Journal of Physiological Anthropology

[39] Noamani A., Nazarahari M., Lewicke J., Vettea A.H., Rouhani H., *Validity of using wearable inertial sensors for assessing the dynamics of standing balance*, 2020, Medical Engineering and Physics, Vol. 77:53–59

[40] Adamová B., Kutilek P., Cakrt O., Svoboda Z., Viteckova S., Smrcka P., *Quantifying postural stability of patients with cerebellar disorder during quiet stance using three-axis accelerometer*, Biomed. Signal Process. Control, 2018

[41] Alkathiry A.A., Sparto P.J., Freund B., Whitney S.L., Mucha, A., Furman, J.M., Collins M.W., Kontos A.P., *Using Accelerometers to Record Postural Sway in Adolescents With Concussion: A Cross-Sectional Study*, 2018, J. Athl. Train.

[42] Roldán-Jiménez C., Cuesta-Vargas A.I., *Studying upper-limb kinematics using inertial sensors: a cross-sectional study*, 2015, BioMed Central

[43] Sun R., Moon Y., McGinnis R., Seagers K., Motl R.W., Sheth N., Wright J.A., Ghaffari R., Patel S., Sosnoff J., *Assessment of Postural Sway in Individuals with Multiple Sclerosis Using a Novel Wearable Inertial Sensor*, 2018, Digit Biomark 2018

[44] Mancini M., Salarian A., Carlson-Kuhta P., Zampieri C., King L., Chiari L., Horak F.B., *ISway: a sensitive, valid and reliable measure of postural control*, 2012, J. Neuroeng. Rehabil., Vol. 9, NO. 1

[45] Jakob V., Küderle A., Kluge F., Klucken J., Eskofier B.M, Winkler J., Winterholler M., Gassner H., *Validation of a Sensor-Based Gait Analysis System with a Gold-Standard Motion Capture System in Patients with Parkinson's Disease*, 2021, sensors

[46] Fusca M., Negrini F., Perego P., Magoni L., Molteni F., Andreoni G., *Validation of a Wearable IMU System for Gait Analysis: Protocol and Application to a New System*

[47] Grimm B., Bolink S., *Evaluating physical function and activity in the elderly patient using wearable motion sensors*, 2017, EFORT Open Rev., Vol. 1:112-120 NO.5

[48] Zijlstra W., Hof A.L., *Assessment of spatio-temporal gait parameters from trunk accelerations during human walking*, 2003, Gait Posture

[49] Supuk T.G., Skelin A.K., Cic M., *Design, development and testing of a low-cost sEMG system and its use in recording muscle activity in human gait*, 2014, Sensors

[50] Faber G.S., Kingma I., Bruijn S.M., van Dieen J.H.. *Optimal inertial sensor location for ambulatory measurement of trunk inclination*, 2009, J Biomech

[51] Howcroft J., Kofman J., Lemaire E.D., *Review of fall risk assessment in geriatric populations using inertial sensors*, 2013, J. Neuroeng. Rehabilit.

[52] Sun R., Sosnoff J.J., *Novel sensing technology in fall risk assessment in older adults: A systematic review*, 2018, BMC Geriatr.

[53] MaetzlerW., Domingos J., Srulijes K., Ferreira J.J., Bloem B.R., *Quantitative wearable sensors for objective assessment of Parkinson's disease*, 2013, Mov. Disord.

[54] Hubble R.P., Naughton G.A., Silburn P.A., Cole M.H., *Wearable Sensor Use for Assessing Standing Balance and Walking Stability in People with Parkinson's Disease: A Systematic Review*, 2015, PLoS ONE

[55] Sun R., McGinnis, R., Sosnoff, J.J., *Novel technology for mobility and balance tracking in patients with multiple sclerosis: A systematic review* , 2018, Expert Rev. Neurother.

[56] Abe Y., Sugaya T., Sakamoto M., *Postural Control Characteristics during Single Leg Standing of Individuals with a History of Ankle Sprain: Measurements Obtained Using a Gravicorder and Head and Foot Accelerometry*, J. Phys. Ther. Sci., 2014, Vol. 26:447–450

[57] Ehsani H., Mohler J., Marlinski V., Rashedi E., Toosizadeh N., *The influence of mechanical vibration on local and central balance control*, 2018, J. Biomech.

[58] Nguyen N., Phan D., Pathirana P.N., Horne M., Power, L., Szmulewicz D., *Quantification of Axial Abnormality Due to Cerebellar Ataxia with Inertial Measurements Sensors*, 2018

[59] Guo L., Xiong S., *Accuracy of Base of Support Using an Inertial Sensor Based Motion Capture System*, 2017, Sensors

[60] Bzduskova D., Valkovic P., Hirjakova Z., Kimijanova J., Hlavacka F., *Parkinson's disease versus ageing: Different postural responses to soleus muscle vibration*, Gait Posture, 2018

[61] Kutilek P., Svoboda Z., Cakrt O., Hána K., Chovanec M., *Postural Stability Evaluation of Patients Undergoing Vestibular Schwannoma Microsurgery Employing the Inertial Measurement Unit* , 2018, Journal of Healthcare Engineering

[62] Alessandrini M., Micarelli A., Viziano A., Pavone I., Costantini G., Casali D., Paolizzo F., Saggio G., *Body-worn triaxial accelerometer coherence and reliability related to static posturography in unilateral vestibular failure*, 2017, Acta Otorhinolaryngol Italica

[63] Doherty C., Zhao L., Ryan J., Komaba Y., Inomata A., Caulfield B., *Quantification of postural control deficits in patients with recent concussion: An inertial-sensor based approach*, Clin. Biomech., 2017

[64] Kim K.G., Lucarevic J., Bennett C., Gaunaurd I., Gailey R., Agrawal V., *Testing the assumption of normality in body sway area calculations during unipedal stance tests with an inertial sensor*, 2016, Proc. Annu. Int. Conf. IEEE Eng. Med. Biol. Soc. EMBS, Vol. 2016: 4987–4990

[65] Melecky R., Socha V., Kutilek P., Hanakova L., Takac P., Schlenker J., Svoboda Z., *Quantification of Trunk Postural Stability Using Convex Polyhedron of the Time-Series Accelerometer Data*, 2016, J. Healthc. Eng.

[66] Hejda J., Cakrt, O., Socha, V., Schlenker J., Kutilek P., *3-D trajectory of body sway angles: A technique for quantifying postural stability*, 2015, Biocybern. Biomed. Eng., Vol.35:185–191 NO.3

[67] Neville C., Ludlow C., Rieger B., *Measuring postural stability with an inertial sensor: Validity and sensitivity*, 2015, Med. Devices Evid. Res., Vol. 8:447–455

[68] Halicka' Z., Lobotkova' J., Buckova' K., Hlavacka F., *Effectiveness of different visual biofeedback signals for human balance improvement*, 2014, Gait Posture Vol.39:410–414

[69] Heebner N.R., Akins J.S., Lephart S.M., Sell T.C., *Reliability and validity of an accelerometry based measure of static and dynamic postural stability in healthy and active individuals*, 2015, Gait Posture, Vol.41:535–539

[70] Hsieh K.L., Roach K.L., Wajda D.A., Sosnoff J.J, *Smartphone technology can measure postural stability anddiscriminate fall risk in older adults*, 2019, Gait Posture, Vol. 67:160–16

[71] Mancini M., Carlson-Kuhta P., Zampieri C.,Nutt J. G., Chiari L., Horak F.B., *Postural sway as a marker of progression in Parkinson's disease: A pilot longitudinal study*, 2012, Gait Posture, Vol. 36:471–476

[72] Mancini M., Carlson-Kuhta P., Zampieri C.,Nutt J. G., Chiari L., *Trunk Accelerometry Reveals Postural Instability in Untreated Parkinson's Disease HHS Public Access*, 2011, Park. Relat Disord, Vol. 17:557–562, NO. 7

[73] Rouis A., Rezzoug N., Gorce P., *Validity of a low-cost wearable device for body sway parameter evaluation*, 2014, Comput. Methods Biomech. Biomed. Engin. 2014, Vol. 17:182–183

[74] Whitney S., Roche J., Marchetti G., Lin C., Steed D., Furman G., Musolino M., Redfern M., *A comparison of accelerometry and center of pressure measures during computerized dynamic posturography: A measure of balance*, 2011, Gait Posture, Vol.33:594–599

[75] Frames C., Soangra R., Lockhart T.E., *Assessment of postural stability using inertial measurement unit on inclined surfaces in healthy adults*, 2013, Biomed. Sci. Instrum., Vol. 49:234–42

[76] Sadun A.S., Jalani J., Sukor J.A., *Force Sensing Resistor (FSR): A Brief Overview and the Low Cost Sensor for Active Compliance Control*, 2016

[77] https://www.tekscan.com/blog/flexiforce/how-does-force-sensing-resistor-fsr-work

[78] https://x-io.co.uk/ngimu/